A Metabolomics Approach to Improving CHO Cell Productivity

A dissertation submitted by

Grace Yao

in partial fulfillment of the requirements for the degree of

Doctor of Philosophy

in

Chemical and Biological Engineering

Tufts University

February 2023

Advisor: Kyongbum Lee, Ph.D.

Abstract

Chinese Hamster Ovary (CHO) cells are widely used in the biopharmaceutical industry to produce therapeutic recombinant proteins such as monoclonal antibodies for myriad clinical applications. Technological advances in the past few decades have greatly increased the productivity of CHO cells, allowing for more efficient, robust, and flexible production. Most of these advances have come from improved growth and longevity of cells, with perfusion cultures being the most extreme case and able to sustain cell densities of over 100 million cells/mL over the course of weeks or even months. However, as we approach the physical limitations of cell growth-based productivity improvement, we need to instead look at increasing the specific productivity (qP) of each individual cell to continue making progress towards higher titer and volumetric efficiency. This is necessary to meet the growing demand for biologics in a cost-effective and sustainable way. Growth and qP are closely connected as they both require significant amounts of energy from a limited pool within cells. Thus, increases in qP will often correlate with decreases in growth, resulting in similar final volumetric titer. Finding ways to enhance qP enough to overcome any loss in growth and increase overall titer is a complex challenge. In this work, we endeavored to use a metabolomics approach on a library of CHO clones producing IgG on an industrial level to identify novel, low-cost strategies for improving qP without compromising cell growth.

First, we performed untargeted metabolomics on supernatants from fed-batch production of these clones and found metabolites that were significantly correlated with qP. Two of these metabolites, aspartate and cysteine, were found to have significant positive correlations in separate sets of clones producing different recombinant proteins, so they may be useful as early indicators of high-qP cell lines during clone selection. Having a panel of early indicators may shorten timelines or

help to overcome limitations of the clone selection process such as unoptimized media conditions. Another metabolite of interest identified through pathway enrichment analysis was citrate. When added directly to cell culture, citrate was able to increase both qP and volumetric titer for multiple clones, showing potential utility as a media supplement.

In order to elucidate the mechanism of qP improvement upon citrate addition, we used 13C-labeled citrate as a stable isotopic tracer that cellular enzymes cannot distinguish from naturally occurring citrate. As a key intermediate of the TCA cycle, citrate could be augmenting TCA cycle flux, which generates additional ATP that can be used for protein production, by entering as a substrate. However, citrate uptake and conversion into downstream metabolites was not increased by citrate supplementation, suggesting an alternative mechanism was at play. Through metabolic flux analysis of clones that did and did not respond positively to citrate addition, we discovered significant correlations between qP response and intracellular fluxes in pathways connected to but not in the TCA cycle. The significant fluxes included catabolism of aromatic and branched-chain amino acids as well as flux through the α-ketoglutarate-malate transporter, part of the malate-aspartate shuttle. These results may signify a more regulatory role for citrate in terms of qP improvement rather than being directly used as a substrate for the TCA cycle. Further studies, for example using RNA-seq or proteomics, are warranted to study the regulatory impact of citrate supplementation.

Acknowledgements

The work in this thesis was only realized with the support of many contributors at Tufts University and Bristol Myers Squibb. First and foremost, I would like to thank my advisor, Professor Kyongbum Lee, not only for the constant, thoughtful guidance throughout my time as a student in his lab, but also for his unwavering encouragement, generous trust, and kind understanding of the difficulties of balancing graduate research with a full-time industry position. I am so appreciative and admiring of his ability to push his students to independently ask challenging questions while providing insightful nudges in the right direction whenever we need help. Immensely knowledgeable about a vast range of topics, excellent at making interdisciplinary connections, diplomatic and clear in communicating, he has been an ideal advisor, and I am fortunate to have learned from him.

I am also deeply grateful to Dr. Kathryn Aron for her patient mentorship, flexibility, advocacy, and inspirational leadership on this journey. Without her, this project may never have left the ground. Our many discussions were essential to developing my confidence as a scientist and the quality of my research, and I couldn't have asked for a better role model to shape my growth. Next, I want to thank my incredible committee members, Dr. Michael Borys, Professor Emmanuel Tzanakakis and Professor Rebecca Scheck. They have shown me continual willingness to help in any way, especially throughout the trials of a global pandemic, and provided valuable feedback, helping me to think deeply with scientific rigor and to learn how to best prioritize my work.

I'd like to thank the past and present members of the Lee Lab who have spent time and effort collaborating and sharing knowledge while also providing camaraderie and motivation along the way, especially Karin Yanagi, Ming Lei, Nick Alden, Ece Gülşan, Sophie Girard, Jenner Tresan,

Seoyoung Park, Pomai Yamaguchi, Jingyun Yang, Smitha Krishnan, and Gautham Sridharan, plus honorary members from our neighboring lab Trevor Nicks and Sean Sullivan. Similarly, so many colleagues at Bristol Myers Squibb have enriched my life with their friendship, advice, and support: Kyle McHugh, Jeff Swanberg, Zhuangrong Huang, Shayna Sizelove, Jessica Roberge, Sue Egan, and many more. I am also indebted to all others who have supported this work including numerous Process Development Upstream, Cell Line Development, and Analytical colleagues, and those who helped allow me this opportunity at BMS in the first place, including Zhengjian Li, Morrey Atkinson, and Girish Pendse.

Finally, I want to extend my sincere appreciation to my friends and family who have brought light and balance to my life. Thanks to Tracy and Erik, Julie, Ploy, Steph, Julia, Esther, and too many others to name for always being ready to lend an ear or give me a pep talk. Thanks to my parents, Linda and Charles, and my brother Jeff for fostering an environment growing up that led me to develop focus, persistence, and ambition, without which I would never have made it to this point. Most importantly, Minh and Rusty have been by my side through all these years, and I feel so lucky to have such a loving family to care for me and cheer me on.

Contents

List of Figures

List of Tables

Chapter 1. Introduction: Biopharmaceutical production of monoclonal antibodies in Chinese Hamster Ovary cells

1.1 Biopharmaceutical Production

Biopharmaceuticals, also known as biologics, are medicines which are produced through biological process, usually in living cells. These molecules are larger and more complex than the other major category of drugs, small molecules, which are well-defined and made through chemical synthesis. Biologics include treatments such as monoclonal antibodies (mAbs), other recombinant proteins, hormones, gene and cell therapies, and vaccines (Makurvet, 2021). The manufacturing process, which usually involves genetic modification to living cells, is a major reason why biologics are more expensive than small molecules, in addition to the cost of administration to patients in medical facilities because they are not in pill form (Rozek, 2013). Despite the cost, the global biopharmaceutical market, projected to reach >$380 billion by 2024, has been continually expanding, led by therapeutic mAbs with high specificity and affinity for targets (Tsumoto et al., 2019).

Monoclonal antibody drugs are used to treat many types of disease, but the top sellers include many immunotherapy products such as Opdivo (nivolumab), Keytruda (pembrolizumab), which are both anti-PD-1, Rituxan (rituximab), targeting CD20, or chemotherapy products such as Herceptin (trastuzumab), and Avastin (bevacizumab). Widely prescribed drugs for autoimmune and inflammatory diseases like arthritis, psoriasis or Crohn's disease are also monoclonal antibodies, such as Humira (adalimumab), Remicade (infliximab) and Stelara (ustekinumab) (Lu et al., 2020). These mAbs can be created in several ways, but the most popular is the traditional mouse hybridoma technique, where mice are immunized with desired antigens, triggering an immune response. Harvested splenocytes are used to generate hybridoma cells that secrete IgG

antibodies. These murine antibodies can be humanized by grafting the complementary-determining region (CDR), which targets the antigen, into a human framework sequence (Lu et al., 2020).

Typical human antibodies are composed of two light chains (LC) and two heavy chains (HC), with each LC linked to an HC and the two HCs linked together via disulfide bridges. Each side of the Y-shaped antibody molecule consists of the "antigen-binding" Fab region which includes the light chain and first two domains of the heavy chain, and the "crystallizable" Fc region which includes two constant domains of the heavy chain. Within the Fab region, there is a variable domain and a constant domain for each of the light and heavy chains. The variable heavy and variable light chains are connected by a short polypeptide linker and together this is the scFv, or single-chain variable fragment which is where the CDR is grafted (Chiu et al., 2019).

During the production, secretion, and purification of the mAbs, they experience many post-translational modifications (PTMs). These PTMs are considered product quality attributes (PQAs), many of which monitored and controlled within predefined acceptance criteria to maintain consistent drug safety and efficacy. Examples of PTMs include deamidation, glycation, disulfide reduction, and C-terminal lysine clipping (X. Xu et al., 2019). One of the most important and most heterogeneous PTMs that can significantly affect potency and pharmacokinetics is N-linked glycosylation. N-linked glycans are typically complex branched oligosaccharide structures with one or more monosaccharides attached, and their initial formation starts in the endoplasmic reticulum, followed by trimming and modifications in the Golgi apparatus (Cymer et al., 2018). Glycosylation can help stabilize the Fc region heavy chains, impact serum half-life, affect binding to Fc receptors, and modulate immune-mediated effector functions such as ADCC (antibody-

dependent cellular cytotoxicity), CDC (complement dependent cytotoxicity), and ADCP (antibody dependent cellular phagocytosis) (Shrivastava et al., 2022).

Because these PTMs have major implications for safety, efficacy, stability, and bioactivity, it is critical to synthesize therapeutic proteins in host cells capable of performing PTMs compatible with use in humans. Thus, most biologics are made in mammalian cell lines such as CHO (Chinese hamster ovary), HEK 293 (human embryonic kidney), NS0 (murine myeloma), SP2/0 (murine hybridoma) or BHK (baby hamster kidney) cells. To date, CHO cells have been the host of choice for production of mAbs for several reasons. Since there have been many regulatory approvals for therapeutics made in CHO cells, they are considered well established to have appropriate safety and efficacy profiles for over two decades (Hong et al., 2018). They are also capable of relatively high productivity and consistently good growth in chemically defined, serum-free suspension cultures suitable for large industrial scale bioreactors (Tihanyi & Nyitray, 2020).

Although CHO cells are well-characterized due to their popularity, there is room for further improvements, especially with respect to cell specific productivity. Higher protein titers can reduce costs for patients and help maintain an edge over competing therapeutics. Biosimilars, while not as popular or easy to produce as small molecule generics due to greater molecular complexity, are still being developed for many drugs, adding to the pressure to lower manufacturing costs. Meanwhile, industry trends are driving a shift towards smaller batches often produced in single-use bioreactors with small footprints, enabling flexible multiproduct facilities. These single-use bioreactors can accommodate intense bioprocesses and are designed to translate well between scales, require fewer resources for operation including turnaround between batches (Frank, 2018). Higher protein productivity would add to manufacturing flexibility by reducing the number of batches required to adapt to dynamic clinical and market demands.

1.2 Chinese Hamster Ovary Cell Lines

CHO cells were first isolated and immortalized in the late 1950s by Theodore Puck from an ovarian biopsy of *Cricetulus griseus* (Puck et al., 1958). Through extensive mutagenesis and cloning, variants of the original CHO cell line have been established for higher protein yield. An early development was the mutation of dihydrofolate reductase (DHFR) in the CHO-K1 subclone (Zhu et al., 2007). Because this essential enzyme is required for synthesis of purines and certain amino acids, transgenes such as mAb protein constructs could be stably introduced in these DHFR-deficient CHO-DXB11 cells upon co-transfection with the *dhfr* gene, as cells only survive when DHFR is recombinantly co-expressed (G Urlaub & Chasin, 1980; Wigler et al., 1980). Later, this technology was expanded to deleting both DHFR alleles, resulting in the CHO-DG44 cell line (G. Urlaub et al., 1983). Even greater selection pressure can be applied by exposing transfected cells to methotrexate (MTX), a DHFR inhibitor, effectively acting as a gene amplification system leading to higher copy numbers and antibody production (Tihanyi & Nyitray, 2020). The other widely-used selection system relies on a strategy initially considered in NS0 cell lines, knocking out glutamine synthetase (GS), which is again reintroduced alongside the gene of interest (Bebbington et al., 1992). GS is responsible for synthesizing glutamine from glutamate, so cells that do not express the exogenous selection marker copy of GS cannot grow in glutamine-free medium. Methionine sulfoximine (MSX), a GS inhibitor, can be used in CHO-GS knockout systems to improve selection stringency by eliminating background GS expression.

To efficiently generate the targeted biallelic elimination of these target genes, zinc-finger nucleases (ZFNs) have been used in recent years to cause a site-specific double-strand break. This technology exploits the mutagenic, error-prone nature of the non-homologous end joining-mediated DNA repair to achieve disruption and can even be employed in multi-gene knockouts (Liu et al., 2010).

The BMS-proprietary cell lines in this work all originate from a GS-/- host cell line created from the CHO-K1 lineage using ZFNs.

To produce our CHO clones, the host cell line is first transfected by electroporation with the target vectors containing the recombination protein, resulting in random integration of the expression plasmid. These cells are then pooled and plated as master wells (MW). The top master wells then undergo FACS sorting for single cell cloning, and these clones are cultured and screened for the best growth, productivity, genetic stability, and product quality matches, especially for attributes that affect potency and pharmacokinetics (Bolisetty et al., 2020). Combined with natural clonal variation, the unpredictable effects of random integration causes the selection process to be a typically 6-12 month effort that is highly intensive in time, labor, and capital (W. Yang et al., 2022).

In recent years, targeted integration (TI) has been gaining popularity. By integrating the plasmid into a preselected genomic site characterized to have high transcriptional activity and eliminating a source of clonal variability, more consistent phenotypes and expression levels can be attained. Integrating multiple copies of the plasmid at a genomic locus or integrating it at multiple "hotspots" has been shown to increase productivity (Carver et al., 2020; Sergeeva et al., 2020). While promising, this strategy needs further development before being used widely at the industrial scale, as there can be diminishing returns on multicopy integration at a single site and finding hotspots is still a challenge (W. Yang et al., 2022). Additionally, while greater consistency or predictability is beneficial for robustness in the screening process, the diversity in the random integration strategy provides opportunity for occasionally generating better clones than could be achieved with targeted integration. Thus, characterizing stable high producers from random integration, including their integration sites, is valuable in better understanding CHO cell

phenotypes and finding favorable landing pads (Dhiman et al., 2020; Stadermann et al., 2022). Because so many clones are generated for clone selection, most of the screening is performed using high-throughput methods at small scales, for example in microplates, conical tubes, or miniature bioreactors. Once a clone is selected, a cell bank is made and a process must be developed to optimize its cell culture for performance at bench, clinical, and eventually commercial scales.

1.3 Chinese Hamster Ovary Bioprocesses

At BMS, this process starts with thawing a vial from the bank into a shake flask containing growth media. The cells are grown in a shaking incubator and passaged every 3-4 days into successively larger volumes for several weeks. This seed train is then used to inoculate seed (*N*-2 and *N*-1) bioreactors, which can include WAVE rocking bioreactors and/or stirred-tank bioreactors. These seed bioreactors can be operated in a variety of modes, from batch to fed-batch to perfusion, often depending on facility fit. Batch mode, meaning the cells are allowed to grow with little intervention, is the simplest and usually achieves the lowest cell-density out of the three. Since it is desirable to keep the cells in a high-viability exponential growth phase so they grow well when seeded into the production stage, batch mode would likely only be operated to a maximum of around 10×10^6 to 15×10^6 cells/mL. In fed-batch, the culture is periodically supplemented with boluses of rich media to replenish nutrients that cells have taken up and can grow to at least 20×10^6 cells/mL. Perfusion, the most intensified mode, uses alternating tangential flow devices (ATFs) to retain cells but exchange the media to both remove waste metabolites and provide fresh nutrients and can achieve very high cell densities nearing 200×10^6 cells/mL. The *N*-1 seed bioreactor is used to inoculate the production (*N*) stage bioreactor, which again can be operated in different modes. For example, efforts are underway to develop various intensified processes. These intensified processes can include a hybrid form of perfusion called high productivity harvest in which

perfusion is used in the last few days of a fed-batch culture to maintain high viability and often increase product yield. Another option is steady-state perfusion which incorporates a cell bleed to keep the culture at a predetermined cell density and can usually achieve a more continuous product stream with longer culture duration with higher cell viability. Currently, fed-batch culture is the most commonly used bioprocess mode, usually lasting around two weeks (ideal for a regular manufacturing cadence) but the process period may vary based on product quality attributes that are impacted by duration, followed by harvest and downstream purification.

Many operating conditions can be tested and optimized, such as working volumes or other bioreactor parameters including agitation, pH control, dissolved oxygen setpoint, and feeding strategy (Yee et al., 2018). One of the most critical conditions that can affect culture performance is the formulation of basal and feed media. These media can sometimes be commercial products purchased off-the-shelf but are usually proprietary compositions developed over time using empirical data. Depending on the specific clone, even platform media engineered to support a wide range of clones from the parental cell line may need to be supplemented with amino acids that are depleted particularly quickly or other biological precursor molecules to enhance product yield or product quality.

Media improvement can be achieved based on performance in DoE studies and/or analytical assessment of spent media (cell culture supernatant) and the product itself. In addition to viable cell density (VCD), viability, cell size, pH, and dissolved oxygen levels, key metabolites are measured daily during the production stage to monitor culture health. Glucose and glutamine are the main carbon and nitrogen sources for CHO cells, and their metabolism leads to the release of waste byproducts lactate and ammonia. Via glutaminolysis, glutamine enters the TCA cycle in the form of a-ketoglutarate. If glutamine is not available as in CHO-GS systems, the cells will uptake

glutamate instead. The GS catalyzes ATP hydrolysis of glutamate and condensation with ammonia to produce glutamine (Zhang et al., 2006). Thus, in many CHO-GS cultures, glutamate consumption is seen to occur until enough glutamine has been produced, at which point glutamate may accumulate if it is being fed. Likewise, some amount of ammonia may also be consumed towards the early stage of a culture before it starts accumulating from glutamine metabolism.

As for glucose and lactate metabolism, often different phenotypes are observed over the course of a production run. During exponential growth, cells are usually in a glycolytic state, consuming glucose and producing lactate. After this initial stage, some cultures may exhibit a transition to a lactate-consuming culture. This lactate switch is generally regarded as desirable as it prevents the acidification of the medium which may result in base addition. Also, it has been associated with metabolic efficiency as glucose directed towards aerobic glycolysis, which produces two net moles of ATP per mole of glucose, decreases and flux towards oxidative phosphorylation, which results in a net of 36 moles of ATP per mole of glucose, increases. Cultures that do not exhibit the lactate switch are often lower productivity, and if "lactate runaway" occurs in which the lactate accumulates to toxic levels, viability of the culture may be negatively impacted. The mechanism of the switch is not fully understood, although a leading hypothesis identifies the redox state of the cell as a likely trigger (Hartley et al., 2018). Nevertheless, many approaches have been developed to control the lactate switch and an accompanying switch from growth to protein production. One approach is metabolic engineering focused on rational knockouts or overexpression of genes targeting pyruvate metabolism. At the process level, engineering approaches include dynamic feeding strategies limiting glucose to a minimum level that avoids complete depletion, replacing it with alternative energy sources such as galactose, adding copper, or implementing a pH or temperature shift (Hartley et al., 2018; Qian et al., 2011; S. Xu et al., 2016). However, though

these approaches can cause a lactate switch to occur, they may negatively impact other performance attributes such as glycosylation or charge variants. From a process development perspective, the initial selection of a clone with desirable metabolite trends in production is the most straightforward way to ensure a favorable lactate profile.

Taken together, these desirable metabolite trends are overall reflective of a high yield culture. Antibody yield or volumetric titer is a product of growth and qP (specific productivity), or how much target protein each individual cell produces over time. Many high producers can reach high cell densities during the exponential growth phase, quickly converting glucose to lactate in glycolysis independent of mitochondrial metabolism. These high producers can then shift resources towards the TCA cycle and oxidative phosphorylation, associated with a higher qP state (Templeton et al., 2013). These cells may have increased mitochondrial oxidative capacity compared to low producers, which may not be able to produce ATP as efficiently and consequently generate less of the energy needed for protein production (Zagari et al., 2013).

The first of these two factors, growth, has been extensively studied with the aim of increasing production stage VCDs. Cell engineering approaches have largely focused on cell death inhibition, for example by overexpression of Bcl-2 or c-Myc, anti-apoptotic proteins, or knocking out pro-apoptotic proteins such as Bax and Bak which can be activated by stress signals such as nutrient deprivation, ER stress, and heat (Ifandi & Al-Rubeai, 2003; Tang et al., 2022; Tey et al., 2000). Other cell engineering approaches target growth inhibitors and toxic metabolites, such as lactate, or more recently byproducts from branched chain amino acid catabolism (Mulukutla et al., 2019).

Media development can also significantly improve growth – the required balance of amino acids, lipids, vitamins, and key energy sources such as carbohydrates can vary from clone to clone and can often be optimized stoichiometrically by calculating experimental consumption rates. Salts,

growth factors and trace elements are also important in regulating cell proliferation, not to mention other non-nutritional components such as buffers and surfactants, resulting in complex formulations of several dozen medium components (Ritacco et al., 2018). Directly identifying specific growth issues related to metabolism and signaling pathways can streamline efforts to optimize these components by taking advantage of modern analytical technologies, for instance multiomics profiling or Process Analytical Technology (PAT) which supports real-time measurements and feedback loop control, to highly customize media to each specific cell line.

As mentioned earlier, perfusion can be effective in increasing cell growth if the media has been designed to support very high cell densities, which may require rebalancing components, removing unnecessary components, and adjusting osmolality. However, logistical challenges including large volumes of perfusion media and storage of perfusate without downstream processing that can support a continuous product stream have limited the application of this technology. Furthermore, there are also technical challenges such as product retention, membrane fouling, and high cell densities leading to debris in the supernatant which can often lead to column clogging and sieving, where product accumulates inside reactors instead of passing into the perfusate (Su et al., 2021). In internal experiments, we have found that we may be reaching the limitations of cell density with perfusion as column clogging occurs at VCDs higher than 200×10^6 cells/mL.

As ever higher cell densities become more difficult to attain, raising specific productivity may be a more promising avenue for increasing volumetric titers. Through the cell engineering and media optimization already discussed, qPs have increased significantly over the past two decades from ~10 pg/cell/day to as high as a reported 90 pg/cell/day (Wurm, 2004). While this figure is impressive, most industrial cell lines are not as productive, and the high end of typical benchmarking levels is in the range of 30-50 pg/cell/day with final titers of up to 10 g/L (Reinhart

et al., 2019). Out of the many studies performed to increase overall titer, few have attempted to isolate improvement in growth phenotypes, often the main source of titer increase, from any change in qP. Separating the two is difficult because cells that are very efficient at directing energy towards growth may be less efficient at protein production, and vice versa.

Decoupling cell growth and protein production is a strategy that could potentially improve both aspects by letting cells proliferate without any metabolic burden from the recombinant expression before switching over to antibody production. This switch may be induced using a constructed gene expression system combined with a proliferation control strategy (Donaldson et al., 2021). In these systems, cells are cultured to the desired cell density before halting growth and inducing expression of the recombinant protein with an inducer such as tetracycline, doxycycline, or cumate (Lam et al., 2017; Poulain et al., 2017).

However, current control methods for halting proliferation after cell density has reached the desired level often impact pathways other than cell growth. A commonly used method is inducing mild hypothermia by shifting the culture temperature from 36-37°C to 30-35°C, which can successfully arrest cell growth in the G1 phase. In some cases, temperature shifts can cause other off-target effects and reduce global protein translation, which may negatively impact productivity and product quality (Bedoya-López et al., 2016). Hyperosmolality also inhibits cell growth and has been shown to enhance qP (Pfizenmaier et al., 2015). However, this effect is inconsistent, the cellular response to osmotic stress can induce premature senescence and the formation of micronuclei, a marker of chromosome aberration (Romanova et al., 2021). Chemical techniques to induce cell cycle arrest include the addition of sodium butyrate or DMSO, which has been shown to lead to G1-phase accumulation and increased specific productivity but also triggers apoptosis in some cases, which may undermine the benefits (Kumar et al., 2007).

Another potential growth-related tradeoff to consider is between cell number and cell size. In the above studies, stressors used to limit cell growth and increase qP – hypothermia, cell cycle arrest, hyperosmolality – also showed correlations between higher qP and increased cell diameter. In recent study, stressing cells by limiting CO2 supply or oversupplying glucose also decreases cell growth and leads to cell enlargement and qP increase (Schellenberg et al., 2022). Even small increases in diameter can lead to increased capacity for protein synthesis, processing, and export machinery (Lloyd et al., 2000; Pan et al., 2017). Taken together, these studies show that cell growth, individual cell size, and qP are interconnected in a highly complex manner.

As a result, few bioprocess levers have been discovered to consistently enhance qP with minimal impact to cell growth such that overall titer is increased. A proteomic profiling attempted to reveal proteins that were reflective of a sustained productivity phenotype and found differential expression in four proteins involved in protein translation and folding as well as three involved in glucose metabolism (Meleady et al., 2011). Meta-analysis of publicly available transcriptomic datasets has identified potential engineering targets for increasing qP in cell cycle and lysosome pathways (Tamošaitis & Smales, 2018). Despite these and numerous other omics studies on CHO cells, so far most cell engineering efforts have focused on reducing growth inhibitory acting proteins (Jerabek et al., 2022). Engineering focused on increased qP may be less popular possibly because the underlying pathways behind protein productivity are intricate and less well-understood, and strategies that might work for one cell line/product combination may not work for others (Samoudi et al., 2021). So far, successful efforts have mostly targeted the secretory pathway, especially in the context of difficult-to-express genes (Cartwright et al., 2020; Pieper et al., 2017; Samy et al., 2020). While these improvements have potential, there are still questions about whether they can be demonstrated to be generally applicable, and the time and effort required to

test them compared to screening natural genetic variation means they have yet to be widely adopted throughout the industry.

Likewise, medium additives that reliably improve qP in industrial cell lines have been elusive due to the variability of CHO cell phenotypes. For example, valproic acid addition to three different CHO-DG44 cell lines all expressing different molecules showed cell-line specific results. With two cell lines, qP was increased enough to overcome slightly depressed growth to result in higher titer by up to 20%, but the third cell line showed no effect (W. C. Yang et al., 2014). An autophagy-inducing peptide (AIP) was shown to increase qP in fed-batch culture, leading to an overall titer increase of up to twofold (Braasch et al., 2021). Interestingly, addition of the AIP did show reduced peak VCD but increased culture viability. These changes were only shown in one cell line and more investigation would be needed to explore whether this additive is broadly efficacious. Even if the effects of qP-enhancing medium additives may not be applicable to every cell line, having a panel of potential additives to screen may be useful in process development.

1.3 Modeling CHO Cell Culture

As CHO cells are the workhorse of the biologics industry, there is much interest in modeling them to gain insight into cell metabolism and regulation and to systematically find targets for genetic or culture parameter improvements (Traustason et al., 2019). Model-based approaches can be data-driven, based on statistical correlations between input parameters and process outcomes, mechanism-driven, based on existing stoichiometric or kinetic understanding of cells, or a hybrid of the two (Sha et al., 2018). Data-driven models rely on empirical data to train models, and do not take into consideration biologically meaningful relationships between inputs and outputs. On the other hand, mechanistic models strive to translate biological knowledge into a functional system that can quantitatively describe cellular activities.

Over the past decades, many computational, mechanistic models have been developed for CHO cells (Ahn & Antoniewicz, 2011; Nicolae et al., 2014; Nolan & Lee, 2010; Torres et al., 2019). The sequencing of the CHO genome led to a draft genome-scale metabolic model containing all consensus biochemical reactions in CHO cells at the time, called iCHO1766 for the 1,766 included genes (Hefzi et al., 2016; Lewis et al., 2013; Xun Xu et al., 2011). Since then, researchers have augmented this consensus model for various purposes, such as adding the mammalian secretory pathway resulting in iCHO2048s or by a systematic gap-filling approach resulting in iCHO2101 (Fouladiha et al., 2020; Gutierrez et al., 2020). Models focused on quality attributes, such as glycosylation, have also been developed (Galleguillos et al., 2017; Spahn et al., 2016). These genome-scale or similar reconstructions use flux balance analysis (FBA). FBA uses linear programming, introducing objective functions such as cell growth to calculate intracellular fluxes in underdetermined systems where there are far more reactions than metabolites that can be measured and used as constraints. Some common software options to perform FBA include COBRA toolbox, Sybil, and OptFlux (Gelius-Dietrich et al., 2013; Heirendt et al., 2019; Rocha et al., 2010). Models using FBA have been used on industrial cell lines to compare metabolic signatures of high and low producers, suggest strategies for medium optimization, identify engineering targets, and improve feeding strategies for intensified processes (Brunner et al., 2021; Calmels, Arnoult, et al., 2019; Calmels, McCann, et al., 2019; Huang et al., 2020; Huang & Yoon, 2020).

Another approach to study metabolic networks has been to focus on smaller networks that can be determined or overdetermined, such as central metabolism. When the number of unknown intracellular fluxes is the same or less than the number of independent mass balance equations, metabolic flux analysis (MFA) can be used. MFA is often paired with ^{13}C stable isotope labeling

to track carbon distribution throughout the network (Sha et al., 2018). After mass spectrometry analysis of cell pellet samples, intracellular fluxes can be estimated from the mass isotopomer distributions (MIDs) and extracellular exchange fluxes using software such as Metran, INCA, or other models often developed in Matlab (Yoo et al., 2008; Young, 2014). This technique has been used with labeled glucose and GC-MS analysis to compare metabolism of CHO cells at growth and stationary phases, finding that the exponential phase is characterized by higher glycolytic and anaplerotic fluxes, while the stationary phase is characterized by reduced glycolysis and anaplerosis but higher oxidative pentose phosphate pathway flux (Ahn & Antoniewicz, 2011; Sengupta et al., 2011). That finding has been supported by numerous other labeling studies examining antibody production phenotypes in fed-batch cultures, although a lower qP despite comparable oxidative metabolism in perfusion mode has shown that this association may not tell the whole story about productivity (Templeton et al., 2013; Templeton, Smith, et al., 2017; Templeton, Xu, et al., 2017). The aforementioned lactate metabolic switch has also been studied using ^{13}C MFA, labeling glucose, pyruvate, glutamine, and asparagine to provide insight into the stoichiometric requirements of biosynthesis and mAb production (Dean & Reddy, 2013). This depth of knowledge can be useful in media development, as evidenced by a similar study with parallel labeling of glucose and glutamine showing successful reduction of ammonia via rebalancing of medium amino acid composition (McAtee Pereira et al., 2018).

While ^{13}C MFA is a powerful tool, it is important to keep in mind its limitations. The complexity of cell biology means that any rational interventions based on MFA results could potentially have off-target effects, especially because the models represent a very limited number of reactions (Sacco & Young, 2021). As with any model, outputs are highly dependent on inputs and assumptions. Both FBA and MFA typically rely on a pseudo-steady-state assumption (assuming

metabolic and isotopic steady state, respectively) as biological changes in reactors occur over the course of days, slow compared to the timescale of measurements (Karst et al., 2017). When looking for a snapshot to understand cell metabolism at a certain point in time, analyses using this assumption may be sufficient. Nolan and Lee used this assumption but incorporated kinetic rate expressions to obtain a hybrid dynamic flux balance analysis (dFBA) method of modeling to investigate and predict changes over time (Nolan & Lee, 2010, 2012). Dynamic metabolic flux analysis (DMFA) on time-series measurements has also been used to determine CHO cell fluxes at metabolic non-steady state (Leighty & Antoniewicz, 2011). These dynamic models have now been used to describe clonal variation and media changes (Ghorbaniaghdam et al., 2014; Robitaille et al., 2015).

Isotopic nonstationary ^{13}C MFA (Inst-^{13}CMFA) is used when isotopic steady state is not achieved, and current models include reaction reversibility as well as compartmentation separating mitochondrial and cytosolic pools (Nicolae et al., 2014). Compartmented CHO cell models were used to elucidate improvements in qP by a media additive, MTA, that increased flux into the pentose phosphate pathway after cell-cycle arrest and cell size increase, boosting NADPH supply, or by attenuation of the GS selection marker to reduce glutamine overflow (Sacco et al., 2022; Wijaya et al., 2021).

Other recent developments in dynamic modeling include incorporating elementary flux modes to represent the intracellular reaction network as fewer macroscopic reactions (Hagrot et al., 2019; Martínez et al., 2020; Zamorano et al., 2013). Hybrid approaches combining data-driven and mechanistic models are becoming more popular as well, taking advantage of both multivariate statistical analysis and *in silico* modeling (Hong et al., 2022; Popp et al., 2016). These hybrid models have been proposed as digital twins capable of real-time process control and online

optimization (Helgers et al., 2022; Park et al., 2021). This continued trend towards quantitative modeling and advanced process control strategies should help bring us closer to more reliable culture performance, consistent quality, and efficient biomanufacturing product production.

References

Ahn, W. S., & Antoniewicz, M. R. (2011). Metabolic flux analysis of CHO cells at growth and non-growth phases using isotopic tracers and mass spectrometry. *Metabolic Engineering, 13*(5), 598-609. doi:https://doi.org/10.1016/j.ymben.2011.07.002

Bebbington, C. R., Renner, G., Thomson, S., King, D., Abrams, D., & Yarranton, G. T. (1992). High-level expression of a recombinant antibody from myeloma cells using a glutamine synthetase gene as an amplifiable selectable marker. *Biotechnology (N Y), 10*(2), 169-175. doi:10.1038/nbt0292-169

Bedoya-López, A., Estrada, K., Sanchez-Flores, A., Ramírez, O. T., Altamirano, C., Segovia, L., . . . Valdez-Cruz, N. A. (2016). Effect of Temperature Downshift on the Transcriptomic Responses of Chinese Hamster Ovary Cells Using Recombinant Human Tissue Plasminogen Activator Production Culture. *PloS one, 11*(3), e0151529. doi:10.1371/journal.pone.0151529

Bolisetty, P., Tremml, G., Xu, S., & Khetan, A. (2020). Enabling speed to clinic for monoclonal antibody programs using a pool of clones for IND-enabling toxicity studies. *mAbs, 12*(1), 1763727. doi:10.1080/19420862.2020.1763727

Braasch, K., Kryworuchko, M., & Piret, J. M. (2021). Autophagy-inducing peptide increases CHO cell monoclonal antibody production in batch and fed-batch cultures. *Biotechnology and Bioengineering, 118*(5), 1876-1883. doi:https://doi.org/10.1002/bit.27703

Brunner, M., Kolb, K., Keitel, A., Stiefel, F., Wucherpfennig, T., Bechmann, J., . . . Schaub, J. (2021). Application of metabolic modeling for targeted optimization of high seeding density processes. *Biotechnology and Bioengineering, 118*(5), 1793-1804. doi:https://doi.org/10.1002/bit.27693

Calmels, C., Arnoult, S., Ben Yahia, B., Malphettes, L., & Andersen, M. R. (2019). Application of a genome-scale model in tandem with enzyme assays for identification of metabolic signatures of high and low CHO cell producers. *Metabolic Engineering Communications*, e00097. doi:https://doi.org/10.1016/j.mec.2019.e00097

Calmels, C., McCann, A., Malphettes, L., & Andersen, M. R. (2019). Application of a curated genome-scale metabolic model of CHO DG44 to an industrial fed-batch process. *Metabolic Engineering, 51*, 9-19. doi:https://doi.org/10.1016/j.ymben.2018.09.009

Cartwright, J. F., Arnall, C. L., Patel, Y. D., Barber, N. O. W., Lovelady, C. S., Rosignoli, G., . . . James, D. C. (2020). A platform for context-specific genetic engineering of recombinant protein production by CHO cells. *Journal of Biotechnology, 312*, 11-22. doi:https://doi.org/10.1016/j.jbiotec.2020.02.012

Carver, J., Ng, D., Zhou, M., Ko, P., Zhan, D., Yim, M., . . . Hu, Z. (2020). Maximizing antibody production in a targeted integration host by optimization of subunit gene dosage and position. *Biotechnol Prog, 36*(4), e2967. doi:https://doi.org/10.1002/btpr.2967

Chiu, M. L., Goulet, D. R., Teplyakov, A., & Gilliland, G. L. (2019). Antibody Structure and Function: The Basis for Engineering Therapeutics. *Antibodies (Basel), 8*(4). doi:10.3390/antib8040055

Cymer, F., Beck, H., Rohde, A., & Reusch, D. (2018). Therapeutic monoclonal antibody N-glycosylation – Structure, function and therapeutic potential. *Biologicals, 52*, 1-11. doi:https://doi.org/10.1016/j.biologicals.2017.11.001

Dean, J., & Reddy, P. (2013). Metabolic analysis of antibody producing CHO cells in fed-batch production. *Biotechnol Bioeng, 110*(6), 1735-1747. doi:10.1002/bit.24826

Dhiman, H., Campbell, M., Melcher, M., Smith, K. D., & Borth, N. (2020). Predicting favorable landing pads for targeted integrations in Chinese hamster ovary cell lines by learning stability characteristics from random transgene integrations. *Computational and Structural Biotechnology Journal, 18*, 3632-3648. doi:https://doi.org/10.1016/j.csbj.2020.11.008

Donaldson, J. S., Dale, M. P., & Rosser, S. J. (2021). Decoupling Growth and Protein Production in CHO Cells: A Targeted Approach. *Frontiers in Bioengineering and Biotechnology, 9*. doi:10.3389/fbioe.2021.658325

Fouladiha, H., Marashi, S.-A., Li, S., Vaziri, B., & Lewis, N. E. (2020). Systematically gap-filling the genome-scale model of CHO cells. *bioRxiv*, 2020.2001.2027.921296. doi:10.1101/2020.01.27.921296

Frank, G. T. (2018). Transformation of biomanufacturing by single-use systems and technology. *Current Opinion in Chemical Engineering, 22*, 62-70. doi:https://doi.org/10.1016/j.coche.2018.09.006

Galleguillos, S. N., Ruckerbauer, D., Gerstl, M. P., Borth, N., Hanscho, M., & Zanghellini, J. (2017). What can mathematical modelling say about CHO metabolism and protein glycosylation? *Computational and Structural Biotechnology Journal, 15*, 212-221. doi:https://doi.org/10.1016/j.csbj.2017.01.005

Gelius-Dietrich, G., Desouki, A. A., Fritzemeier, C. J., & Lercher, M. J. (2013). sybil – Efficient constraint-based modelling in R. *BMC systems biology, 7*(1), 125. doi:10.1186/1752-0509-7-125

Ghorbaniaghdam, A., Chen, J., Henry, O., & Jolicoeur, M. (2014). Analyzing clonal variation of monoclonal antibody-producing CHO cell lines using an in silico metabolomic platform. *PloS one, 9*(3), e90832. doi:10.1371/journal.pone.0090832

Gutierrez, J. M., Feizi, A., Li, S., Kallehauge, T. B., Hefzi, H., Grav, L. M., . . . Lewis, N. E. (2020). Genome-scale reconstructions of the mammalian secretory pathway predict metabolic costs and limitations of protein secretion. *Nature Communications, 11*(1), 68. doi:10.1038/s41467-019-13867-y

Hagrot, E., Oddsdóttir, H. Æ., Mäkinen, M., Forsgren, A., & Chotteau, V. (2019). Novel column generation-based optimization approach for poly-pathway kinetic model applied to CHO cell culture. *Metabolic Engineering Communications, 8*, e00083. doi:https://doi.org/10.1016/j.mec.2018.e00083

Hartley, F., Walker, T., Chung, V., & Morten, K. (2018). Mechanisms driving the lactate switch in Chinese hamster ovary cells. *Biotechnol Bioeng, 115*(8), 1890-1903. doi:10.1002/bit.26603

Hefzi, H., Ang, K. S., Hanscho, M., Bordbar, A., Ruckerbauer, D., Lakshmanan, M., . . . Lewis, N. E. (2016). A Consensus Genome-scale Reconstruction of Chinese Hamster Ovary Cell Metabolism. *Cell Systems, 3*(5), 434-443.e438. doi:https://doi.org/10.1016/j.cels.2016.10.020

Heirendt, L., Arreckx, S., Pfau, T., Mendoza, S. N., Richelle, A., Heinken, A., . . . Fleming, R. M. T. (2019). Creation and analysis of biochemical constraint-based models using the COBRA Toolbox v.3.0. *Nature Protocols, 14*(3), 639-702. doi:10.1038/s41596-018-0098-2

Helgers, H., Schmidt, A., & Strube, J. (2022). Towards Autonomous Process Control—Digital Twin for CHO Cell-Based Antibody Manufacturing Using a Dynamic Metabolic Model. *Processes, 10*(2), 316. Retrieved from https://www.mdpi.com/2227-9717/10/2/316

Hong, J. K., Choi, D.-H., Park, S.-Y., Silberberg, Y. R., Shozui, F., Nakamura, E., . . . Lee, D.-Y. (2022). Data-driven and model-guided systematic framework for media development in CHO cell culture. *Metabolic Engineering, 73*, 114-123. doi:https://doi.org/10.1016/j.ymben.2022.07.003

Hong, J. K., Lakshmanan, M., Goudar, C., & Lee, D.-Y. (2018). Towards next generation CHO cell line development and engineering by systems approaches. *Current Opinion in Chemical Engineering, 22*, 1-10. doi:https://doi.org/10.1016/j.coche.2018.08.002

Huang, Z., Xu, J., Yongky, A., Morris, C. S., Polanco, A. L., Reily, M., . . . Yoon, S. (2020). CHO cell productivity improvement by genome-scale modeling and pathway analysis: Application to feed supplements. *Biochemical Engineering Journal, 160*, 107638. doi:https://doi.org/10.1016/j.bej.2020.107638

Huang, Z., & Yoon, S. (2020). Identifying metabolic features and engineering targets for productivity improvement in CHO cells by integrated transcriptomics and genome-scale metabolic model. *Biochemical Engineering Journal, 159*, 107624. doi:https://doi.org/10.1016/j.bej.2020.107624

Ifandi, V., & Al-Rubeai, M. (2003). Stable transfection of CHO cells with the c-myc gene results in increased proliferation rates, reduces serum dependency, and induces anchorage independence. *Cytotechnology, 41*(1), 1-10. doi:10.1023/a:1024203518501

Jerabek, T., Keysberg, C., & Otte, K. (2022). The potential of emerging sub-omics technologies for CHO cell engineering. *Biotechnology Advances, 59*, 107978. doi:https://doi.org/10.1016/j.biotechadv.2022.107978

Karst, D. J., Steinhoff, R. F., Kopp, M. R. G., Soos, M., Zenobi, R., & Morbidelli, M. (2017). Isotope labeling to determine the dynamics of metabolic response in CHO cell perfusion bioreactors using MALDI-TOF-MS. *Biotechnol Prog, 33*(6), 1630-1639. doi:10.1002/btpr.2539

Kumar, N., Gammell, P., & Clynes, M. (2007). Proliferation control strategies to improve productivity and survival during CHO based production culture : A summary of recent methods employed and the effects of proliferation control in product secreting CHO cell lines. *Cytotechnology, 53*(1-3), 33-46. doi:10.1007/s10616-007-9047-6

Lam, C., Santell, L., Wilson, B., Yim, M., Louie, S., Tang, D., . . . Misaghi, S. (2017). Taming hyperactive hDNase I: Stable inducible expression of a hyperactive salt- and actin-resistant variant of human deoxyribonuclease I in CHO cells. *Biotechnol Prog, 33*(2), 523-533. doi:https://doi.org/10.1002/btpr.2439

Leighty, R. W., & Antoniewicz, M. R. (2011). Dynamic metabolic flux analysis (DMFA): A framework for determining fluxes at metabolic non-steady state. *Metabolic Engineering, 13*(6), 745-755. doi:https://doi.org/10.1016/j.ymben.2011.09.010

Lewis, N. E., Liu, X., Li, Y., Nagarajan, H., Yerganian, G., O'Brien, E., . . . Palsson, B. O. (2013). Genomic landscapes of Chinese hamster ovary cell lines as revealed by the Cricetulus griseus draft genome. *Nature Biotechnology, 31*(8), 759-765. doi:10.1038/nbt.2624

Liu, P.-Q., Chan, E. M., Cost, G. J., Zhang, L., Wang, J., Miller, J. C., . . . Gregory, P. D. (2010). Generation of a triple-gene knockout mammalian cell line using engineered zinc-finger nucleases. *Biotechnology and Bioengineering, 106*(1), 97-105. doi:https://doi.org/10.1002/bit.22654

Lloyd, D. R., Holmes, P., Jackson, L. P., Emery, A. N., & Al-Rubeai, M. (2000). Relationship between cell size, cell cycle and specific recombinant protein productivity. *Cytotechnology, 34*(1), 59-70. doi:10.1023/A:1008103730027

Lu, R.-M., Hwang, Y.-C., Liu, I. J., Lee, C.-C., Tsai, H.-Z., Li, H.-J., & Wu, H.-C. (2020). Development of therapeutic antibodies for the treatment of diseases. *Journal of Biomedical Science, 27*(1), 1. doi:10.1186/s12929-019-0592-z

Makurvet, F. D. (2021). Biologics vs. small molecules: Drug costs and patient access. *Medicine in Drug Discovery, 9*, 100075. doi:https://doi.org/10.1016/j.medidd.2020.100075

Martínez, J. A., Bulté, D. B., Contreras, M. A., Palomares, L. A., & Ramírez, O. T. (2020). Dynamic Modeling of CHO Cell Metabolism Using the Hybrid Cybernetic Approach With a Novel Elementary Mode Analysis Strategy. *Frontiers in Bioengineering and Biotechnology, 8*. doi:10.3389/fbioe.2020.00279

McAtee Pereira, A. G., Walther, J. L., Hollenbach, M., & Young, J. D. (2018). (13) C Flux Analysis Reveals that Rebalancing Medium Amino Acid Composition can Reduce Ammonia Production while Preserving Central Carbon Metabolism of CHO Cell Cultures. *Biotechnol J, 13*(10), e1700518. doi:10.1002/biot.201700518

Meleady, P., Doolan, P., Henry, M., Barron, N., Keenan, J., O'Sullivan, F., . . . Clynes, M. (2011). Sustained productivity in recombinant Chinese Hamster Ovary (CHO) cell lines:

proteome analysis of the molecular basis for a process-related phenotype. *BMC Biotechnology, 11*(1), 78. doi:10.1186/1472-6750-11-78

Mulukutla, B. C., Mitchell, J., Geoffroy, P., Harrington, C., Krishnan, M., Kalomeris, T., . . . Hiller, G. W. (2019). Metabolic engineering of Chinese hamster ovary cells towards reduced biosynthesis and accumulation of novel growth inhibitors in fed-batch cultures. *Metabolic Engineering, 54*, 54-68. doi:https://doi.org/10.1016/j.ymben.2019.03.001

Nicolae, A., Wahrheit, J., Bahnemann, J., Zeng, A.-P., & Heinzle, E. (2014). Non-stationary 13C metabolic flux analysis of Chinese hamster ovary cells in batch culture using extracellular labeling highlights metabolic reversibility and compartmentation. *BMC systems biology, 8*, 50-50. doi:10.1186/1752-0509-8-50

Nolan, R., & Lee, K. (2010). Dynamic model of CHO cell metabolism. *Metabolic Engineering, 13*, 108-124. doi:10.1016/j.ymben.2010.09.003

Nolan, R., & Lee, K. (2012). Dynamic model for CHO cell engineering. *J Biotechnol, 158*, 24-33. doi:10.1016/j.jbiotec.2012.01.009

Pan, X., Dalm, C., Wijffels, R. H., & Martens, D. E. (2017). Metabolic characterization of a CHO cell size increase phase in fed-batch cultures. *Appl Microbiol Biotechnol, 101*(22), 8101-8113. doi:10.1007/s00253-017-8531-y

Park, S.-Y., Park, C.-H., Choi, D.-H., Hong, J. K., & Lee, D.-Y. (2021). Bioprocess digital twins of mammalian cell culture for advanced biomanufacturing. *Current Opinion in Chemical Engineering, 33*, 100702. doi:https://doi.org/10.1016/j.coche.2021.100702

Pfizenmaier, J., Matuszczyk, J.-C., & Takors, R. (2015). Changes in intracellular ATP-content of CHO cells as response to hyperosmolality. *Biotechnol Prog, 31*(5), 1212-1216. doi:https://doi.org/10.1002/btpr.2143

Pieper, L. A., Strotbek, M., Wenger, T., Gamer, M., Olayioye, M. A., & Hausser, A. (2017). Secretory pathway optimization of CHO producer cells by co-engineering of the mitosRNA-1978 target genes CerS2 and Tbc1D20. *Metabolic Engineering, 40*, 69-79. doi:https://doi.org/10.1016/j.ymben.2017.01.003

Popp, O., Müller, D., Didzus, K., Paul, W., Lipsmeier, F., Kirchner, F., . . . Beaucamp, N. (2016). A hybrid approach identifies metabolic signatures of high-producers for chinese hamster ovary clone selection and process optimization. *Biotechnol Bioeng, 113*(9), 2005-2019. doi:10.1002/bit.25958

Poulain, A., Perret, S., Malenfant, F., Mullick, A., Massie, B., & Durocher, Y. (2017). Rapid protein production from stable CHO cell pools using plasmid vector and the cumate gene-switch. *Journal of Biotechnology, 255*, 16-27. doi:https://doi.org/10.1016/j.jbiotec.2017.06.009

Puck, T. T., Cieciura, S. J., & Robinson, A. (1958). Genetics of somatic mammalian cells. III. Long-term cultivation of euploid cells from human and animal subjects. *J Exp Med, 108*(6), 945-956. doi:10.1084/jem.108.6.945

Qian, Y., Khattak, S. F., Xing, Z., He, A., Kayne, P. S., Qian, N. X., . . . Li, Z. J. (2011). Cell culture and gene transcription effects of copper sulfate on Chinese hamster ovary cells. *Biotechnol Prog, 27*(4), 1190-1194. doi:10.1002/btpr.630

Reinhart, D., Damjanovic, L., Kaisermayer, C., Sommeregger, W., Gili, A., Gasselhuber, B., . . . Kunert, R. (2019). Bioprocessing of Recombinant CHO-K1, CHO-DG44, and CHO-S: CHO Expression Hosts Favor Either mAb Production or Biomass Synthesis. *Biotechnol J, 14*(3), 1700686. doi:https://doi.org/10.1002/biot.201700686

Ritacco, F. V., Wu, Y., & Khetan, A. (2018). Cell culture media for recombinant protein expression in Chinese hamster ovary (CHO) cells: History, key components, and optimization strategies. *Biotechnol Prog, 34*(6), 1407-1426. doi:https://doi.org/10.1002/btpr.2706

Robitaille, J., Chen, J., & Jolicoeur, M. (2015). A Single Dynamic Metabolic Model Can Describe mAb Producing CHO Cell Batch and Fed-Batch Cultures on Different Culture Media. *PloS one, 10*(9), e0136815-e0136815. doi:10.1371/journal.pone.0136815

Rocha, I., Maia, P., Evangelista, P., Vilaça, P., Soares, S., Pinto, J. P., . . . Rocha, M. (2010). OptFlux: an open-source software platform for in silico metabolic engineering. *BMC systems biology, 4*(1), 45. doi:10.1186/1752-0509-4-45

Romanova, N., Niemann, T., Greiner, J. F. W., Kaltschmidt, B., Kaltschmidt, C., & Noll, T. (2021). Hyperosmolality in CHO culture: Effects on cellular behavior and morphology. *Biotechnology and Bioengineering, 118*(6), 2348-2359. doi:https://doi.org/10.1002/bit.27747

Rozek, R. (2013). Economic Aspects of Small and Large Molecule Pharmaceutical Technologies. *Advances in Economics and Business, 1*, 258-269. doi:10.13189/aeb.2013.010303

Sacco, S. A., Tuckowski, A. M., Trenary, I., Kraft, L., Betenbaugh, M. J., Young, J. D., & Smith, K. D. (2022). Attenuation of glutamine synthetase selection marker improves product titer and reduces glutamine overflow in Chinese hamster ovary cells. *Biotechnology and Bioengineering, 119*(7), 1712-1727. doi:https://doi.org/10.1002/bit.28084

Sacco, S. A., & Young, J. D. (2021). 13C metabolic flux analysis in cell line and bioprocess development. *Current Opinion in Chemical Engineering, 34*, 100718. doi:https://doi.org/10.1016/j.coche.2021.100718

Samoudi, M., Masson, H. O., Kuo, C.-C., Robinson, C. M., & Lewis, N. E. (2021). From omics to cellular mechanisms in mammalian cell factory development. *Current Opinion in Chemical Engineering, 32*, 100688. doi:https://doi.org/10.1016/j.coche.2021.100688

Samy, A., Kaneyoshi, K., & Omasa, T. (2020). Improvement of Intracellular Traffic System by Overexpression of KDEL Receptor 1 in Antibody-Producing CHO Cells. *Biotechnol J, 15*(6), 1900352. doi:https://doi.org/10.1002/biot.201900352

Schellenberg, J., Nagraik, T., Wohlenberg, O. J., Ruhl, S., Bahnemann, J., Scheper, T., & Solle, D. (2022). Stress-induced increase of monoclonal antibody production in CHO cells. *Engineering in Life Sciences, 22*(5), 427-436. doi:https://doi.org/10.1002/elsc.202100062

Sengupta, N., Rose, S. T., & Morgan, J. A. (2011). Metabolic flux analysis of CHO cell metabolism in the late non-growth phase. *Biotechnol Bioeng, 108*(1), 82-92. doi:10.1002/bit.22890

Sergeeva, D., Lee, G. M., Nielsen, L. K., & Grav, L. M. (2020). Multicopy Targeted Integration for Accelerated Development of High-Producing Chinese Hamster Ovary Cells. *ACS Synthetic Biology, 9*(9), 2546-2561. doi:10.1021/acssynbio.0c00322

Sha, S., Huang, Z., Wang, Z., & Yoon, S. (2018). Mechanistic modeling and applications for CHO cell culture development and production. *Current Opinion in Chemical Engineering, 22*, 54-61. doi:https://doi.org/10.1016/j.coche.2018.08.010

Shrivastava, A., Joshi, S., Guttman, A., & Rathore, A. S. (2022). N-Glycosylation of monoclonal antibody therapeutics: A comprehensive review on significance and characterization. *Analytica Chimica Acta, 1209*, 339828. doi:https://doi.org/10.1016/j.aca.2022.339828

Spahn, P. N., Hansen, A. H., Hansen, H. G., Arnsdorf, J., Kildegaard, H. F., & Lewis, N. E. (2016). A Markov chain model for N-linked protein glycosylation – towards a low-parameter tool for model-driven glycoengineering. *Metabolic Engineering, 33*, 52-66. doi:https://doi.org/10.1016/j.ymben.2015.10.007

Stadermann, A., Gamer, M., Fieder, J., Lindner, B., Fehrmann, S., Schmidt, M., . . . Gorr, I. H. (2022). Structural analysis of random transgene integration in CHO manufacturing cell lines by targeted sequencing. *Biotechnology and Bioengineering, 119*(3), 868-880. doi:https://doi.org/10.1002/bit.28012

Su, Y., Wei, Z., Miao, Y., Sun, L., Shen, Y., Tang, Z., . . . Tian, J. (2021). Optimized process operations reduce product retention and column clogging in ATF-based perfusion cell cultures. *Appl Microbiol Biotechnol, 105*(24), 9125-9136. doi:10.1007/s00253-021-11662-8

Tamošaitis, L., & Smales, C. M. (2018). Meta-Analysis of Publicly Available Chinese Hamster Ovary (CHO) Cell Transcriptomic Datasets for Identifying Engineering Targets to Enhance Recombinant Protein Yields. *Biotechnol J, 13*(10), 1800066. doi:https://doi.org/10.1002/biot.201800066

Tang, D., Lam, C., Bauer, N., Auslaender, S., Snedecor, B., Laird, M. W., & Misaghi, S. (2022). Bax and Bak knockout apoptosis-resistant Chinese hamster ovary cell lines significantly improve culture viability and titer in intensified fed-batch culture process. *Biotechnol Prog, 38*(2), e3228. doi:https://doi.org/10.1002/btpr.3228

Templeton, N., Dean, J., Reddy, P., & Young, J. D. (2013). Peak antibody production is associated with increased oxidative metabolism in an industrially relevant fed-batch CHO cell culture. *Biotechnol Bioeng, 110*(7), 2013-2024. doi:10.1002/bit.24858

Templeton, N., Smith, K. D., McAtee-Pereira, A. G., Dorai, H., Betenbaugh, M. J., Lang, S. E., & Young, J. D. (2017). Application of (13)C flux analysis to identify high-productivity CHO metabolic phenotypes. *Metab Eng, 43*(Pt B), 218-225. doi:10.1016/j.ymben.2017.01.008

Templeton, N., Xu, S., Roush, D. J., & Chen, H. (2017). (13)C metabolic flux analysis identifies limitations to increasing specific productivity in fed-batch and perfusion. *Metab Eng, 44*, 126-133. doi:10.1016/j.ymben.2017.09.010

Tey, B. T., Singh, R. P., Piredda, L., Piacentini, M., & Al-Rubeai, M. (2000). Influence of bcl-2 on cell death during the cultivation of a Chinese hamster ovary cell line expressing a chimeric antibody. *Biotechnol Bioeng, 68*(1), 31-43. doi:10.1002/(sici)1097-0290(20000405)68:1<31::aid-bit4>3.0.co;2-l

Tihanyi, B., & Nyitray, L. (2020). Recent advances in CHO cell line development for recombinant protein production. *Drug Discovery Today: Technologies, 38*, 25-34. doi:https://doi.org/10.1016/j.ddtec.2021.02.003

Torres, M., Berrios, J., Rigual, Y., Latorre, Y., Vergara, M., Dickson, A. J., & Altamirano, C. (2019). Metabolic flux analysis during galactose and lactate co-consumption reveals enhanced energy metabolism in continuous CHO cell cultures. *Chemical Engineering Science, 205*, 201-211. doi:https://doi.org/10.1016/j.ces.2019.04.049

Traustason, B., Cheeks, M., & Dikicioglu, D. (2019). Computer-Aided Strategies for Determining the Amino Acid Composition of Medium for Chinese Hamster Ovary Cell-Based Biomanufacturing Platforms. *Int J Mol Sci, 20*(21). doi:10.3390/ijms20215464

Tsumoto, K., Isozaki, Y., Yagami, H., & Tomita, M. (2019). Future perspectives of therapeutic monoclonal antibodies. *Immunotherapy, 11*(2), 119-127. doi:10.2217/imt-2018-0130

Urlaub, G., & Chasin, L. A. (1980). Isolation of Chinese hamster cell mutants deficient in dihydrofolate reductase activity. *Proceedings of the National Academy of Sciences, 77*(7), 4216-4220. doi:doi:10.1073/pnas.77.7.4216

Urlaub, G., Käs, E., Carothers, A. M., & Chasin, L. A. (1983). Deletion of the diploid dihydrofolate reductase locus from cultured mammalian cells. *Cell, 33*(2), 405-412. doi:10.1016/0092-8674(83)90422-1

Wigler, M., Perucho, M., Kurtz, D., Dana, S., Pellicer, A., Axel, R., & Silverstein, S. (1980). Transformation of mammalian cells with an amplifiable dominant-acting gene. *Proceedings of the National Academy of Sciences, 77*(6), 3567-3570. doi:doi:10.1073/pnas.77.6.3567

Wijaya, A. W., Verhagen, N., Teleki, A., & Takors, R. (2021). Compartment-specific 13C metabolic flux analysis reveals boosted NADPH availability coinciding with increased cell-specific productivity for IgG1 producing CHO cells after MTA treatment. *Engineering in Life Sciences, 21*(12), 832-847. doi:https://doi.org/10.1002/elsc.202100057

Wurm, F. M. (2004). Production of recombinant protein therapeutics in cultivated mammalian cells. *Nature Biotechnology, 22*(11), 1393-1398. doi:10.1038/nbt1026

Xu, S., Hoshan, L., & Chen, H. (2016). Improving lactate metabolism in an intensified CHO culture process: productivity and product quality considerations. *Bioprocess and Biosystems Engineering, 39*(11), 1689-1702. doi:10.1007/s00449-016-1644-3

Xu, X., Huang, Y., Pan, H., Molden, R., Qiu, H., Daly, T. J., & Li, N. (2019). Quantitation and modeling of post-translational modifications in a therapeutic monoclonal antibody from single- and multiple-dose monkey pharmacokinetic studies using mass spectrometry. *PloS one, 14*(10), e0223899. doi:10.1371/journal.pone.0223899

Xu, X., Nagarajan, H., Lewis, N. E., Pan, S., Cai, Z., Liu, X., . . . Wang, J. (2011). The genomic sequence of the Chinese hamster ovary (CHO)-K1 cell line. *Nature Biotechnology, 29*(8), 735-741. doi:10.1038/nbt.1932

Yang, W., Zhang, J., Xiao, Y., Li, W., & Wang, T. (2022). Screening Strategies for High-Yield Chinese Hamster Ovary Cell Clones. *Frontiers in Bioengineering and Biotechnology, 10*. doi:10.3389/fbioe.2022.858478

Yang, W. C., Lu, J., Nguyen, N. B., Zhang, A., Healy, N. V., Kshirsagar, R., . . . Huang, Y.-M. (2014). Addition of Valproic Acid to CHO Cell Fed-Batch Cultures Improves Monoclonal Antibody Titers. *Molecular Biotechnology, 56*(5), 421-428. doi:10.1007/s12033-013-9725-x

Yee, J., Rehmann, M., Yao, G., Sowa, S., Aron, K., Tian, J., . . . Li, Z. J. (2018). Advances in process control strategies for mammalian fed-batch cultures. *Current Opinion in Chemical Engineering, 22*, 34-41. doi:10.1016/j.coche.2018.09.002

Yoo, H., Antoniewicz, M. R., Stephanopoulos, G., & Kelleher, J. K. (2008). Quantifying reductive carboxylation flux of glutamine to lipid in a brown adipocyte cell line. *J Biol Chem, 283*(30), 20621-20627. doi:10.1074/jbc.M706494200

Young, J. D. (2014). INCA: a computational platform for isotopically non-stationary metabolic flux analysis. *Bioinformatics, 30*(9), 1333-1335. doi:10.1093/bioinformatics/btu015

Zagari, F., Jordan, M., Stettler, M., Broly, H., & Wurm, F. M. (2013). Lactate metabolism shift in CHO cell culture: the role of mitochondrial oxidative activity. *New Biotechnology, 30*(2), 238-245. doi:https://doi.org/10.1016/j.nbt.2012.05.021

Zamorano, F., Vande Wouwer, A., Jungers, R. M., & Bastin, G. (2013). Dynamic metabolic models of CHO cell cultures through minimal sets of elementary flux modes. *J Biotechnol, 164*(3), 409-422. doi:10.1016/j.jbiotec.2012.05.005

Zhang, F., Sun, X., Yi, X., & Zhang, Y. (2006). Metabolic characteristics of recombinant Chinese hamster ovary cells expressing glutamine synthetase in presence and absence of glutamine. *Cytotechnology, 51*(1), 21-28. doi:10.1007/s10616-006-9010-y

Zhu, M. M., Mollet, M., & Hubert, R. S. (2007). Industrial Production of Therapeutic Proteins: Cell Lines, Cell Culture, and Purification. In J. A. Kent (Ed.), *Kent and Riegel's Handbook of Industrial Chemistry and Biotechnology* (pp. 1421-1448). Boston, MA: Springer US.

Chapter 2. A Metabolomics Approach to Increasing CHO Cell Productivity

2.1 Abstract

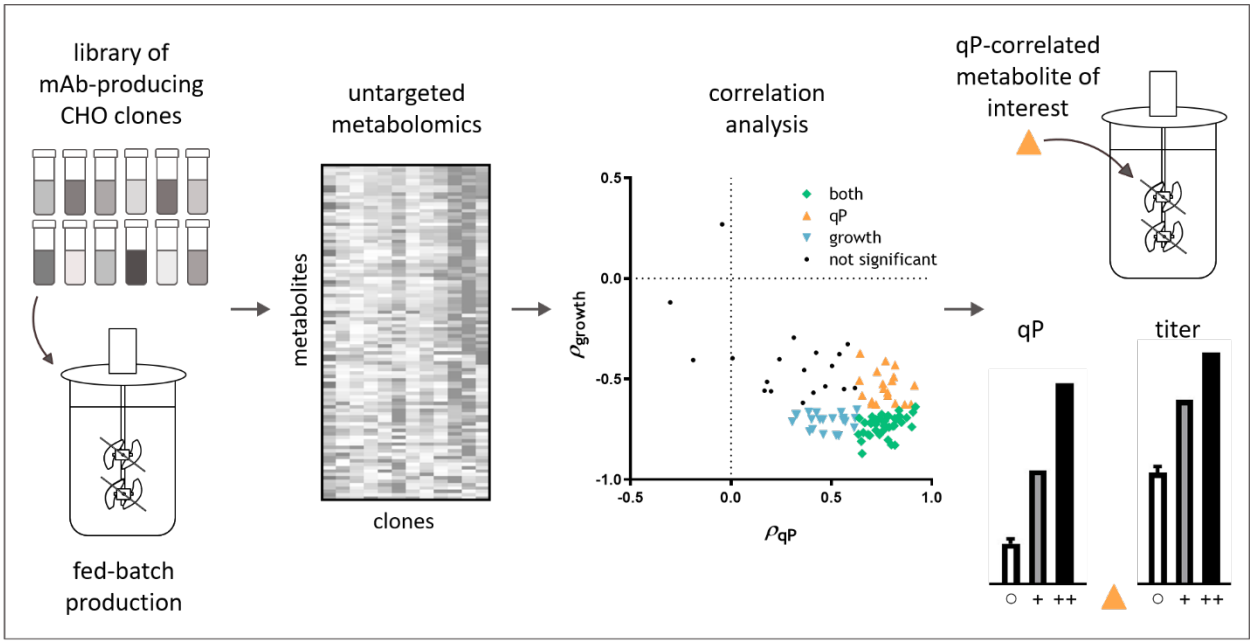

Much progress has been made in improving the viable cell density of bioreactor cultures in monoclonal antibody production from Chinese hamster ovary (CHO) cells; however, specific productivity (qP) has not been increased to the same degree. In this work, we analyzed a library of 24 antibody-expressing CHO cell clones to identify metabolites that positively associate with qP and could be used for clone selection or medium supplementation. An initial library of 12 clones, each producing one of two antibodies, was analyzed using untargeted LC-MS experiments. Metabolic model-based annotation followed by correlation analysis detected 73 metabolites that significantly correlated with growth, qP, or both. Of these, metabolites in the alanine, aspartate, and glutamate metabolism pathway, and the TCA cycle showed the strongest association with qP. To evaluate whether these metabolites could be used as indicators to identify clones with potential for high productivity, we performed targeted LC-MS experiments on a second library of 12 clones

expressing a third antibody. These experiments found that aspartate and cystine were positively correlated with qP, confirming the results from untargeted analysis. To investigate whether qP correlated metabolites reflected endogenous metabolic activity beneficial for productivity, several of these metabolites were tested as medium additives during cell culture. Medium supplementation with citrate improved qP by up to 490% and more than doubled the titer. Together, these studies demonstrate the potential for using metabolomics to discover novel metabolite additives that yield higher volumetric productivity in biologics production processes.

2.2 Introduction

Chinese hamster ovary (CHO) cells are widely used for manufacturing of biopharmaceutical proteins, especially monoclonal antibodies (mAbs). Maximizing upstream productivity allows for greater facility flexibility, smaller footprints, and lower costs for patients. Over recent decades, CHO cell culture processes have gradually improved in volumetric productivity to reach recombinant protein titers on the order of 10 g/L in fed-batch production (Handlogten et al., 2018; Y.-M. Huang et al., 2010; Takagi et al., 2017). Much of the titer increases seen in the past few years have been due to increased viable cell density (VCD) and sustained viability (Verhagen et al., 2020; Xu et al., 2020). In comparison, cell-specific productivity (qP) has improved to only a limited extent (Templeton, Xu, et al., 2017). As the biomanufacturing industry implements process intensification technologies such as perfusion cell culture in integrated continuous bioprocesses, CHO cell culture processes may soon approach the upper limits of achievable VCDs. This would constrain any further improvements to volumetric productivity. Therefore, there is an urgent need to identify efficient strategies for developing high-producing clones and optimizing media or process conditions not only for VCD but also qP.

To investigate cellular mechanisms leading to different productivity phenotypes in CHO cells, many omics approaches have been used, including transcriptomics and proteomics (Ang et al., 2019; Z. Huang & Yoon, 2020; Morris et al., 2020; Stolfa et al., 2018). Although challenges persist in metabolite identification, untargeted metabolomics has been increasingly adopted for characterizing the metabolic profiles of industrially relevant CHO cells cultured in bioreactors (W. P. Chong, Goh, et al., 2009; Mohmad-Saberi et al., 2013). Recent studies have used metabolomics experiments to identify metabolites associated with apoptosis, hypoxia and ROS generation, or growth inhibition (W. P. Chong et al., 2011; Gao et al., 2016; Mulukutla et al., 2017). Only a few

studies have examined cellular productivity (Morris et al., 2020). Notably, Chong et al. analyzed intracellular metabolites from several CHO cell clones showing high or low productivity and found that metabolites related to redox status regulation were elevated in high producers (W. P. Chong et al., 2012). Dean and Reddy compared metabolic fluxes between a low- and a high-productivity cell line using isotope labeling experiments, identifying differences in glycolysis, the TCA cycle, and lactate metabolism; Templeton et al. found similar differences among multiple low- and high-productivity cell lines (Dean & Reddy, 2013; Templeton, Smith, et al., 2017). Recently, Huang et al. used targeted metabolomics data in conjunction with a genome scale modeling approach to optimize media for enhanced qP (Z. Huang et al., 2020). Qian et al. also used targeted metabolomics to connect a decrease in qP over time to elevated lipid oxidation in unstable cell lines (Qian et al., 2020).

These studies have provided important clues linking CHO cell metabolism to qP. However, it remains an open question how metabolic differences drive qP differences and how cellular metabolism could be manipulated to improve qP. In this work, we analyze a library of clones with varying qP producing different mAbs to identify endogenous (CHO cell derived) metabolites that are positively associated with qP and could be used as productivity indicators or medium additives to improve clone selection and cell culture process development. Extracellular samples generated from an initial library of 12 clones with a wide range of qP were used for an untargeted LC-MS metabolomics study. Metabolic model guided annotation and correlation analysis identified a panel of metabolites significantly and specifically associated with qP. Targeted metabolomics experiments using a different set of 12 mAb producing clones confirmed the positive correlations between qP and amino acids identified by the untargeted study. Furthermore, supplementing the

culture medium with a qP-associated central carbon metabolite, citrate, significantly improved qP and final titer.

2.3 Results

2.3.1 Untargeted Metabolomics Identified Endogenous CHO Cell Metabolites That Correlate with qP but Not Growth

A set of 12 clones, six expressing mAb A and six expressing mAb B at industrially relevant titers on the g/L scale, was selected to represent a wide range of growth (Figure 1A), titer (Figure 1B) and productivity profiles (Figure 1C). All 12 clones were cultured in identically operated 5 L bioreactors using the same fed-batch platform process. Detailed qP profiles at different time points are shown in Figure S1A. For all clones, VCD peaked between days 6 and 8, with peak VCD ranging from about 18 to 39 × 10^6 cells/mL. Titer and qP were both the highest for clone A-5. Interestingly, although often higher growth can lead to higher volumetric productivity, clone B-6 displayed the lowest titer and the highest growth, indicating that growth and volumetric titer are not always positively correlated. Across the 12 clones, we detected a significant negative correlation was found between peak VCD and qP (Figure S1B).

A set of 12 clones, six expressing mAb A and six expressing mAb B at industrially relevant titers on the g/L scale, was selected to represent a wide range of growth (Figure 1A), titer (Figure 1B) and productivity profiles (Figure 1C). All 12 clones were cultured in identically operated 5 L bioreactors using the same fed-batch platform process. Detailed qP profiles at different time points are shown in Figure S1A. For all clones, VCD peaked between days 6 and 8, with peak VCD ranging from about 18 to 39 × 10^6 cells/mL. Titer and qP were both the highest for clone A-5. Interestingly, although often higher growth can lead to higher volumetric productivity, clone B-6 displayed the lowest titer and the highest growth, indicating that growth and volumetric titer are

not always positively correlated. Across the 12 clones, we detected a significant negative correlation was found between peak VCD and qP (Figure S1B).

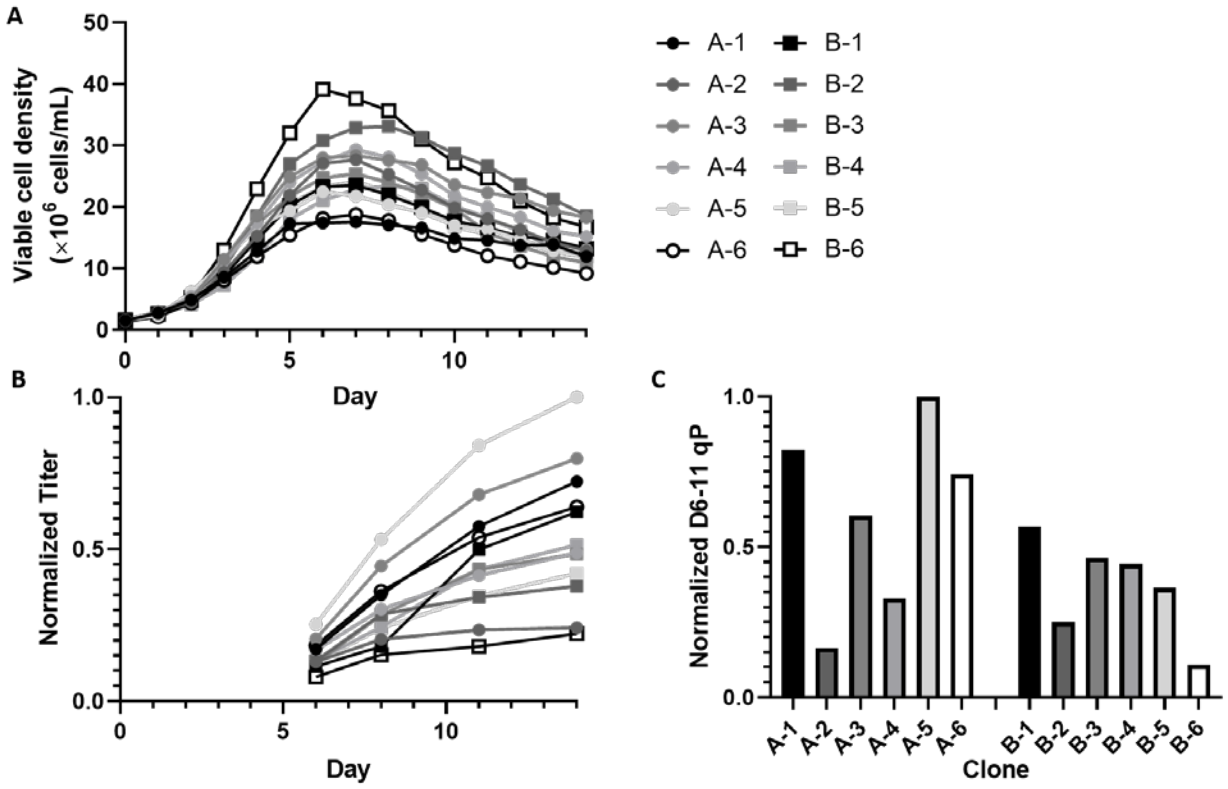

Figure 1. Growth and productivity profiles of 12 clones producing antibody A or B cultured in fed-batch bioreactors under identical process conditions. (**A**) Viable cell density (VCD) was recorded daily. (**B**) Titer was measured in samples collected on days 6, 8, 11, and 14. (**C**) Average qP from day 6 to 11 was calculated from integral VCD and titer.

To determine the clones' metabolite profiles, supernatant samples were collected on days 4 and 7, corresponding to mid-exponential and early stationary phases of the bioreactor cultures. Untargeted LC-MS analysis on the supernatant samples detected 4541 features between the four combinations of LC methods (HILIC or RP, see Materials and Methods) and MS modes (ESI positive or negative), including adducts and features that were detected by multiple methods.

Analysis of the features' accurate mass (*m/z*) and MS/MS spectra using a semi-automated annotation tool mapped 167 of these features to CHO cell metabolites (Alden et al., 2017). A subset of these metabolites was selected for testing against high purity chemical standards to verify the annotations (Figure S2).

Metabolite abundances, represented by extracted ion chromatogram peak areas (AUCs), were normalized to integral VCD to control for the clones' growth rate differences (Figure 2A). Out of the 167 annotated features, 70 features were duplicates detected in more than one analysis method and were eliminated from the correlation analysis as described in the methods section. The remaining 97 annotated and unique features were tested for significant correlations with cell growth or protein production. Pearson and Spearman rank correlation coefficients calculated between each metabolite and average qP or peak VCD gave similar results. Pearson coefficients are shown in Figure 2B and Table S3. There were no significant correlations for the mid-exponential phase (day 4) samples. Early stationary phase (day 7) measurements (normalized AUCs) were significantly correlated with qP, growth, or both for 73 of the 97 features. More than half of the 73 features reached at least level 2 identification (Table S4) based on minimum reporting standards of the Metabolomics Standards Initiative (MSI) (Sumner et al., 2007). Out of the 73 putatively identified and significantly correlated metabolites, about 25% are part of the basal or feed medium, indicating that most of the correlated metabolites result from endogenous metabolism of CHO cells. A delta analysis between day 4 and day 7 iVCD-normalized AUCs was performed to examine whether any cell-specific rates were correlated with qP or growth. In this analysis, 11 metabolites showed a significant positive correlation with qP, and 2 of these showed an additional significant negative correlation with growth. All 11 metabolites were also significant

in the day 7 correlation analysis. Notably, none of them were originally part of the feed or basal medium, indicating that their accumulation was not due to reduced net uptake.

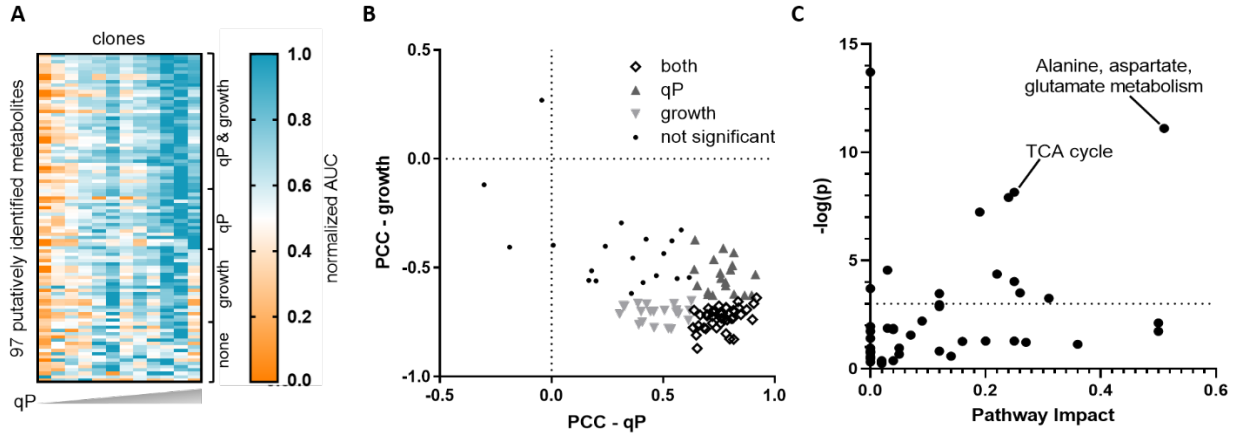

Figure 2. Significant correlations and pathways of extracellular metabolites from untargeted analysis. (**A**) Heatmap of integrated peak areas (AUCs). The AUC of a feature was first normalized to the corresponding sample's viable cell density (VCD), then scaled to the maximum value for the feature across all samples. Clones are ordered from low qP to high qP, while rows are grouped from the top in the following order: correlated with both qP and growth, correlated with qP, correlated with growth, and no significant correlations. (**B**) Scatter plot of Pearson correlation coefficients (PCC) showing significance of correlation for each metabolite with peak VCD (y-axis) and qP (x-axis). Significant correlations with qP (▲), growth (▼), or both (◊) are indicated if the PCC has a *p*-value less than 0.05. Metabolites without any significant correlations are shown by filled dots (●). (**C**) Enrichment (y-axis) and pathway impact (x-axis) analyses using Metaboanalyst were performed on metabolites significantly correlated with qP, including those also correlated with growth. Labels indicate the top four ranked pathways as determined by pathway impact scores from betweenness centrality and significance in pathway enrichment (dotted line represents $p < 0.05$ calculated by modified Fisher's exact test).

In general, metabolites significantly correlating with qP had positive associations (higher extracellular metabolite levels correlated with higher qP), while those significantly correlating with growth had negative associations (Figure 2B). Only three metabolites had negative correlations with qP, while one metabolite had a positive correlation with growth. None of these correlations were significant. This result is consistent with several earlier studies that have shown negative associations between growth and endogenous (CHO cell produced) metabolites accumulating in the culture medium (Pereira et al., 2018). Positive associations between qP and accumulated metabolites could reflect an inverse correlation of qP with growth, possibly due to the metabolic burden of recombinant protein biosynthesis (Altamirano et al., 2001). However, it is important to note that there are some metabolites, e.g., aspartate, that showed no correlation with growth but still positively correlated with qP.

Pathway impact and enrichment analysis on the set of metabolites correlated with qP, including those also correlated with growth, using Metaboanalyst showed that the two pathways with both high pathway impact and enrichment of the metabolites that have significant correlations with qP were the TCA cycle and alanine, aspartate, and glutamate metabolism had (Figure 2C) (J. Chong et al., 2018). Meanwhile, enriched pathways for metabolites that only correlated with growth were aminoacyl-tRNA biosynthesis and tyrosine metabolism (data not shown). The latter is consistent with a recent study reporting a beneficial impact of tyrosine on cell growth (Traustason, 2019).

2.3.2 Targeted Analysis Confirmed Aspartate and Cystine as qP Specific Metabolite Indicators

A fed-batch study with a new set of 12 clones producing a third mAb (molecule C) was performed in Ambr 15 bioreactors to investigate if significant metabolites identified by the untargeted analysis might serve as useful metabolic indicators of high-qP cell lines. Like the clones producing

molecules A and B, these clones exhibited a wide range of growth and productivity profiles (Figure S3).

Supernatant samples from day 7 were analyzed using targeted LC-MS experiments for 34 metabolites that were significantly and positively associated with peak VCD and/or qP in the untargeted analysis. The selection of metabolites was based on commercial availability of standards. The day 7 time point was selected to allow discovery of early indicators of qP and to avoid potentially confounding influences from nutrient starvation that may occur towards the end of a bioreactor run. The targeted analysis again found that aspartate was positively correlated with qP, confirming the association from the untargeted experiment (Figures 3A and 3C). In addition, cystine was tested, as it had a significant negative correlation with growth and a positive correlation with qP, although the latter correlation did not meet the significance threshold of FDR-controlled *p*-value less than 0.05. In the targeted analysis, cystine was found to be significantly and positively correlated with qP (Figure 3B and 3D). Aspartate and cystine were not significantly correlated with growth in the targeted analysis (Figure S4). This indicates that a positive correlation between these two metabolites and qP does not merely reflect the negative correlation between qP and growth.

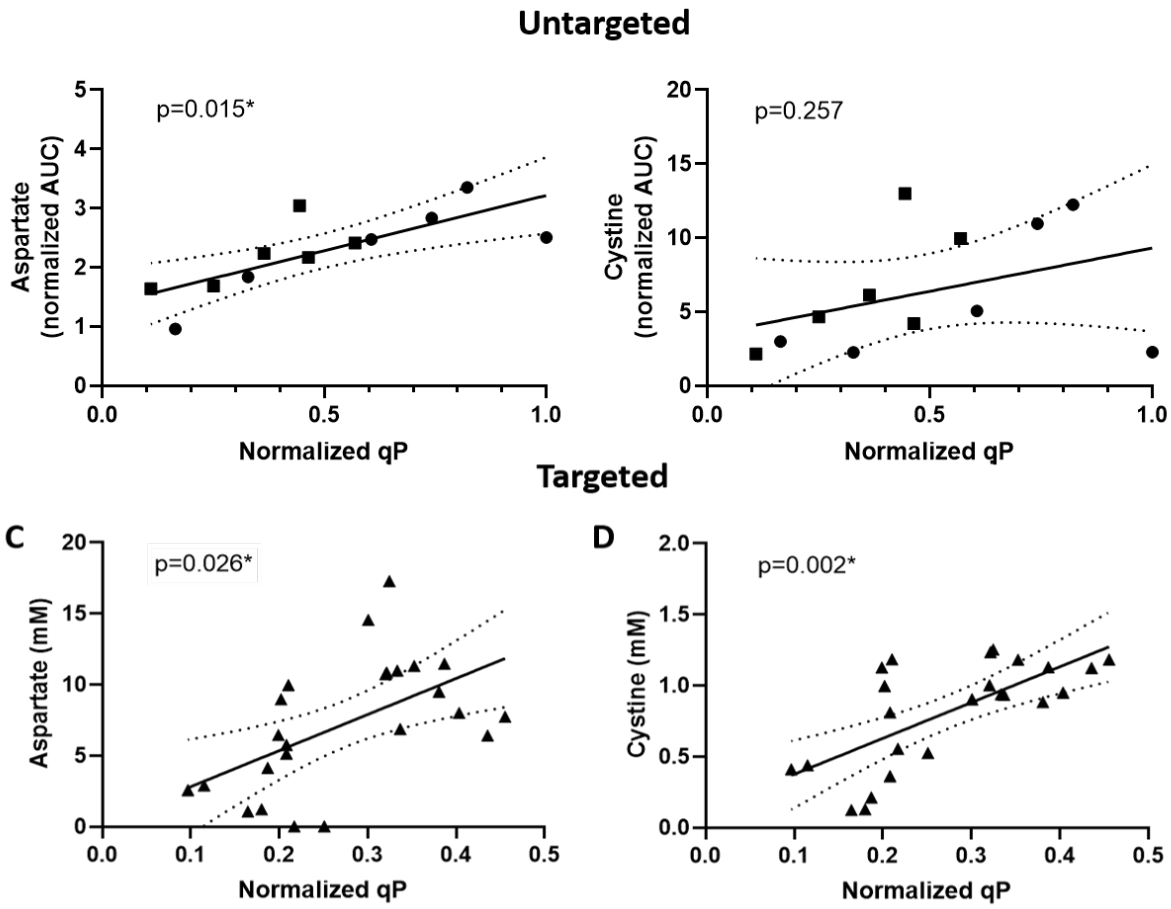

Figure 3. Correlations between day 7 metabolite levels and qP. Aspartate (left panels) and cystine (right panels) levels plotted against specific productivity (qP) for 12 clones expressing mAbs A (●) or B (■) cultured in 5 L bioreactors (**A** and **B**, individual bioreactors) or 12 clones expressing mAb C (▲) cultured in Ambr 250 bioreactors (**C** and **D**, duplicate bioreactors), with * indicating a p-value of <0.05. All qP values were normalized to the maximum qP among all 24 clones. For the untargeted experiment, metabolite levels shown are integrated areas under the curve (AUCs) from extracted ion chromatograms, normalized to VCD. Solid and dotted lines show, respectively, the ordinary least squares regression model and 95% confidence interval for the regression line.

2.3.3 Medium Supplementation with qP Correlated Metabolite Improved qP and Titer

We next investigated whether the metabolites that significantly correlated with qP could be used to improve qP and antibody titer. To this end, an addback study with a D-optimal design was performed with selected metabolites from the TCA cycle and from alanine, aspartate, and glutamate metabolism based on the observation that these two pathways were enriched in the set of metabolites positively correlated with qP (Figure 2C) (Goos & Jones, 2011). The selected metabolites were aspartate, glutamate, 4-aminobutanoate (GABA), and citrate. The lowest- and highest-qP clones expressing mAb A and mAb B were cultured in 50 mL conical tubes using a scaled down version of the fed-batch platform process. The selected metabolites were added to the cultures on day 3 at varying concentrations based on a D-optimal design (Table S2). By day 3, the cells have entered exponential growth, but have not begun antibody production. Day 3 was also early enough to detect potentially negative effects of metabolite supplementation on peak VCD as a proxy for overall growth.

Of the four metabolites tested, only citrate had a clear dose-dependent effect on qP (Figure 4 and S5). The low and medium concentrations of citrate improved qP in three of the four clones, but negatively impacted growth. The high concentration was detrimental to both growth and qP. In the low-qP clone A-2, the low dose of citrate had minimal impact on growth, while improving qP two-fold, resulting in a higher overall titer compared to the control without citrate supplementation.

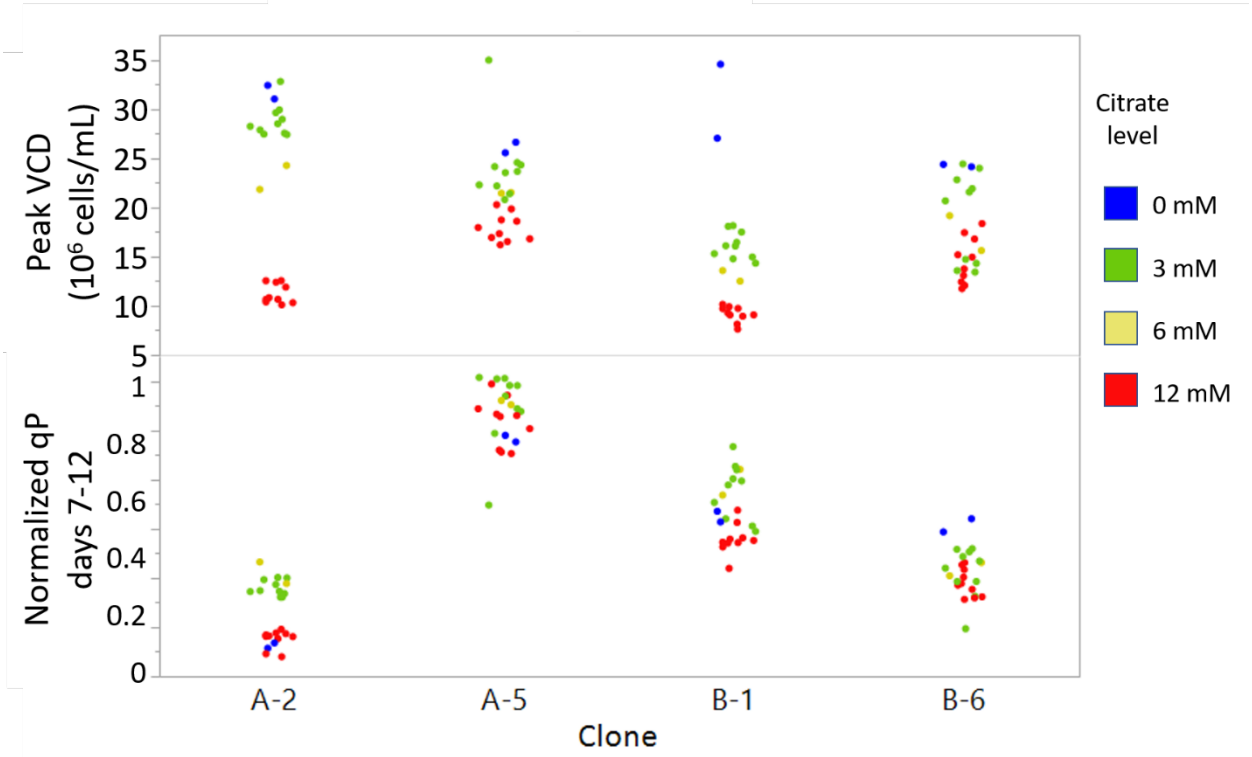

Figure 4. Effects of citrate addition on growth and productivity of selected clones with the highest (A-5, B-1) and lowest (A-2, B-6) qP for mAbs A and B. Citrate was added at 3 different levels as described in Table S2. Grouping of conditions with the same level of citrate indicate dose-dependent changes in both peak VCD and qP.

To determine if citrate addition could improve the qP of other clones and confirm that this effect also occurs under bioreactor conditions, a similar addback experiment was performed with a narrower concentration range using Ambr 250 cultures. Three of the clones expressed molecule A, and three expressed molecule B. In all clones, citrate supplemental reduced peak VCD in a dose-dependent manner (Figure S6). This effect was modest, however, with the highest concentration reducing peak VCDs by 10–35% compared to the controls. In five out of the six clones, citrate addition improved qP in a dose-dependent manner (Figure 5A). In four clones, the qP improvement outweighed the growth reduction, leading to an increase in overall volumetric

titer of 15–107% over the controls without citrate supplementation (Figure 5B). The qP and titer improvements were observed for both mAb A and mAb B producing clones. Dose-dependent changes in metabolite profiles were observed for the five clones showing a positive qP response to citrate addition, including increased accumulation of glutamine, glutamate, and lactate, and reduced accumulation of ammonium (Figure S6). Interestingly, clone A-1, which did not show a positive qP response to citrate addition, also did not show these metabolic responses.

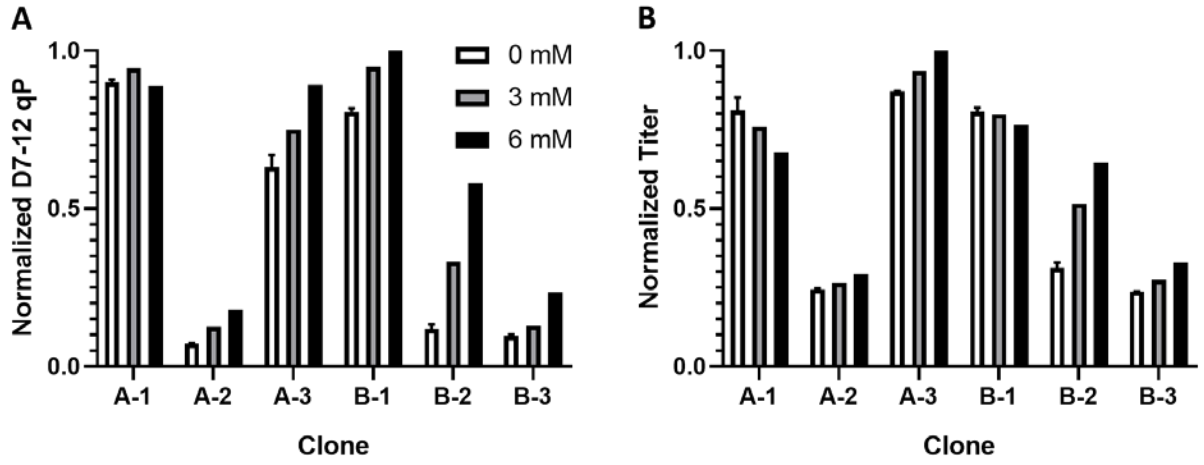

Figure 5. Responses of clones expressing mAb A (A-1 through A-3) or mAb B (B-1 through B-3) to addition of citrate to the culture medium. (**A**) Five out of six clones, each expressing one of two monoclonal antibodies (mAb A or mAb B, indicated by Clones A-1 through 3 and B-1 through 3), showed a dose-dependent increase in qP. (**B**) Four of the clones showed an overall increase in final volumetric titer. Data shown are normalized qP or titer scaled to the highest respective value across the six clones. Error bars show standard deviation across duplicate control cultures.

2.4 Discussion

In this work, a metabolomics approach was used to identify CHO cell metabolites that are associated with productivity, cell growth, or both, across multiple clones producing different

mAbs. These metabolites were also tested for their potential utility in cell culture process development either as a qP indicator or medium additive. These studies identified aspartic acid and cystine as potential clone-independent indicators of qP. The correlation between these metabolites and qP observed in one set of clones producing two different mAbs was validated in a distinct, second set of clones expressing a third mAb. Furthermore, this work showed citrate can function as a culture additive benefiting both qP and volumetric titer in multiple clones under production process conditions.

2.4.1 Tradeoff between Cell Growth and mAb Production

We observed that significant correlations between metabolites accumulating in the fed-batch cultures and growth were almost always negative, whereas correlations with qP were positive. The negative association between growth and metabolite levels observed in the present study is consistent with several previous studies that reported on growth-inhibitory effects of metabolic byproducts, including many of the TCA cycle metabolites, amino acids, and their derivatives reviewed by Pereira et al. (W. P. Chong et al., 2012; Pereira et al., 2018). Well-known examples of growth-inhibitory byproducts include ammonium and lactate, the accumulation of which has been consistently reported to have a negative impact on cell viability and growth (Freund & Croughan, 2018; Lao & Toth, 1997; Noh et al., 2017; Toussaint et al., 2016). Recently, it has been shown that reducing the accumulation of branched chain amino acid (BCAA) catabolites, either by decreasing concentrations of the amino acid precursor or by metabolic engineering of the cell line to limit BCAA transamination, can lead to better growth (Mulukutla et al., 2017; Mulukutla et al., 2019). Alden et al. found that a tryptophan metabolite, 5-hydroxyindole acetaldehyde, negatively correlated with growth, and that tryptophan addition led to growth inhibition (Alden et al., 2020). Although efforts in understanding growth impacts of byproducts can be used to improve

productivity, higher growth may not always lead to increased titers, as qP may be negatively affected by process modifications that favor growth over protein production.

Compared to cell growth, very little has been reported regarding the impact of accumulating metabolites on qP. Unlike cell proliferation, production of a mAb is not native to CHO cells and could place metabolic burdens on the cell that are not subject to endogenous regulatory mechanisms, i.e., the cell is not naturally programmed to achieve balanced mAb production. A reduction in qP could reflect a depletion of biosynthetic precursors or compromised cell viability. In principle, a depletion of carbon, nitrogen or energy resources needed for heterologous protein production could be mitigated by media supplementation or by engineering increased flux through pathways that supply the precursors. However, a reduction in qP due to compromised cell viability could be more complex to address. Collectively, the trends from the fed-batch studies referenced in the previous paragraph suggest declining viability in fed-batch systems is likely due to accumulation of harmful metabolites, rather than nutrient depletion. This is also supported by studies showing that cell density and productivity, as well as high viability, can be maintained for long periods of time in perfusion systems which continuously remove toxic byproducts (Bielser et al., 2018; Warikoo et al., 2012). Conversely, an increase in qP could indicate that more resources are directed towards protein production instead of cell growth and maintenance. Cell growth and heterologous protein production could require different balances of nutrients, and if the culture is operated the same way during both exponential and stationary phases of a fed-batch process, accumulation of metabolites may be seen.

In the present study, we show that almost all significant correlations between qP and metabolites detected in the culture medium are positive, in contrast to correlations between peak VCD and the metabolites. If a metabolite is accumulating in a culture, the cells are consuming less of it (if it is

in the feed or basal media), making an excess of it, or there is a bottleneck in the metabolite's use. This accumulation is more likely to happen when cells enter stationary phase, growth slows, and a larger share of metabolic resources (biosynthetic precursors and energy currency metabolites) is consumed for producing the non-native molecule (Martínez et al., 2013). Before this point, accumulation of metabolites may not differ significantly between low-qP and high-qP cultures. This is consistent with the results of our untargeted analysis on mid-exponential phase (day 4) samples. After the stationary phase begins (day 7), we see that the metabolic profile of cells that grew to a high cell density is different than the metabolic profile of cells that exhibit high qP.

The best-growing cells likely have a flux distribution optimized for growth with minimal overflow of central carbon metabolites. Meanwhile, accumulation of central carbon pathway intermediates may reflect a suboptimal flux distribution for growth but more capacity for a non-natural objective such as producing recombinant protein. This tradeoff could explain why only negative correlations were seen with growth and positive correlations with qP. Additionally, cell culture processes are generally optimized for titer rather than growth, with many processes even limiting proliferation in favor of producing antibody (Fussenegger et al., 1998; Kumar et al., 2007). The platform process used in these studies was indeed previously optimized for antibody expression in the parental cell line, which could be another reason most correlations with qP were positive.

2.4.2 Aspartic Acid and Cystine

Metabolites that correlate with qP across different clones independent of the clones' mAbs could be useful early indicators for selecting high-qP clones. Ideally, such indicators specifically predict qP and are independent of growth. In this work, day 7 aspartic acid and cystine levels in the culture medium were identified as potential indicators that had statistically significant correlations with qP of 24 clones expressing three different molecules. Furthermore, both metabolites showed no

correlation with growth in the targeted analysis. Extracellular metabolites are easily measured indicators that could be used to assess the culture at an early stage of protein production (e.g., day 7 of a 14-day process) to reduce timelines during multiple rounds of clone selection. The indicators could also reveal clones with high-qP potential that may not perform well in initial clone selection due to unoptimized platform culture conditions such as starvation towards the end of a process. Although both aspartic acid and cysteine were present in the basal and feed media used in the study, there were differences in the consumption rates of these amino acids between low-qP and high-qP clones.

A previous study reported that aspartate is produced by mammalian cells when the cells are grown in high glucose/glutamine conditions, whereas the amino acid is consumed by the cells in low glucose/glutamine conditions (Larson et al., 2002). In the presence of excess glucose, as was the case in the present work, aspartate production may have occurred as a byproduct of elevated glucose metabolism in the higher qP clones. Alternatively, the positive correlation between qP and aspartate could reflect the amino acid's involvement in the malate-aspartate shuttle (Eric L. Allen et al., 2016). Overexpression of an aspartate/glutamate carrier in the malate-aspartate shuttle has been shown to increase ATP production in CHO cells (Lasorsa et al., 2003). A high concentration of ATP could deactivate adenosine monophosphate kinase (AMPK) and modulate mTOR signaling, which has been found to promote qP (W. P. Chong, Sim, et al., 2009; Edros et al., 2014). The positive correlation of aspartate with qP could also be linked to increased oxidative phosphorylation, a phenotype associated with higher productivity phases and clones (Templeton, Smith, et al., 2017; Young, 2013).

Cystine was measured in the present study instead of free cysteine, which readily dimerizes to cystine in the presence of oxygen. The accumulation of cystine in high-qP clones could indicate a

more oxidized cell culture environment. Previous studies have reported that having sufficient cysteine in the medium supports high productivity (Ali et al., 2018). Cysteine is an important substrate for synthesis of antioxidants, including taurine and glutathione (GSH), which support high rates of oxidative phosphorylation associated with high-qP cells. A recent study found that a depletion of cysteine in CHO cell culture medium negatively impacted VCD, viability, and qP, and attributed these observations to redox imbalance, endoplasmic reticulum stress, and mitochondrial dysfunction (Ali et al., 2020). The accumulation we observed in high-qP cells could reflect the ability of these cells to supplement feed cysteine with endogenous production. We did not observe a significant trend with methionine, the other sulfur-containing amino acid, but the cells could be sourcing the sulfur by turning over proteins. Further studies, e.g., using isotopic tracers, are warranted to better understand the source of cystine in the medium, the mechanisms behind metabolite-qP correlations and to evaluate more broadly the use of the metabolites as biomarkers of qP.

2.4.3 Citrate Addition Improves qP and Titer

Addition of citrate to the medium on day 3 increased qP for multiple clones in a dose-dependent manner. In the untargeted experiment (Figure 2), citrate correlated positively with qP but negatively with growth. Previous studies have suggested that the accumulation of TCA cycle intermediates in the media may signal a bottleneck that is connected to growth limitation (Carinhas et al., 2013; Sellick et al., 2011; Sellick et al., 2015). In the present study, multiple clones showed a benefit to qP with citrate addition that overcame any impact on growth. One possible explanation for our finding is that metabolism in the clones benefiting from citrate addition has not yet reached a bottleneck, and the added citrate increased the amount of substrate available for the TCA cycle. Zhang et al. postulated this hypothesis in an earlier study which found that feeding various TCA

cycle intermediates led to titer increases (Zhang et al., 2020). Another study reported that feeding TCA cycle intermediates, including citrate, to CHO cells during stationary phase resulted in lower ammonium accumulation and higher glutamate and glutamine concentrations in the culture medium (Gilbert et al., 2013), consistent with findings in this study (Figure S6). These observations could be explained by additional conversion of citrate to α-ketoglutarate (aKG), which would reduce transamination of glutamate and production of ammonium, while increasing flux of glutamate to glutamine. Entry of additional citrate into the TCA cycle could also reduce the demand for cytosolic pyruvate, leaving more pyruvate available for reduction to lactate. This scenario is consistent with the lactate profiles observed in this work. However, current literature suggests that elevated pyruvate flux towards lactate indicates a less efficient metabolic state for antibody production (Alden et al., 2020; Templeton, Smith, et al., 2017). Further investigation into intracellular carbon fluxes may be able to resolve this difference.

An alternative explanation for citrate's effect on qP is that it promotes iron chelation. An earlier study reported that adding sodium citrate in combination with ferric sulfate increased qP (Bai et al., 2011). A future study comparing citrate with the effects of other iron-chelating compounds while examining ATP production in all phases of the cell culture could shed light on the mechanism by which productivity increased. Quality attributes including glycan distribution and charge variants should also be considered in future studies.

The titer improvement seen in this study from medium supplementation of a metabolite identified through untargeted metabolomics on a library of clones followed by correlation analysis shows that this approach has the potential to discover early indicators of qP and beneficial media additives. Although prior studies focused on byproducts that inhibit cell growth, this work sought to identify metabolites that can be added to improve process performance by increasing qP.

Additives such as citrate offer the advantage of flexibility, in that they are easy to introduce at any stage, including during clone selection to provide a better indication of a clone's potential performance. For example, when comparing clones B-2 and B-3 under the same platform process condition, differences in qP and volumetric titer appear to be negligible (Figure 4). However, with the addition of citrate, clone B-2 clearly outperforms B-3 with a 110% increase in final titer over the control condition without citrate. In comparison, other strategies for improving qP, such as genetic modifications or subcloning with higher levels of a selection agent require greater effort and time and have yielded only modest benefit to titer (Gupta et al., 2017; Lao & Toth, 1997; Wilkens & Gerdtzen, 2015). Furthermore, it is an open question if genetic modifications or a subcloning strategy effective for clones producing one mAb also apply to other clones producing a different mAb.

In conclusion, we demonstrate that high-qP associated extracellular metabolites identified by analyzing a library of multiple CHO cell clones producing different mAbs can be used to predict high-qP clones in another library. Through addback studies, we also show that a TCA cycle metabolite positively associated with qP can be used as a medium additive to improve both qP as well as final titer. To our knowledge, this is the first study to identify extracellular metabolites that specifically associate with qP across a large number of CHO cell clones and demonstrate their applications. The metabolomics approach presented here offers practical routes for identifying metabolites to improve clone selection and enhance overall productivity and titer.

2.5 Materials and Methods

2.5.1 Cell Lines

A total of 24 clones derived from a CHO GS KO parental cell line were used in these studies. The parental cell line has been described previously by Morris et al. (Morris et al., 2020). Six clones

expressing mAb A and six expressing mAb B were used for the initial fed-batch cell culture experiments to generate untargeted LC-MS data, and a subset of these 12 clones were used for addback experiments. Twelve other clones expressing mAb C were used for the targeted LC-MS experiment. All 24 clones were single-cell clones selected from multiple transfection pools to increase the likelihood of including diverse phenotypes with a wide range of growth and qP profiles.

2.5.2 Fed-Batch Cell Culture Experiments

Fed-batch experiments were performed on several platforms: 5 L bioreactors, 50 mL conical tubes, and 15 mL and 250 mL bioreactors (Ambr 15 and Ambr 250, Sartorius, Göttingen, Germany). The cells were grown using chemically defined BMS proprietary media. Temperature was maintained at 36.5 °C for all cultures. In bioreactors, dissolved oxygen was maintained above 40% using oxygen sparging and pH was maintained between 6.8–7.4 using sodium carbonate addition and carbon dioxide sparging. In addition to daily concentrated feed, boluses of glucose were supplemented starting on day 2 to maintain a concentration greater than 1 g/L. Cell suspension samples were taken daily over the course of 14 days to monitor growth using a Vi-Cell cell counter (Beckman Coulter, Brea, CA, USA). The daily samples were also analyzed for concentrations of lactate, ammonia, glutamate, and glutamine using a Cedex BioHT (Roche, Basel, Switzerland). Supernatants from the samples centrifuged at 1000× *g* for 5 min were analyzed by Protein-A HPLC for the antibody product.

2.5.3 Untargeted LC-MS

Supernatant samples collected on days 4 and 7 of the fed-batch experiments were diluted 1:10 with HPLC grade water and analyzed for metabolites using information-dependent acquisition (IDA) experiments performed on a quadrupole time-of flight (TOF) mass spectrometer (TripleTOF

5600+, AB Sciex, Framingham, MA, USA). Each sample was run four times with different combinations of chromatography methods and ionization modes (positive and negative). The chromatographic separation was performed with a binary pump HPLC system (1260 Infinity, Agilent, Santa Clara, CA, USA) using either a HILIC column (Phenomenex Luna NH2, Torrance, CA, USA) or a reverse-phase column (Phenomenex Synergi Hydro-RP, Torrance, CA, USA) as described previously (Alden et al., 2017). The gradient methods and mobile phases are described in Supplementary Methods. An example chromatogram can be found in Figure S7.

2.5.4 Feature Annotation

The LC-MS features were annotated with putative chemical identities based on accurate mass (*m/z*) and product ion (MS/MS) spectrum data. The details of the annotation procedure have been previously described (Alden et al., 2017). Briefly, the *m/z* value and MS/MS spectrum of each unique feature was analyzed using the following five annotation tools: Metfrag (Ruttkies et al., 2016), CFM-ID (F. Allen et al., 2015), NIST17 (NIST/EPA/NIH, 2017), Metlin (Tautenhahn et al., 2012), and HMDB (Wishart et al., 2013). For many features, these fives tools returned different annotations. To determine the most likely identity for a feature, we mapped each feature to one or more compounds in a model of CHO cell metabolism based on accurate mass and computed a score reflecting the confidence in the mapping. Some features were putatively identified as the same metabolite in multiple LC-MS methods. For example, tryptophan was detected in negative ionization mode paired with the Synergi column and positive mode with the HILIC column. In these cases, the putatively identified metabolite was represented by the feature responses (i.e., peak areas) from the LC-MS method that detected the highest dynamic range in peak areas across all samples.

2.5.5 Data Analysis

The peak area, representing the integrated area under the curve (AUC) of the extracted ion chromatogram, for each annotated feature was normalized to the integral viable cell density of the corresponding sample. These normalized AUCs were used in correlation analyses with peak VCD and qP calculated from early stationary phase (day 6 or 7, depending on experimental constraints) to mid-stationary phase (day 11 or 12). Before and after this period, respectively, the cells produce little antibody and show significant viability loss. All correlation analyses were performed only within experiments using data from the same timepoints. More detailed qP profiles are available in Figure S1. The qP was calculated using the following equation:

$$\text{Specific productivity } qP \left[\frac{pg}{day \cdot cell}\right] = \frac{titer_2 - titer_1}{iVCD_2 - iVCD_1}$$

Other equations for qP were also tested, including a simple titer/iVCD calculation, and all provided similar results.

Both Pearson and Spearman correlation coefficients were calculated to test for linear and nonlinear relationships in the data, respectively. The *p*-values were controlled for false discovery rate (FDR) using the Benjamini–Hochberg method (Benjamini & Hochberg, 1995). A p-value < 0.05 indicated a significantly correlated metabolite. Similar results were obtained using both correlations. For simplicity, the Pearson correlation coefficients are reported here. The same correlation analysis was also performed on the delta (difference) between day 7 measurements and day 4 measurements.

For pathway enrichment analysis, Metaboanalyst 4.0 was used, supported by the Mus musculus pathway library as the closest organism available [25]. Default selections were used for all other settings: the method for the over-representation analysis was the hypergeometric test, and the node importance measure for pathway topology analysis was relative betweenness centrality.

2.5.6 Targeted LC-MS

Multiple reaction monitoring (MRM) experiments were performed on a triple quadrupole mass spectrometer (6410, Agilent, Santa Clara, CA, USA) for targeted analysis of significantly correlating metabolites identified from the correlation analysis. High purity standards were used to optimize the following MRM parameters for each target analyte: ionization mode, precursor ion, fragmentor voltage for the precursor ion, product ion (i.e., MRM transition), and collision energy for the transition (Table S1). For sample analysis, supernatants were diluted 1:10 and the same HILIC method was used as in the untargeted experiments. The samples were then analyzed in MRM experiments using the optimized acquisition parameters. Example chromatograms can be found in Figure S8.

2.5.7 Addback Experiments

To determine the effects of significantly correlating metabolites on specific growth and productivity, addback experiments were carried out in 50 mL conical tubes and the Ambr 250. The fed-batch cell culture experiments were performed as described above, except that varying doses of selected compounds were added in bolus to the culture medium on day 3. Each compound was added from a stock solution in a low, medium, or high concentration according to a D-optimal design (Table S2). Control conditions used water addition to maintain the same volume as test conditions. Multiple concentrations were used to determine whether the cultures would exhibit a dose-dependent response in growth or protein production.

2.6 Acknowledgements

We would like to thank the process development analytics group at Bristol Myers Squibb for HPLC analysis of product titer.

References

Alden, N., Krishnan, S., Porokhin, V., Raju, R., McElearney, K., Gilbert, A., & Lee, K. (2017). Biologically Consistent Annotation of Metabolomics Data. *Analytical Chemistry, 89*(24), 13097-13104. doi:10.1021/acs.analchem.7b02162

Alden, N., Raju, R., McElearney, K., Lambropoulos, J., Kshirsagar, R., Gilbert, A., & Lee, K. (2020). Using Metabolomics to Identify Cell Line-Independent Indicators of Growth Inhibition for Chinese Hamster Ovary Cell-based Bioprocesses. *Metabolites, 10*(5), 199. doi:10.3390/metabo10050199

Ali, A. S., Chen, R., Raju, R., Kshirsagar, R., Gilbert, A., Zang, L., . . . Ivanov, A. R. (2020). Multi-Omics Reveals Impact of Cysteine Feed Concentration and Resulting Redox Imbalance on Cellular Energy Metabolism and Specific Productivity in CHO Cell Bioprocessing. *Biotechnol J, n/a*(n/a), 1900565. doi:10.1002/biot.201900565

Ali, A. S., Raju, R., Kshirsagar, R., Ivanov, A. R., Gilbert, A., Zang, L., & Karger, B. L. (2018). Multi-Omics Study on the Impact of Cysteine Feed Level on Cell Viability and mAb Production in a CHO Bioprocess. *Biotechnol J*, e1800352. doi:10.1002/biot.201800352

Allen, Eric L., Ulanet, Danielle B., Pirman, D., Mahoney, Christopher E., Coco, J., Si, Y., . . . Smolen, Gromoslaw A. (2016). Differential Aspartate Usage Identifies a Subset of Cancer Cells Particularly Dependent on OGDH. *Cell Reports, 17*(3), 876-890. doi:https://doi.org/10.1016/j.celrep.2016.09.052

Allen, F., Greiner, R., & Wishart, D. (2015). Competitive fragmentation modeling of ESI-MS/MS spectra for putative metabolite identification. *Metabolomics, 11*(1), 98-110. doi:10.1007/s11306-014-0676-4

Altamirano, C., Cairó, J. J., & Gòdia, F. (2001). Decoupling cell growth and product formation in Chinese hamster ovary cells through metabolic control. *Biotechnol Bioeng, 76*(4), 351-360. doi:10.1002/bit.10096

Ang, K. S., Hong, J., Lakshmanan, M., & Lee, D. Y. (2019). Toward Integrated Multi-omics Analysis for Improving CHO Cell Bioprocessing. In H. F. K. G.M. Lee, S.Y. Lee, J. Nielsen and G. Stephanopoulos (Ed.), *Cell Culture Engineering* (pp. 163-184).

Bai, Y., Wu, C., Zhao, J., Liu, Y. H., Ding, W., & Ling, W. L. (2011). Role of iron and sodium citrate in animal protein-free CHO cell culture medium on cell growth and monoclonal antibody production. *Biotechnol Prog, 27*(1), 209-219. doi:10.1002/btpr.513

Benjamini, Y., & Hochberg, Y. (1995). Controlling the False Discovery Rate: A Practical and Powerful Approach to Multiple Testing. *Journal of the Royal Statistical Society: Series B (Methodological), 57*(1), 289-300. doi:10.1111/j.2517-6161.1995.tb02031.x

Bielser, J.-M., Wolf, M., Souquet, J., Broly, H., & Morbidelli, M. (2018). Perfusion mammalian cell culture for recombinant protein manufacturing – A critical review. *Biotechnology Advances, 36*(4), 1328-1340. doi:https://doi.org/10.1016/j.biotechadv.2018.04.011

Carinhas, N., Duarte, T. M., Barreiro, L. C., Carrondo, M. J. T., Alves, P. M., & Teixeira, A. P. (2013). Metabolic signatures of GS-CHO cell clones associated with butyrate treatment and culture phase transition. *Biotechnology and Bioengineering, 110*(12), 3244-3257. doi:doi:10.1002/bit.24983

Chong, J., Soufan, O., Li, C., Caraus, I., Li, S., Bourque, G., . . . Xia, J. (2018). MetaboAnalyst 4.0: towards more transparent and integrative metabolomics analysis. *Nucleic Acids Res, 46*(W1), W486-w494. doi:10.1093/nar/gky310

Chong, W. P., Goh, L. T., Reddy, S. G., Yusufi, F. N., Lee, D. Y., Wong, N. S., . . . Ho, Y. S. (2009). Metabolomics profiling of extracellular metabolites in recombinant Chinese Hamster Ovary fed-batch culture. *Rapid Commun Mass Spectrom, 23*(23), 3763-3771. doi:10.1002/rcm.4328

Chong, W. P., Sim, L. C., Wong, K. T., & Yap, M. G. (2009). Enhanced IFNgamma production in adenosine-treated CHO cells: a mechanistic study. *Biotechnol Prog, 25*(3), 866-873. doi:10.1002/btpr.118

Chong, W. P., Thng, S. H., Hiu, A. P., Lee, D. Y., Chan, E. C., & Ho, Y. S. (2012). LC-MS-based metabolic characterization of high monoclonal antibody-producing Chinese hamster ovary cells. *Biotechnol Bioeng, 109*(12), 3103-3111. doi:10.1002/bit.24580

Chong, W. P., Yusufi, F. N., Lee, D. Y., Reddy, S. G., Wong, N. S., Heng, C. K., . . . Ho, Y. S. (2011). Metabolomics-based identification of apoptosis-inducing metabolites in recombinant fed-batch CHO culture media. *J Biotechnol, 151*(2), 218-224. doi:10.1016/j.jbiotec.2010.12.010

Dean, J., & Reddy, P. (2013). Metabolic analysis of antibody producing CHO cells in fed-batch production. *Biotechnol Bioeng, 110*(6), 1735-1747. doi:10.1002/bit.24826

Edros, R., McDonnell, S., & Al-Rubeai, M. (2014). The relationship between mTOR signalling pathway and recombinant antibody productivity in CHO cell lines. *BMC Biotechnology, 14*(1), 15. doi:10.1186/1472-6750-14-15

Freund, N. W., & Croughan, M. S. (2018). A Simple Method to Reduce both Lactic Acid and Ammonium Production in Industrial Animal Cell Culture. *Int J Mol Sci, 19*(2). doi:10.3390/ijms19020385

Fussenegger, M., Schlatter, S., Dätwyler, D., Mazur, X., & Bailey, J. E. (1998). Controlled proliferation by multigene metabolic engineering enhances the productivity of Chinese hamster ovary cells. *Nature Biotechnology, 16*(5), 468-472. doi:10.1038/nbt0598-468

Gao, Y., Ray, S., Dai, S., Ivanov, A. R., Abu-Absi, N. R., Lewis, A. M., . . . Karger, B. L. (2016). Combined metabolomics and proteomics reveals hypoxia as a cause of lower productivity on scale-up to a 5000-liter CHO bioprocess. *Biotechnol J, 11*(9), 1190-1200. doi:10.1002/biot.201600030

Gilbert, A., McElearney, K., Kshirsagar, R., Sinacore, M. S., & Ryll, T. (2013). Investigation of metabolic variability observed in extended fed batch cell culture. *Biotechnol Prog, 29*(6), 1519-1527. doi:10.1002/btpr.1787

Goos, P., & Jones, B. (2011). *Optimal design of experiments: a case study approach*: John Wiley & Sons.

Gupta, S. K., Srivastava, S. K., Sharma, A., Nalage, V. H. H., Salvi, D., Kushwaha, H., . . . Shukla, P. (2017). Metabolic engineering of CHO cells for the development of a robust protein production platform. *PloS one, 12*(8), e0181455-e0181455. doi:10.1371/journal.pone.0181455

Handlogten, M. W., Lee-O'Brien, A., Roy, G., Levitskaya, S. V., Venkat, R., Singh, S., & Ahuja, S. (2018). Intracellular response to process optimization and impact on productivity and product aggregates for a high-titer CHO cell process. *Biotechnology and Bioengineering, 115*(1), 126-138. doi:10.1002/bit.26460

Huang, Y.-M., Hu, W., Rustandi, E., Chang, K., Yusuf-Makagiansar, H., & Ryll, T. (2010). Maximizing productivity of CHO cell-based fed-batch culture using chemically defined

media conditions and typical manufacturing equipment. *Biotechnol Prog, 26*(5), 1400-1410. doi:10.1002/btpr.436

Huang, Z., Xu, J., Yongky, A., Morris, C. S., Polanco, A. L., Reily, M., . . . Yoon, S. (2020). CHO cell productivity improvement by genome-scale modeling and pathway analysis: Application to feed supplements. *Biochemical Engineering Journal, 160*, 107638. doi:https://doi.org/10.1016/j.bej.2020.107638

Huang, Z., & Yoon, S. (2020). Identifying metabolic features and engineering targets for productivity improvement in CHO cells by integrated transcriptomics and genome-scale metabolic model. *Biochemical Engineering Journal, 159*, 107624. doi:https://doi.org/10.1016/j.bej.2020.107624

Kumar, N., Gammell, P., & Clynes, M. (2007). Proliferation control strategies to improve productivity and survival during CHO based production culture : A summary of recent methods employed and the effects of proliferation control in product secreting CHO cell lines. *Cytotechnology, 53*(1-3), 33-46. doi:10.1007/s10616-007-9047-6

Lao, M.-S., & Toth, D. (1997). Effects of Ammonium and Lactate on Growth and Metabolism of a Recombinant Chinese Hamster Ovary Cell Culture. *Biotechnol Prog, 13*(5), 688-691. doi:10.1021/bp9602360

Larson, T. M., Gawlitzek, M., Evans, H., Albers, U., & Cacia, J. (2002). Chemometric evaluation of on-line high-pressure liquid chromatography in mammalian cell cultures: Analysis of amino acids and glucose. *Biotechnology and Bioengineering, 77*(5), 553-563. doi:10.1002/bit.10116

Lasorsa, F. M., Pinton, P., Palmieri, L., Fiermonte, G., Rizzuto, R., & Palmieri, F. (2003). Recombinant expression of the Ca(2+)-sensitive aspartate/glutamate carrier increases

mitochondrial ATP production in agonist-stimulated Chinese hamster ovary cells. *J Biol Chem, 278*(40), 38686-38692. doi:10.1074/jbc.M304988200

Martínez, V. S., Dietmair, S., Quek, L.-E., Hodson, M. P., Gray, P., & Nielsen, L. K. (2013). Flux balance analysis of CHO cells before and after a metabolic switch from lactate production to consumption. *Biotechnology and Bioengineering, 110*(2), 660-666. doi:10.1002/bit.24728

Mohmad-Saberi, S. E., Hashim, Y. Z., Mel, M., Amid, A., Ahmad-Raus, R., & Packeer-Mohamed, V. (2013). Metabolomics profiling of extracellular metabolites in CHO-K1 cells cultured in different types of growth media. *Cytotechnology, 65*(4), 577-586. doi:10.1007/s10616-012-9508-4

Morris, C., Polanco, A., Yongky, A., Xu, J., Zhuangrong, H., Zhao, J., . . . Yoon, S. (2020). Bigdata analytics identifies metabolic inhibitors and promoters for productivity improvement and optimization of monoclonal antibody (mAb) production process. *Bioresources and Bioprocessing, 7*. doi:10.1186/s40643-020-00318-6

Mulukutla, B. C., Kale, J., Kalomeris, T., Jacobs, M., & Hiller, G. W. (2017). Identification and control of novel growth inhibitors in fed-batch cultures of Chinese hamster ovary cells. *Biotechnol Bioeng, 114*(8), 1779-1790. doi:10.1002/bit.26313

Mulukutla, B. C., Mitchell, J., Geoffroy, P., Harrington, C., Krishnan, M., Kalomeris, T., . . . Hiller, G. W. (2019). Metabolic engineering of Chinese hamster ovary cells towards reduced biosynthesis and accumulation of novel growth inhibitors in fed-batch cultures. *Metabolic Engineering, 54*, 54-68. doi:https://doi.org/10.1016/j.ymben.2019.03.001

NIST/EPA/NIH. (2017). Mass Spectral Library NIST, Version 17. In (6 June 2017 ed.).

Noh, S. M., Park, J. H., Lim, M. S., Kim, J. W., & Lee, G. M. (2017). Reduction of ammonia and lactate through the coupling of glutamine synthetase selection and downregulation of lactate dehydrogenase-A in CHO cells. *Appl Microbiol Biotechnol, 101*(3), 1035-1045. doi:10.1007/s00253-016-7876-y

Pereira, S., Kildegaard, H. F., & Andersen, M. R. (2018). Impact of CHO Metabolism on Cell Growth and Protein Production: An Overview of Toxic and Inhibiting Metabolites and Nutrients. *Biotechnol J, 13*(3), e1700499. doi:10.1002/biot.201700499

Qian, Y., Sowa, S. W., Aron, K. L., Xu, P., Langsdorf, E., Warrack, B., . . . Li, Z. J. (2020). New insights into genetic instability of an industrial CHO cell line by orthogonal omics. *Biochemical Engineering Journal, 164*, 107799. doi:https://doi.org/10.1016/j.bej.2020.107799

Ruttkies, C., Schymanski, E. L., Wolf, S., Hollender, J., & Neumann, S. (2016). MetFrag relaunched: incorporating strategies beyond in silico fragmentation. *Journal of Cheminformatics, 8*(1), 3. doi:10.1186/s13321-016-0115-9

Sellick, C. A., Croxford, A. S., Maqsood, A. R., Stephens, G., Westerhoff, H. V., Goodacre, R., & Dickson, A. J. (2011). Metabolite profiling of recombinant CHO cells: Designing tailored feeding regimes that enhance recombinant antibody production. *Biotechnology and Bioengineering, 108*(12), 3025-3031. doi:10.1002/bit.23269

Sellick, C. A., Croxford, A. S., Maqsood, A. R., Stephens, G. M., Westerhoff, H. V., Goodacre, R., & Dickson, A. J. (2015). Metabolite profiling of CHO cells: Molecular reflections of bioprocessing effectiveness. *Biotechnol J, 10*(9), 1434-1445. doi:10.1002/biot.201400664

Stolfa, G., Smonskey, M. T., Boniface, R., Hachmann, A. B., Gulde, P., Joshi, A. D., . . . Campbell, A. (2018). CHO-Omics Review: The Impact of Current and Emerging

Technologies on Chinese Hamster Ovary Based Bioproduction. *Biotechnol J, 13*(3), e1700227. doi:10.1002/biot.201700227

Sumner, L. W., Amberg, A., Barrett, D., Beale, M. H., Beger, R., Daykin, C. A., . . . Viant, M. R. (2007). Proposed minimum reporting standards for chemical analysis Chemical Analysis Working Group (CAWG) Metabolomics Standards Initiative (MSI). *Metabolomics, 3*(3), 211-221. doi:10.1007/s11306-007-0082-2

Takagi, Y., Kikuchi, T., Wada, R., & Omasa, T. (2017). The enhancement of antibody concentration and achievement of high cell density CHO cell cultivation by adding nucleoside. *Cytotechnology, 69*(3), 511-521. doi:10.1007/s10616-017-0066-7

Tautenhahn, R., Cho, K., Uritboonthai, W., Zhu, Z., Patti, G. J., & Siuzdak, G. (2012). An accelerated workflow for untargeted metabolomics using the METLIN database. *Nat Biotechnol, 30*(9), 826-828. doi:10.1038/nbt.2348

Templeton, N., Smith, K. D., McAtee-Pereira, A. G., Dorai, H., Betenbaugh, M. J., Lang, S. E., & Young, J. D. (2017). Application of (13)C flux analysis to identify high-productivity CHO metabolic phenotypes. *Metab Eng, 43*(Pt B), 218-225. doi:10.1016/j.ymben.2017.01.008

Templeton, N., Xu, S., Roush, D. J., & Chen, H. (2017). (13)C metabolic flux analysis identifies limitations to increasing specific productivity in fed-batch and perfusion. *Metab Eng, 44*, 126-133. doi:10.1016/j.ymben.2017.09.010

Toussaint, C., Henry, O., & Durocher, Y. (2016). Metabolic engineering of CHO cells to alter lactate metabolism during fed-batch cultures. *Journal of Biotechnology, 217*, 122-131. doi:https://doi.org/10.1016/j.jbiotec.2015.11.010

Traustason, B. (2019). Amino Acid Requirements of the Chinese Hamster Ovary Cell Metabolism during Recombinant Protein Production. *bioRxiv*, 796490. doi:10.1101/796490

Verhagen, N., Teleki, A., Heinrich, C., Schilling, M., Unsöld, A., & Takors, R. (2020). S-adenosylmethionine and methylthioadenosine boost cellular productivities of antibody forming Chinese Hamster ovary cells. *Biotechnol Bioeng*. doi:10.1002/bit.27484

Warikoo, V., Godawat, R., Brower, K., Jain, S., Cummings, D., Simons, E., . . . Konstantinov, K. (2012). Integrated continuous production of recombinant therapeutic proteins. *Biotechnology and Bioengineering, 109*(12), 3018-3029. doi:https://doi.org/10.1002/bit.24584

Wilkens, C. A., & Gerdtzen, Z. P. (2015). Comparative metabolic analysis of CHO cell clones obtained through cell engineering, for IgG productivity, growth and cell longevity. *PloS one, 10*(3), e0119053-e0119053. doi:10.1371/journal.pone.0119053

Wishart, D. S., Jewison, T., Guo, A. C., Wilson, M., Knox, C., Liu, Y., . . . Scalbert, A. (2013). HMDB 3.0--The Human Metabolome Database in 2013. *Nucleic Acids Res, 41*(Database issue), D801-807. doi:10.1093/nar/gks1065

Xu, J., Rehmann, M. S., Xu, M., Zheng, S., Hill, C., He, Q., . . . Li, Z. J. (2020). Development of an intensified fed-batch production platform with doubled titers using N-1 perfusion seed for cell culture manufacturing. *Bioresources and Bioprocessing, 7*(1), 17. doi:10.1186/s40643-020-00304-y

Young, J. D. (2013). Metabolic flux rewiring in mammalian cell cultures. *Current opinion in biotechnology, 24*(6), 1108-1115. doi:10.1016/j.copbio.2013.04.016

Zhang, X., Jiang, R., Lin, H., & Xu, S. (2020). Feeding tricarboxylic acid cycle intermediates improves lactate consumption and antibody production in Chinese hamster ovary cell cultures. *Biotechnol Prog, n/a*(n/a), e2975. doi:10.1002/btpr.2975

2.7 Supplementary Information

LC-MS Methods

Untargeted analysis was performed as described in Alden et al., 2017. In brief, information-dependent acquisition (IDA) experiments were performed on a QTOF, consisting of a TOF MS survey scan and four dependent product ion (MS/MS) scans for the highest intensity unique masses in each scan. Fragmentation was triggered when precursor ion counts rose quickly over several scans, ensuring ions were selected near the top of their LC peaks.

Reverse phase (RP) chromatography method

- Column: Phenomenex Synergi Hydro-RP
  - Solvents:
    - A: 0.1% formic acid in water
    - B: 0.1% formic acid in methanol
  - Column temperature: 15°C
  - Flow rate: 0.2 mL/min
  - Ion source: Turbo spray (ESI)
  - Ion source Gas 1: 35
  - Ion source Gas 2: 45
  - Curtain Gas: 25
  - Temperature: 450C
  - IonSpray Voltage Floating: ±4500 V

Gradient:

Time (min)	%B
0-8	3
8-38	3 → 95
38-45	95
45-47	95 → 3
47-55	3

Hydrophilic interaction chromatography (HILIC) method

- Column: Phenomenex Luna NH2
- Solvents
  - A: 95:5 water:acetonitrile + 20mM ammonium acetate, pH to 9.45 using ammonium hydroxide
  - B: 100% acetonitrile
- Column temperature: 25°C
- Flow rate: 0.3 mL/min

Gradient:

Time (min)	%B
0-15	85 → 0
15-28	0
28-30	0 → 85
30-60	85

- Ion source: Turbo spray (ESI)
- Ion source Gas 1: 35
- Ion source Gas 2: 45
- Curtain Gas: 25
- Temperature: 450C
- IonSpray Voltage Floating: ±5500 V

For the QQQ targeted experiment, the HILIC method above was used with a modified gradient:

Gradient:

Time (min)	**%B**
0-15	85 → 0
15-20	0
20-25	0 → 85
25-30	85

Ion source: ESI
Source parameters
Gas temp: 350C
Gas flow: 11 l/min
Nebulizer: 50 psi
Capillary: Positive 4000V Negative 4500V

Table S1. MRM transitions and instrument parameters for targeted analysis

Compound Name	Mass	Precursor	Product	approx RT	CE	Frag	Polarity
4-aminobutanoate (GABA)	103.06	104.1	87.1	8.9	5	60	Positive
5-hydroxy-L-tryptophan	220.09	221.1	204.1	8.3	5	90	Positive
Adenosine	267.1	268.1	136.1	5.5	9	90	Positive
Biotin	244.09	245.1	227.1	9.7	5	90	Positive
Citrate	192.03	191	111.1	16.2	9	60	Negative
D-gluconic acid	196.16	195.2	75	11	17	90	Negative
D-glucuronate	194.04	193	73.1	11.6	9	90	Negative
Folate	441.14	440.1	310.9	17.3	21	147	Negative
Fumaric acid	116.01	115	71.1	16.1	5	60	Negative
Glycine	75.03	76	30.2	15	5	60	Positive
Guanine	151.05	152.1	135.1	7.1	17	120	Positive
Hypoxanthine	136.04	137	55.1	7.3	33	120	Positive
Inosine	268.08	269.1	137.1	5.2	5	60	Positive
L-2-aminoadipate	161.12	162.1	98.2	11.9	13	90	Positive
L-alanine	89.04	90.1	44.2	15	9	30	Positive
L-arginine	174.11	175.1	70.2	9.5	25	90	Positive
L-aspartate	133.04	132	88.1	11.7	9	60	Negative
L-cysteine	121.02	122	59.1	16	25	60	Positive
L-Cystine	240.02	239	120.1	11.9	5	60	Negative
L-Glutamate	147.05	148.1	84.1	11.7	13	60	Positive
L-histidine	155.07	156.1	110.1	9.1	9	90	Positive
L-isoleucine	131.1	132.1	86.2	6.6	5	60	Positive
L-leucine	131.1	132.1	86.2	6.6	5	60	Positive
L-lysine	146.1	147.1	84.2	10.2	13	90	Positive
L-methionine	149.05	148	47.1	7.4	9	60	Negative
L-Phenylalanine	165.08	166.1	120.1	7.1	9	60	Positive
L-proline	115.06	116.1	70.1	8	13	90	Positive
L-threonine	119.06	118	74.1	8.5	9	60	Negative
L-tryptophan	204.09	205.1	188.1	7.3	5	60	Positive
L-tyrosine	181.07	182.1	136.1	8.1	9	90	Positive
Methionine sulfoxide	165.04	166	74.1	8.9	9	90	Positive
S-malate	134.02	133	115.1	6.6	9	60	Negative
Succinate	118.03	117	73.1	15.5	9	60	Negative
Uridine	244.07	245.1	113	4.9	5	60	Positive

Table S2. Experimental design for add-back screening study

Exp. #	Clone	L-aspartic acid sodium salt monohydrate (mM)	γ-Aminobutyric acid (mM)	Sodium citrate (mM)	L-glutamic acid (mM)
1	B-6	0.72	20	3	0.76
2	B-1	0.72	5	3	0.76
3	B-6	0.18	5	12	0.19
4	B-1	0.72	20	12	0.19
5	A-5	0.36	10	6	0.38
6	A-5	0.72	5	3	0.76
7	B-1	0.36	10	6	0.38
8	B-1	0.18	20	3	0.18
9	A-2	0.72	5	12	0.76
10	A-2	0.72	5	3	0.76
11	A-2	0.36	10	6	0.38
12	B-6	0.18	5	3	0.76
13	B-1	0.72	20	12	0.19
14	B-6	0.72	5	12	0.76
15	A-2	0.72	20	12	0.19
16	A-5	0.36	10	6	0.38
17	A-5	0.72	20	3	0.76
18	A-2	0.18	20	12	0.76
19	A-5	0.72	5	3	0.19
20	A-2	0.72	20	12	0.19
21	B-6	0.72	20	12	0.76
22	A-2	0.72	5	3	0.76
23	A-2	0.36	10	6	0.38
24	A-2	0.18	5	12	0.19
25	A-2	0.72	20	3	0.76
26	B-6	0.18	5	3	0.76
27	B-6	0.36	10	6	0.38
28	B-1	0.72	5	3	0.76
29	B-1	0.18	5	12	0.19
30	B-6	0.72	5	3	0.19
31	A-2	0.72	5	12	0.76
32	A-5	0.18	5	12	0.19
33	B-1	0.72	20	3	0.76
34	B-1	0.72	20	12	0.76
35	B-1	0.18	20	12	0.76
36	B-6	0.18	20	3	0.19
37	B-6	0.18	20	3	0.19

Exp. #	Clone	L-aspartic acid sodium salt monohydrate (mM)	γ-Aminobutyric acid (mM)	Sodium citrate (mM)	L-glutamic acid (mM)
38	B-1	0.36	10	6	0.38
39	B-1	0.18	20	3	0.19
40	A-5	0.72	20	12	0.19
41	B-6	0.36	10	6	0.38
42	A-5	0.18	5	3	0.76
43	A-2	0.72	20	3	0.76
44	B-6	0.72	5	3	0.19
45	A-5	0.72	20	12	0.19
46	A-5	0.72	20	12	0.76
47	B-6	0.18	20	12	0.76
48	B-6	0.18	5	12	0.19
49	B-6	0.72	20	12	0.76
50	A-5	0.18	20	3	0.19
51	A-2	0.72	5	3	0.19
52	A-5	0.18	20	12	0.76
53	B-1	0.18	5	3	0.76
54	A-2	0.18	5	3	0.76
55	A-2	0.18	5	12	0.19
56	B-6	0.72	5	3	0.76
57	A-5	0.72	5	12	0.76
58	B-1	0.18	5	12	0.19
59	A-5	0.18	20	12	0.76
60	B-6	0.72	20	12	0.19
61	B-1	0.72	5	3	0.19
62	A-5	0.72	5	3	0.19
63	B-6	0.18	20	12	0.76
64	A-2	0.18	20	12	0.76
65	A-5	0.72	5	12	0.76
66	A-2	0.72	20	12	0.76
67	B-1	0.18	5	3	0.76
68	B-6	0.72	20	12	0.18
69	B-1	0.72	5	12	0.76
70	A-2	0.18	20	3	0.19
71	B-1	0.72	5	3	0.19
72	B-1	0.72	20	12	0.76
73	A-5	0.72	5	3	0.76
74	A-5	0.18	20	3	0.19
75	B-6	0.72	5	3	0.76
76	A-5	0.72	20	3	0.76

Exp. #	Clone	L-aspartic acid sodium salt monohydrate (mM)	γ-Aminobutyric acid (mM)	Sodium citrate (mM)	L-glutamic acid (mM)
77	A-2	0.72	20	12	0.76
78	A-2	0.18	20	3	0.19
79	B-1	0.72	5	12	0.76
80	B-1	0.72	20	3	0.76
81	A-5	0.72	20	12	0.76
82	A-2	0.72	5	3	0.19
83	A-5	0.18	5	3	0.76
84	A-2	0.18	5	3	0.76
85	A-5	0.18	5	12	0.19
86	B-6	0.72	5	12	0.76
87	B-6	0.72	20	3	0.76
88	B-1	0.18	20	12	0.76
89	B-1	0	0	0	0
90	B-1	0	0	0	0
91	A-2	0	0	0	0
92	A-2	0	0	0	0
93	B-6	0	0	0	0
94	B-6	0	0	0	0
95	A-5	0	0	0	0
96	A-5	0	0	0	0

A D-optimal design of 96 conditions was used to screen four metabolites for qP-enhancing potential.

Table S3. Pearson correlation coefficients between annotated metabolites and qP or growth.

	Correlation with qP		Correlation with growth	
Annotated metabolite	**Correlation coefficient**	**p-value**	**Correlation coefficient**	**p-value**
L-Glutamate 5-semialdehyde	0.817	0.008	-0.829	0.030
2-Oxobutanoate	0.799	0.010	-0.827	0.030
2-Hydroxy-dATP	0.901	0.002	-0.738	0.032
Biotin	0.875	0.004	-0.692	0.032
cis-Aconitate	0.815	0.008	-0.696	0.032
Citrate	0.822	0.008	-0.700	0.032
Biotin amide	0.813	0.008	-0.732	0.032
D-Glucuronate	0.806	0.009	-0.734	0.032
5-Hydroxyindoleacetaldehyde	0.787	0.011	-0.739	0.032
L-Formylkynurenine	0.782	0.011	-0.803	0.032
N-Acetyl-D-mannosamine	0.787	0.011	-0.740	0.032
N-Acetylneuraminate	0.772	0.013	-0.736	0.032
Adenosine	0.766	0.014	-0.708	0.032
L-Tryptophan	0.762	0.014	-0.732	0.032
L-Arginine	0.758	0.015	-0.756	0.032
5-Hydroxy-L-tryptophan	0.755	0.015	-0.707	0.032
alpha-D-Glucose	0.740	0.019	-0.776	0.032
Guanine	0.732	0.021	-0.702	0.032
7,8-Dihydroneopterin 3'-triphosphate	0.722	0.022	-0.700	0.032
Inosine	0.722	0.022	-0.724	0.032
L-Histidine	0.697	0.028	-0.721	0.032
L-Phenylalanine	0.697	0.028	-0.715	0.032
L-Isoleucine	0.691	0.029	-0.780	0.032
L-Methionine	0.683	0.031	-0.776	0.032
5-Acetylamino-6-formylamino-3-methyluracil	0.667	0.038	-0.717	0.032
L-methionine-S-oxide	0.658	0.041	-0.767	0.032
Sorbitol 6-phosphate	0.649	0.044	-0.810	0.032
Leukotriene C4	0.639	0.046	-0.695	0.032
Sucrose	0.635	0.048	-0.775	0.032
Glycine	0.839	0.007	-0.684	0.034
L-2-Aminoadipate	0.784	0.011	-0.684	0.034
Folate	0.781	0.011	-0.683	0.034
Dihydrobiopterin	0.751	0.016	-0.675	0.036
L-Glutamate	0.907	0.002	-0.665	0.038
Succinate	0.836	0.007	-0.656	0.041
5-Oxoproline	0.918	0.002	-0.638	0.049
4-Aminobutanoate	0.897	0.002	-0.626	0.053
Farnesylcysteine	0.865	0.005	-0.626	0.053

L-Alanine	0.722	0.022	-0.627	0.053
sn-Glycero-3-phospho-1-inositol	0.818	0.008	-0.621	0.054
5,10-Methenyltetrahydrofolate	0.700	0.027	-0.623	0.054
UDP-N-acetyl-alpha-D-glucosamine	0.701	0.027	-0.611	0.058
Uridine	0.780	0.011	-0.582	0.072
Glycolate	0.653	0.042	-0.582	0.072
(R)-Mevalonate	0.779	0.011	-0.567	0.079
L-Aspartate	0.760	0.015	-0.548	0.088
(R)-5-Phosphomevalonate	0.914	0.002	-0.531	0.097
Fumarate	0.756	0.015	-0.524	0.102
(S)-1-Pyrroline-5-carboxylate	0.802	0.009	-0.509	0.113
sn-Glycero-3-phosphoethanolamine	0.640	0.046	-0.507	0.113
D-Gluconic acid	0.810	0.009	-0.489	0.128
2-Hydroxy-dAMP	0.817	0.008	-0.430	0.182
(S)-Malate	0.770	0.013	-0.410	0.205
Hypoxanthine	0.643	0.045	-0.372	0.249
3-Cyano-L-alanine	0.618	0.056	-0.696	0.032
3-Aminopropanal	0.614	0.057	-0.741	0.032
2,5-Dioxopentanoate	0.569	0.085	-0.711	0.032
L-Proline	0.558	0.092	-0.704	0.032
L-Tyrosine	0.536	0.105	-0.782	0.032
D-Sorbitol	0.524	0.116	-0.780	0.032
L-Threonine	0.506	0.132	-0.696	0.032
1-(5-Phospho-D-ribosyl)-5-amino-4-imidazolecarboxylate	0.460	0.178	-0.775	0.032
L-Lysine	0.458	0.178	-0.701	0.032
L-Leucine	0.443	0.191	-0.702	0.032
Carboxyphosphamide	0.406	0.234	-0.750	0.032
S-Adenosyl-L-homocysteine	0.401	0.240	-0.700	0.032
4-Fumarylacetoacetate	0.391	0.252	-0.761	0.032
Dopamine	0.305	0.375	-0.713	0.032
L-Cysteine	0.327	0.344	-0.676	0.036
D-myo-Inositol 1,2-cyclic phosphate	0.322	0.351	-0.674	0.036
2-Aminobut-2-enoate	0.549	0.098	-0.665	0.038
5-Guanidino-2-oxopentanoate	0.426	0.211	-0.667	0.038
L-Cystine	0.387	0.257	-0.663	0.038
Dopaquinone	0.627	0.052	-0.652	0.042
Betaine	0.358	0.296	-0.618	0.055
Pterine	0.411	0.229	-0.568	0.079

6-Phospho-D-gluconate	0.200	0.575	-0.560	0.081
L-Glutamine	0.167	0.637	-0.558	0.082
L-Pipecolate	0.617	0.056	-0.545	0.089
Taurine	0.469	0.169	-0.536	0.094
L-Asparagine	0.180	0.613	-0.513	0.109
Guanidinoacetate	0.365	0.286	-0.455	0.158
5,10-Methylenetetrahydrofolate	0.503	0.134	-0.435	0.178
L-Serine	-0.188	0.598	-0.405	0.209
D-Glycerate	0.241	0.492	-0.401	0.213
(S)-3-Methyl-2-oxopentanoic acid	0.008	0.986	-0.396	0.218
1,2-Dibromoethane	0.540	0.103	-0.376	0.245
L-Cysteate	0.424	0.211	-0.368	0.252
3-Methoxy-4-hydroxyphenylglycolaldehyde	0.581	0.077	-0.326	0.314
3,4-Dihydroxymandelate	0.313	0.366	-0.293	0.368
1D-myo-Inositol 1,3,4,5,6-pentakisphosphate	-0.044	0.915	0.270	0.406
Alcophosphamide	-0.302	0.378	-0.119	0.717

Table S4. Metabolites reaching at least MSI level 2 identification.

dataSrc	mz	RT	ppm	Confirmed with standard	Annotation	Match Factor
HilNeg	74.02558	618.8435	11.40		Glycine	597
HilNeg	105.0188	759.329	4.68		Glyceric acid	917
HilNeg	114.0546	574.902	12.58	X	L-Proline	661
HilNeg	118.05	610.716	7.92		Threonine	668
HilNeg	145.0613	616.1975	3.70	X	L-Glutamine	947
HilNeg	164.0372	639.561	9.39	X	L-methionine S-Oxide	761
HilNeg	195.0502	800.8455	4.01		D-gluconic acid	782
HilNeg	239.016	853.677	2.12		L-Cystine	938
HilNeg	440.1362	1229.261	8.49	X	Folic acid	899
HilPos	77.02329	503.784	0.36		Glycolic acid	700
HilPos	106.0484	636.0098	13.71	X	Serine	876
HilPos	130.0864	673.7855	1.05		Pipecolic acid	729
HilPos	133.0606	631.9407	1.19	X	L-Asparagine	976
HilPos	137.0451	411.3256	5.14	X	Hypoxanthine	911
HilPos	152.0564	527.1319	1.81		Guanine	523
HilPos	156.0764	646.861	2.24	X	L-Histidine	926
HilPos	175.1187	636.9453	1.52		L-Arginine	990
HilPos	176.0728	582.9782	12.74		5-hydroxyindoleacetaldehyde	*
HilPos	221.0889	519.4064	14.41		5-hydroxy-l-tryptophan	684
SynNeg	88.04049	881.1325	1.02	X	L-alanine	587
SynNeg	101.0244	920.672	0.02	X	2-oxobutanoate	659
SynNeg	112.0399	1289.605	5.04		(S)-1-Pyrroline-5-carboxylate	504
SynNeg	115.003	882.8115	5.77		Fumaric acid	582
SynNeg	117.019	2587.291	3.00	X	Succinate	887

SynNeg	132.03	883.0335	1.89	X	L-aspartic acid	988
SynNeg	133.0136	1382.16	4.67	X	Malic acid	987
SynNeg	145.0975	717.552	4.88	X	L-Lysine	719
SynNeg	146.0455	910.85	2.49	X	L-Glutamic acid	752
SynNeg	148.0433	1443.241	3.48	X	L-Methionine	636
SynNeg	160.0607	1154.211	5.31	X	L-2-aminoadipic acid	806
SynNeg	162.0414	2615.492	4.31		Pterine	798
SynNeg	164.0717	2816.974	0.18	X	L-phenylalanine	903
SynNeg	173.0082	2452.754	5.06		cis-aconitic acid	572
SynNeg	180.0666	2490.638	0.33	X	L-tyrosine	922
SynNeg	191.0193	2453.592	2.28	X	Citric acid	970
SynNeg	193.0348	928.936	2.80		D-glucuronic acid	965
SynNeg	203.0826	2984.451	0.06	X	L-tryptophan	962
SynNeg	346.0572	2337.519	3.92		Adenosine monophosphate	815
SynPos	115.0496	2885.132	5.10		3-Cyano-L-alanine	483
SynPos	245.092	3140.981	13.97	X	Biotin	905

*No score but see Alden et al, *Metabolites* 2020, *10*(5), 199; https://doi.org/10.3390/metabo10050199

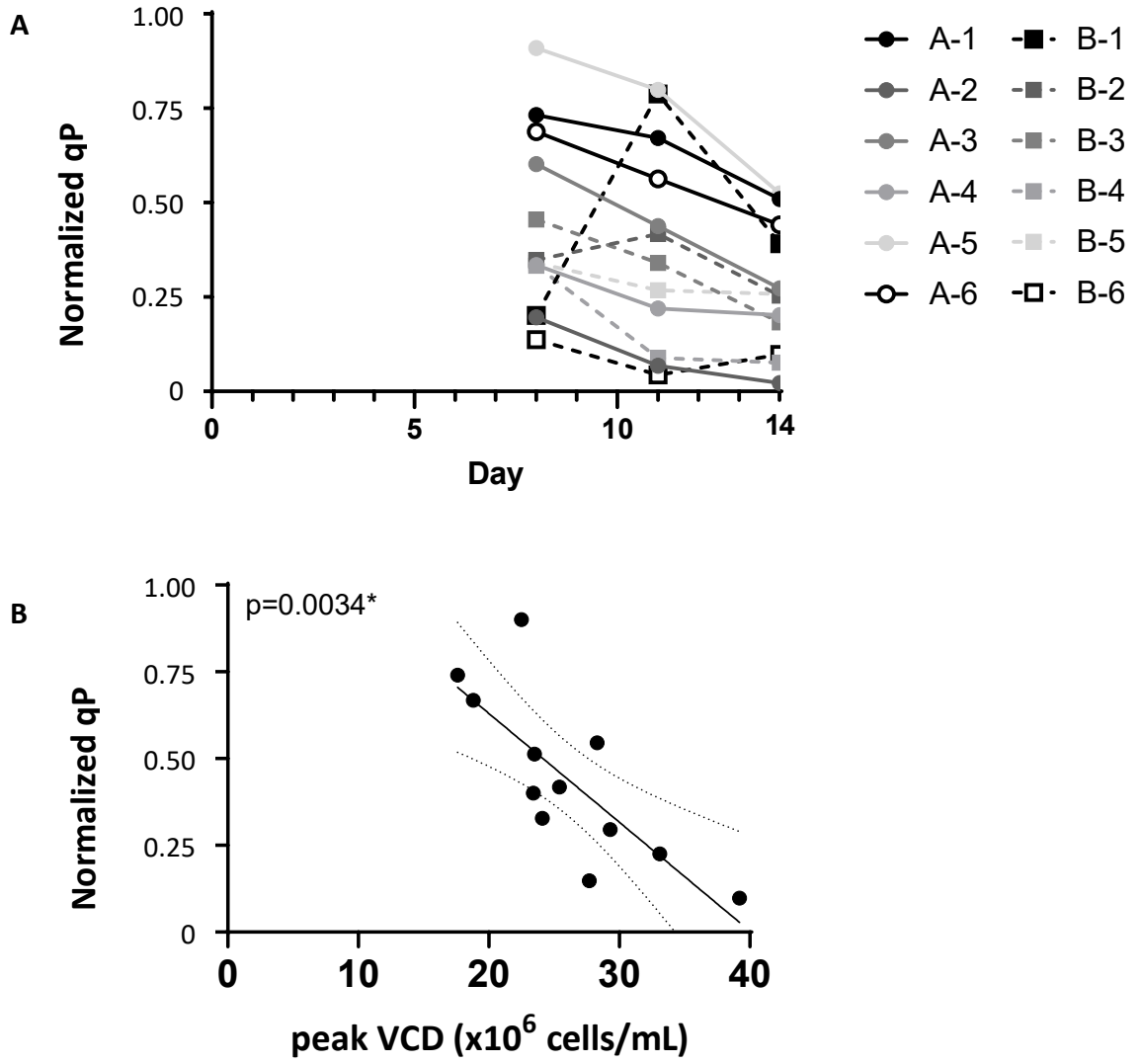

Figure S1. Time profiles of qP for twelve clones producing mAb A and mAb B. (A) For the overall comparison of qP in Figure 1C, titers from days 6 and 11 were used. More detailed qP profiles for each clone are shown here, using titer data available on days 6, 8, 11, and 14. (B) Peak VCD was negatively correlated with qP (days 6-11), indicating a tradeoff between productivity and growth.

Figure S2. Mirror plot examples. The red spectra are from samples; the blue spectra are from standards. Spectral scores (head to tail match factors and reverse match factors) in green indicate the similarity of the unknown spectrum to the library spectrum on the NIST scale of 0 (no matching peaks) to 999 (perfect match).

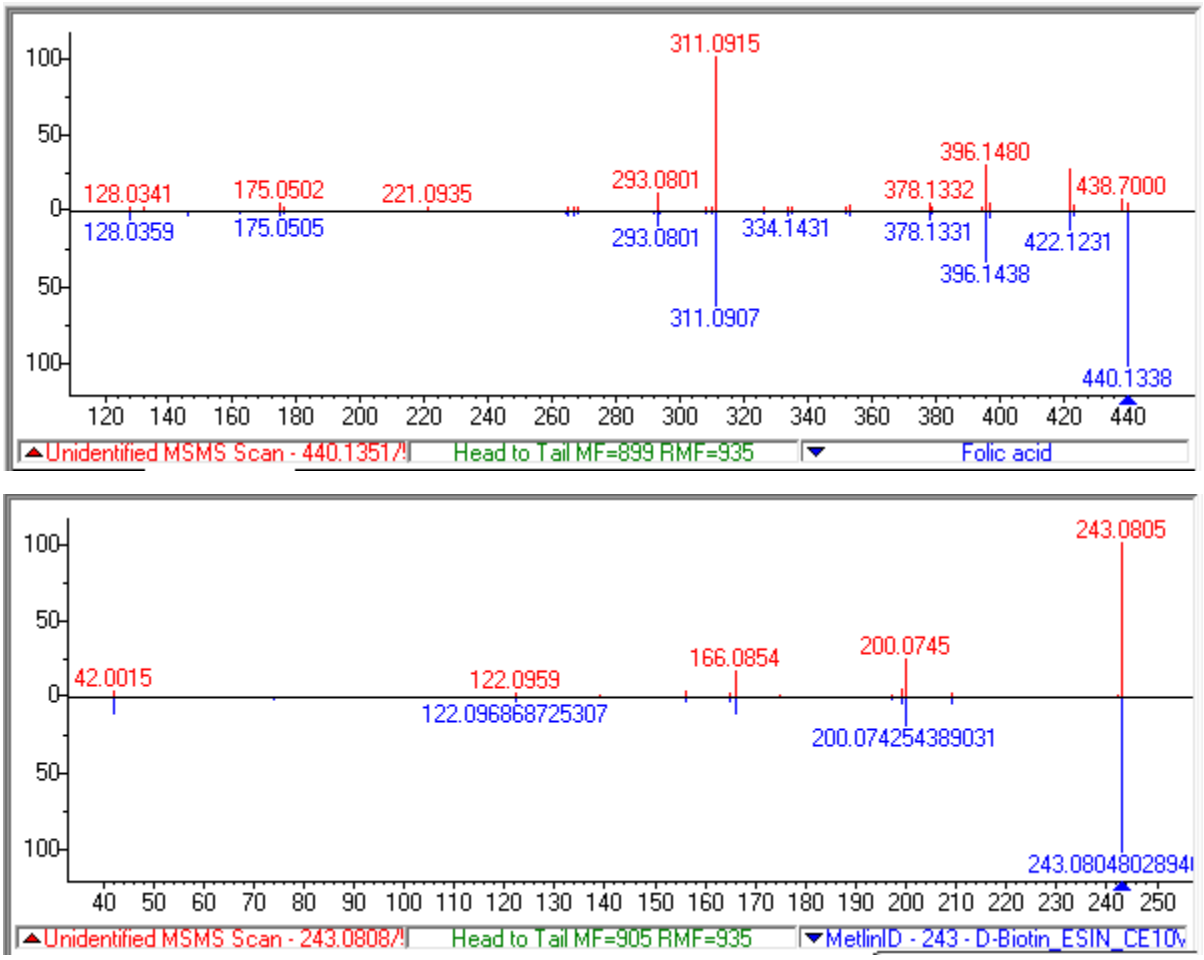

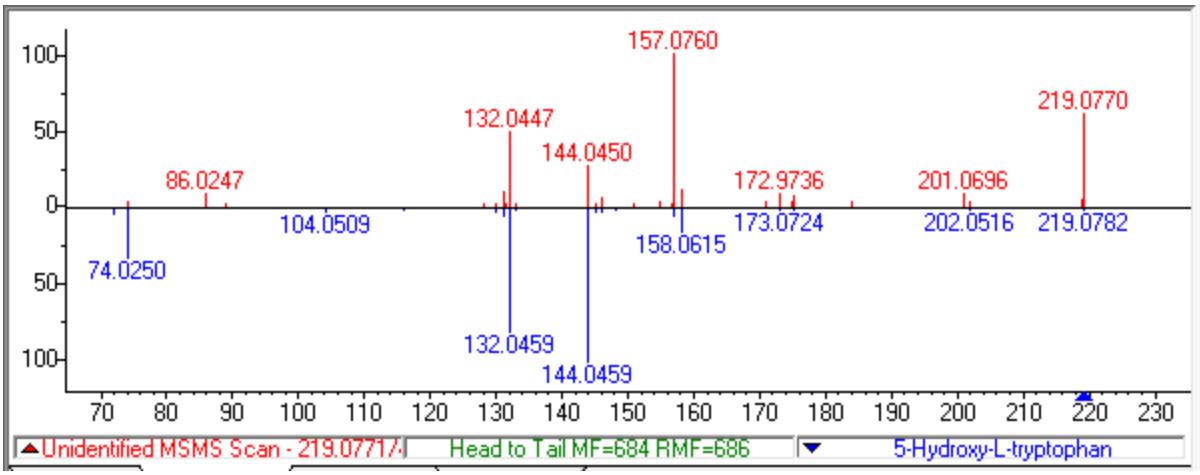
157.0760
219.0770
132.0447
144.0450
86.0247
172.9736
201.0696
104.0509
173.0724
202.0516
219.0782
158.0615
74.0250
132.0459
144.0459
Unidentified MSMS Scan - 219.0771
Head to Tail MF=684 RMF=686
5-Hydroxy-L-tryptophan

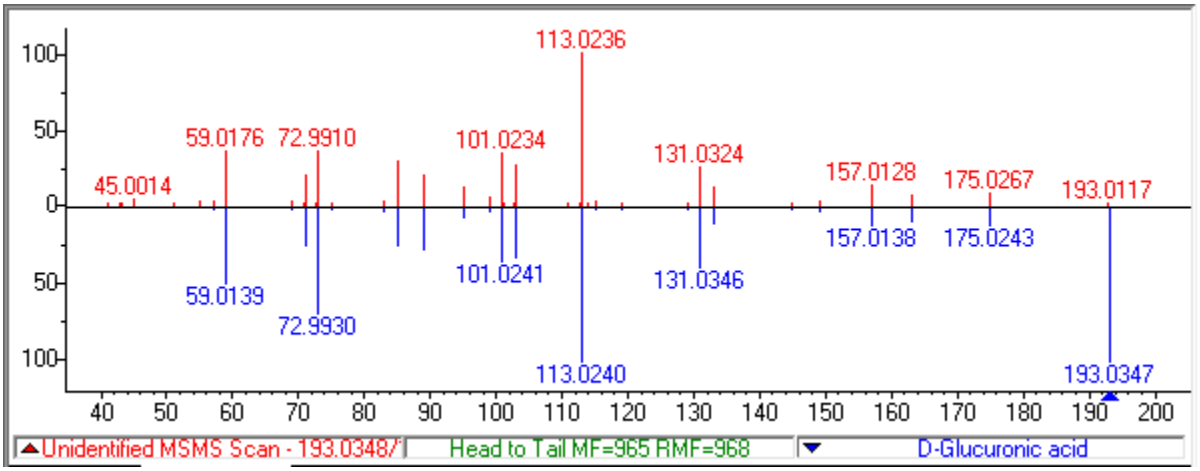
113.0236
59.0176
72.9910
101.0234
131.0324
157.0128
175.0267
193.0117
45.0014
157.0138
175.0243
59.0139
101.0241
131.0346
72.9930
113.0240
193.0347
Unidentified MSMS Scan - 193.0348
Head to Tail MF=965 RMF=968
D-Glucuronic acid

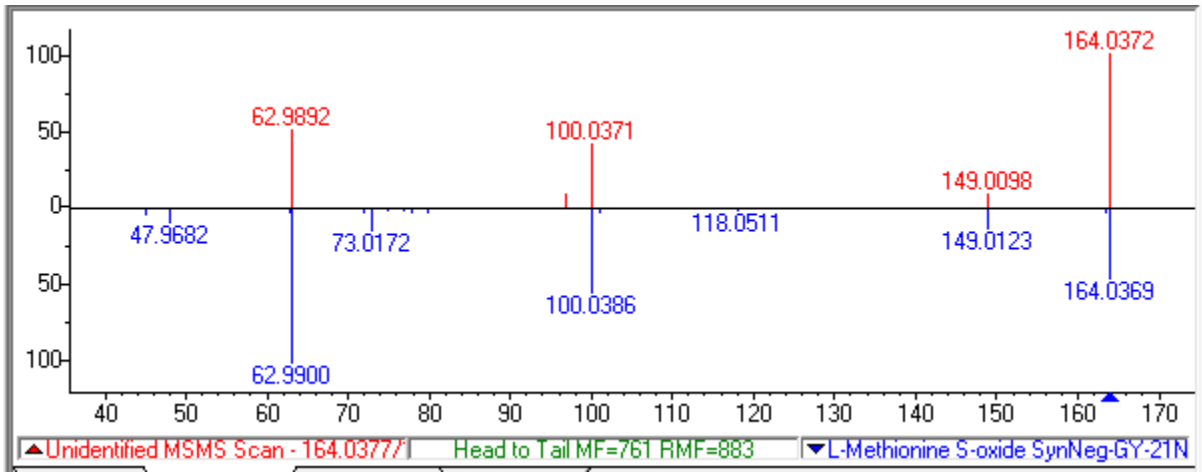
164.0372
62.9892
100.0371
149.0098
47.9682
73.0172
118.0511
149.0123
100.0386
164.0369
62.9900
Unidentified MSMS Scan - 164.0377
Head to Tail MF=761 RMF=883
L-Methionine S-oxide SynNeg-GY-21N

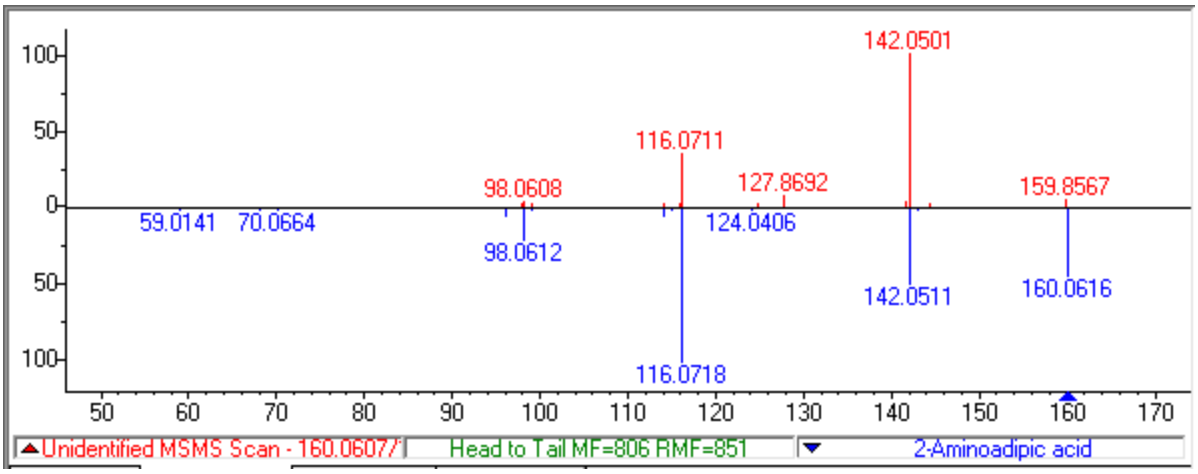
142.0501
116.0711
98.0608
127.8692
159.8567
59.0141
70.0664
124.0406
98.0612
142.0511
160.0616
116.0718
Unidentified MSMS Scan - 160.0607
Head to Tail MF=806 RMF=851
2-Aminoadipic acid

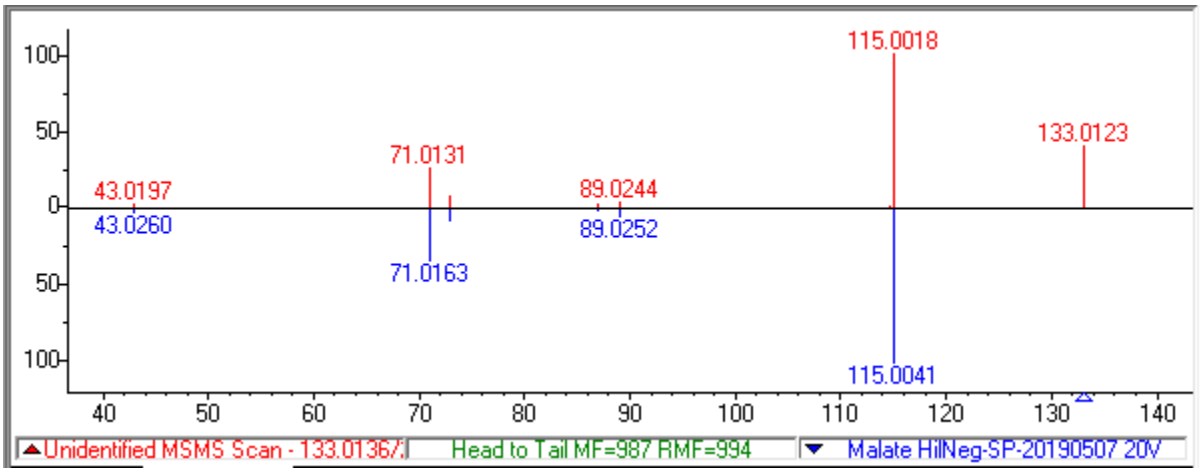
115.0018
133.0123
71.0131
43.0197
89.0244
43.0260
89.0252
71.0163
115.0041
Unidentified MSMS Scan - 133.0136
Head to Tail MF=987 RMF=994
Malate HilNeg-SP-20190507 20V

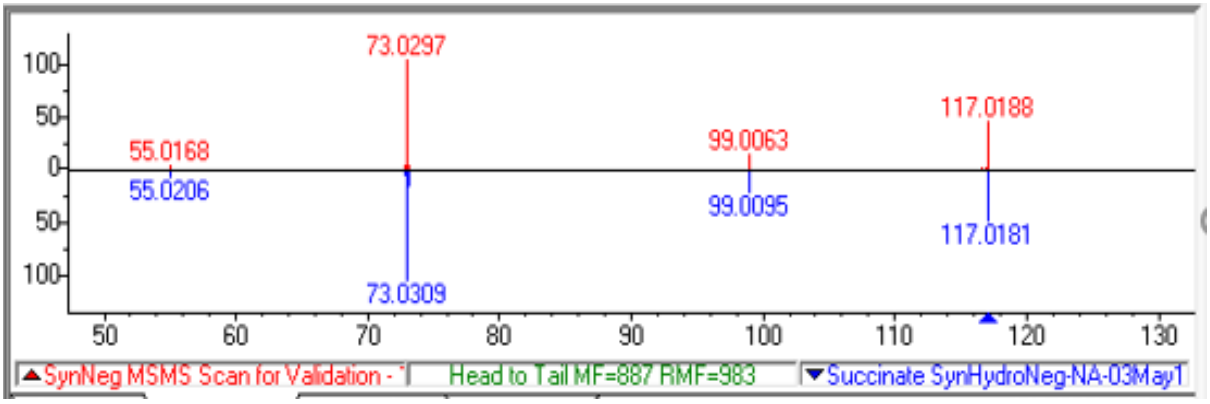
73.0297
117.0188
55.0168
99.0063
55.0206
99.0095
117.0181
73.0309
SynNeg MSMS Scan for Validation -
Head to Tail MF=887 RMF=983
Succinate SynHydroNeg-NA-03May1

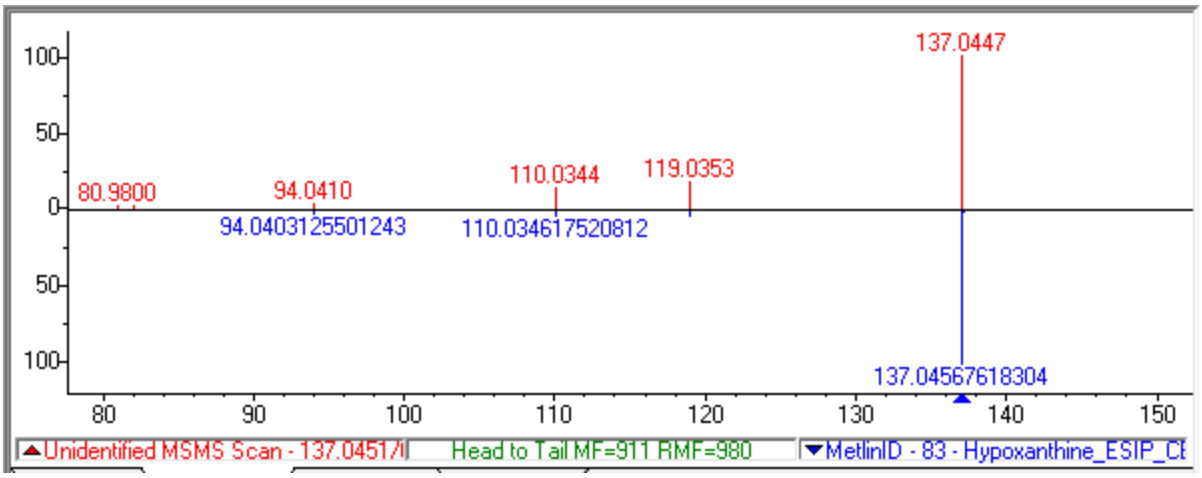
137.0447
80.9800
94.0410
110.0344
119.0353
94.0403125501243
110.034617520812
137.04567618304
Unidentified MSMS Scan - 137.04517
Head to Tail MF=911 RMF=980
MetlinID - 83 - Hypoxanthine_ESIP_Cl

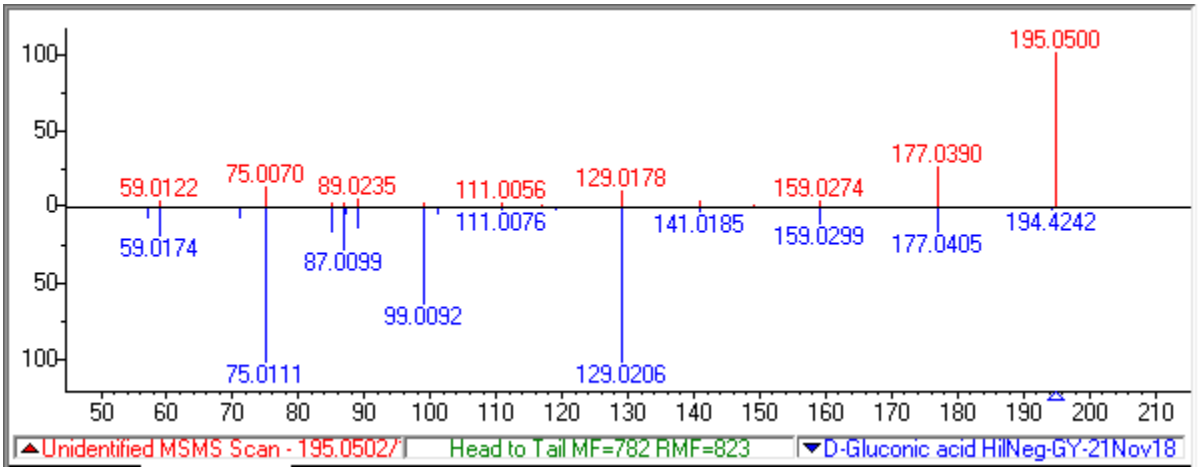
195.0500
177.0390
59.0122
75.0070
89.0235
111.0056
129.0178
159.0274
111.0076
141.0185
159.0299
177.0405
194.4242
59.0174
87.0099
99.0092
75.0111
129.0206
Unidentified MSMS Scan - 195.0502
Head to Tail MF=782 RMF=823
D-Gluconic acid HilNeg-GY-21Nov18

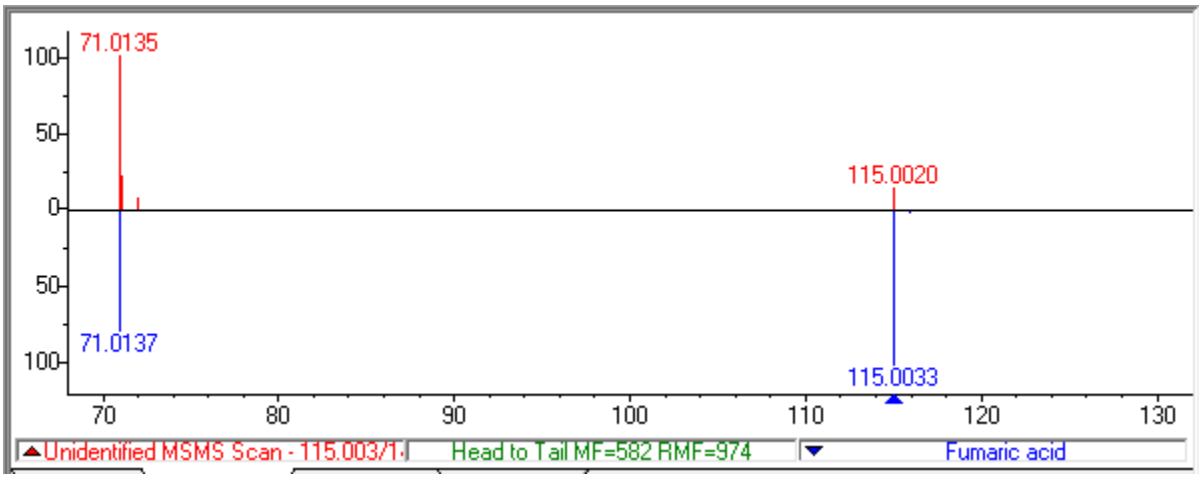
71.0135
115.0020
71.0137
115.0033
Unidentified MSMS Scan - 115.003/1
Head to Tail MF=582 RMF=974
Fumaric acid

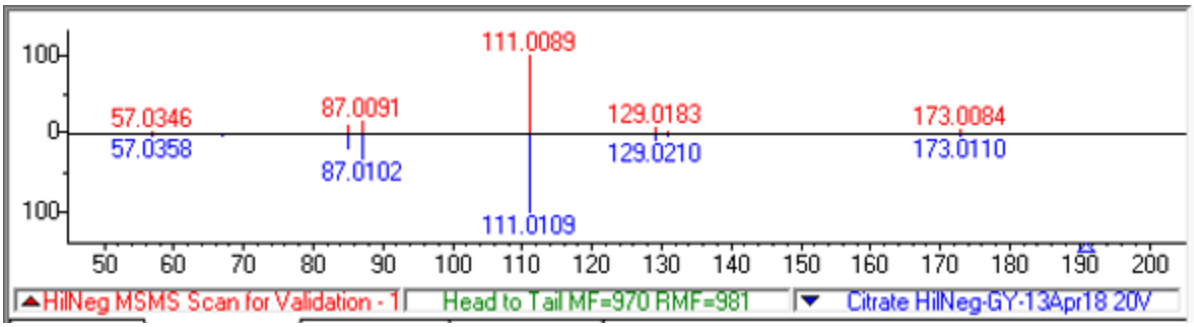
111.0089
100
57.0346
57.0358
87.0091
87.0102
0
129.0183
129.0210
173.0084
173.0110
100
111.0109
50 60 70 80 90 100 110 120 130 140 150 160 170 180 190 200
HilNeg MSMS Scan for Validation - 1
Head to Tail MF=970 RMF=981
Citrate HilNeg-GY-13Apr18 20V

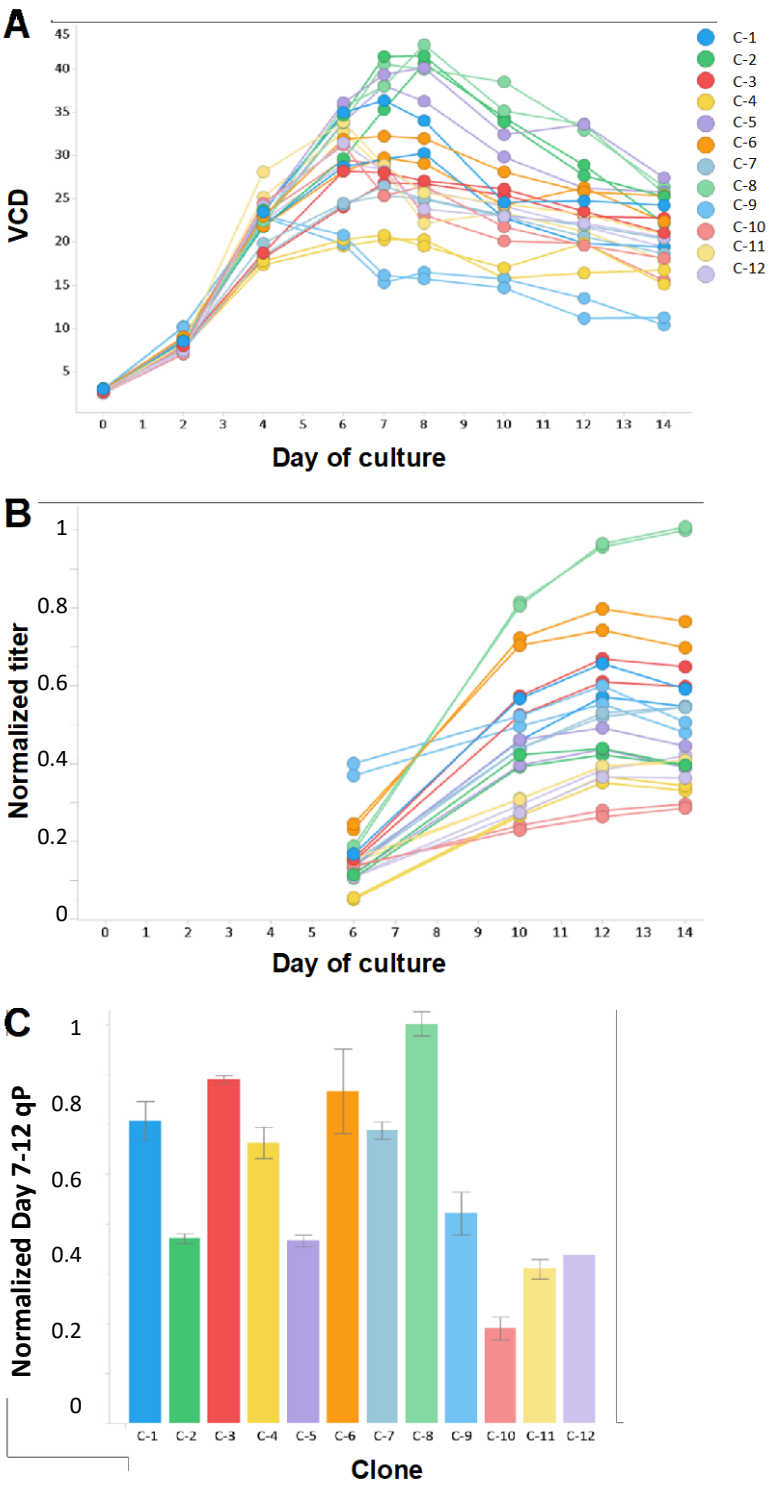

Figure S3. Growth and productivity profiles of mAb C experiment. A set of 12 clones expressing mAb C was cultured in duplicate in Ambr 15 bioreactors using the same fed-batch process as the 5-L bioreactor cultures used for the first set of 12 clones expressing mAb A or mAb B. (A)

Growth and (B) productivity profiles. (C) Average qP was calculated for correlation analysis from Day 7 and Day 12 titers. Error bars indicate standard deviation between duplicates.

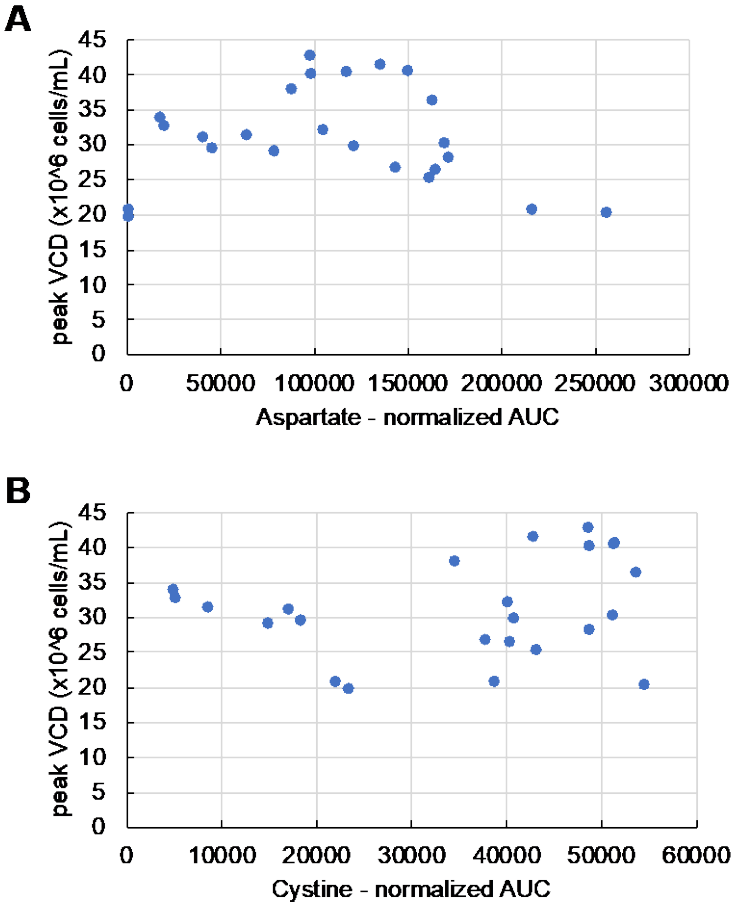

Figure S4. Correlations between Day 7 metabolite levels and peak VCD. (A) Aspartate and (B) cystine AUCs in the targeted experiment were normalized to Day 7 VCDs and plotted against peak VCD. Calculations of both Pearson and Spearman's rank correlation coefficients showed that there were no significant correlations between the metabolite levels and peak VCD.

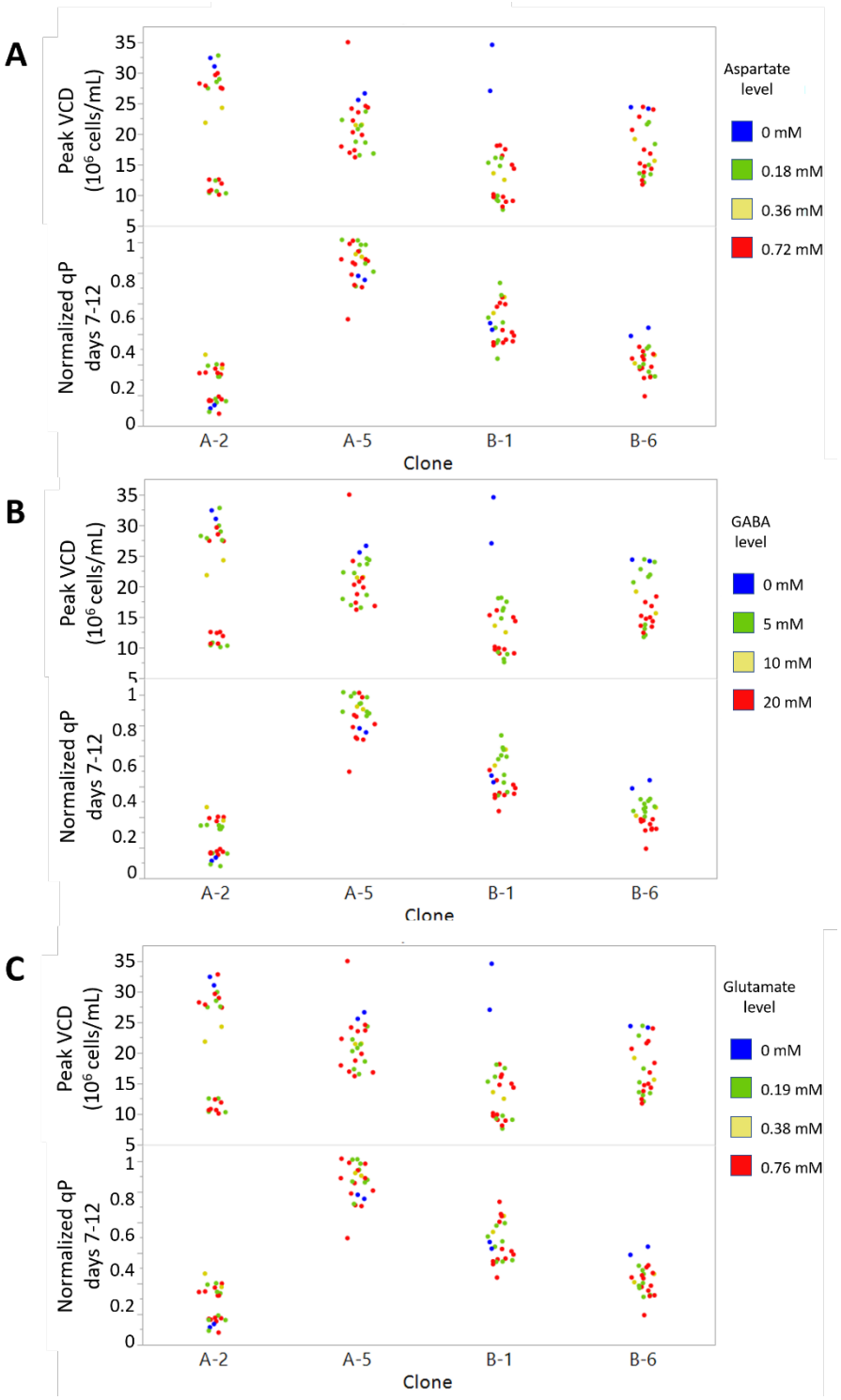

Figure S5. Productivity and growth in the add-back screening study. Data shown are cell-specific productivity (qP) and peak VCD of the 96 conditions (Table S2). (A) Aspartate, (B) GABA, (C) glutamate. Colors indicate metabolite level. Value 0 represents the control and 3 represents the

highest level of the indicated metabolite. In contrast to citrate (Figure 4), these metabolites did not show consistent responses in qP or VCD. High-qP clones used in this study were A-5 and B-1. Low-qP clones were A-2 and B-6.

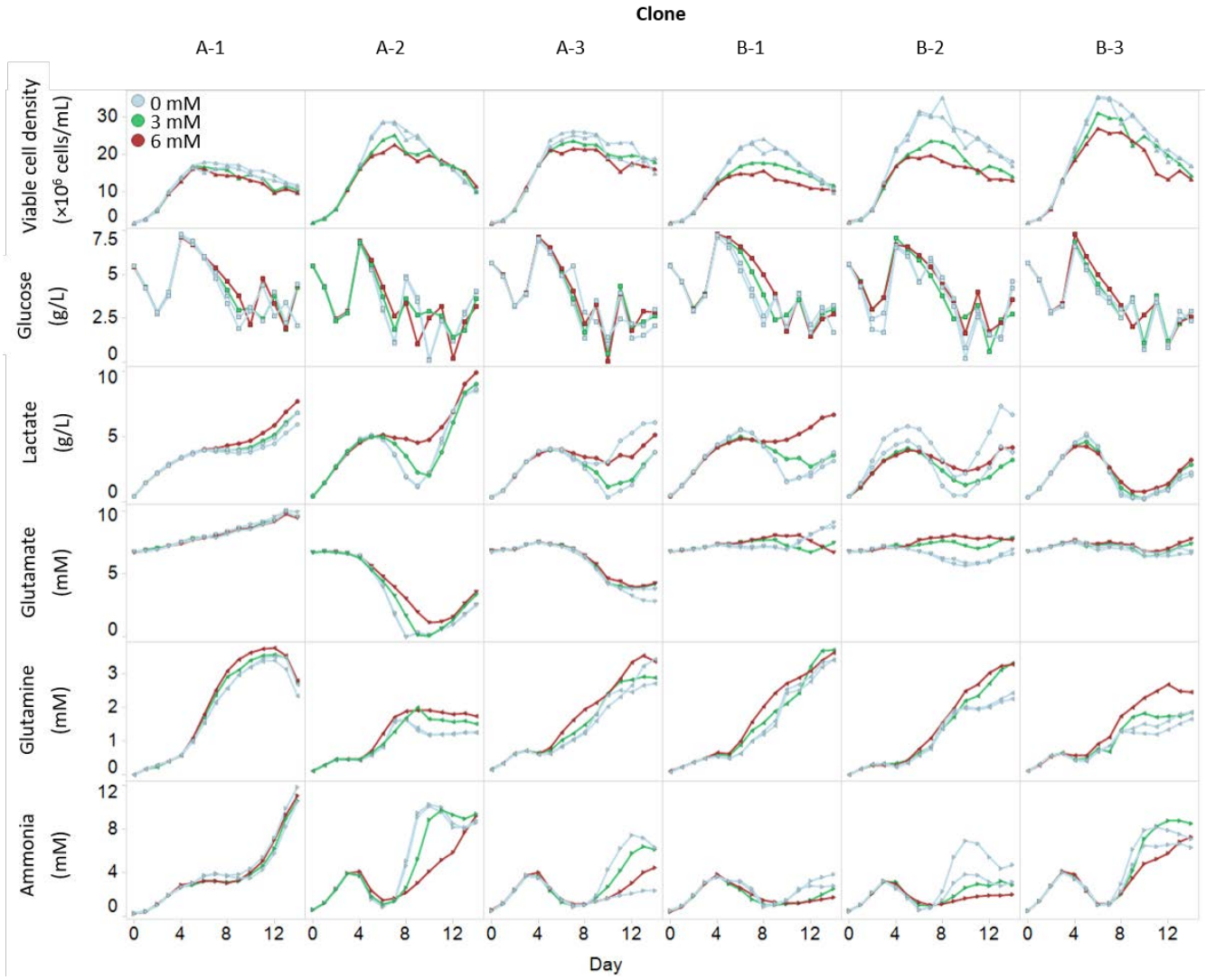

Figure S6. Metabolite profiles for citrate add-back study in Ambr 250 reactors. Line colors represent different amounts of citrate supplementation. The control condition was performed in duplicate. For all but one clone (A-1), we observed a dose-dependent decrease in peak VCD, an increase in lactate accumulation, and a decrease in lactate accumulation with the addition of citrate. We also saw slightly increased glutamate and glutamine concentrations.

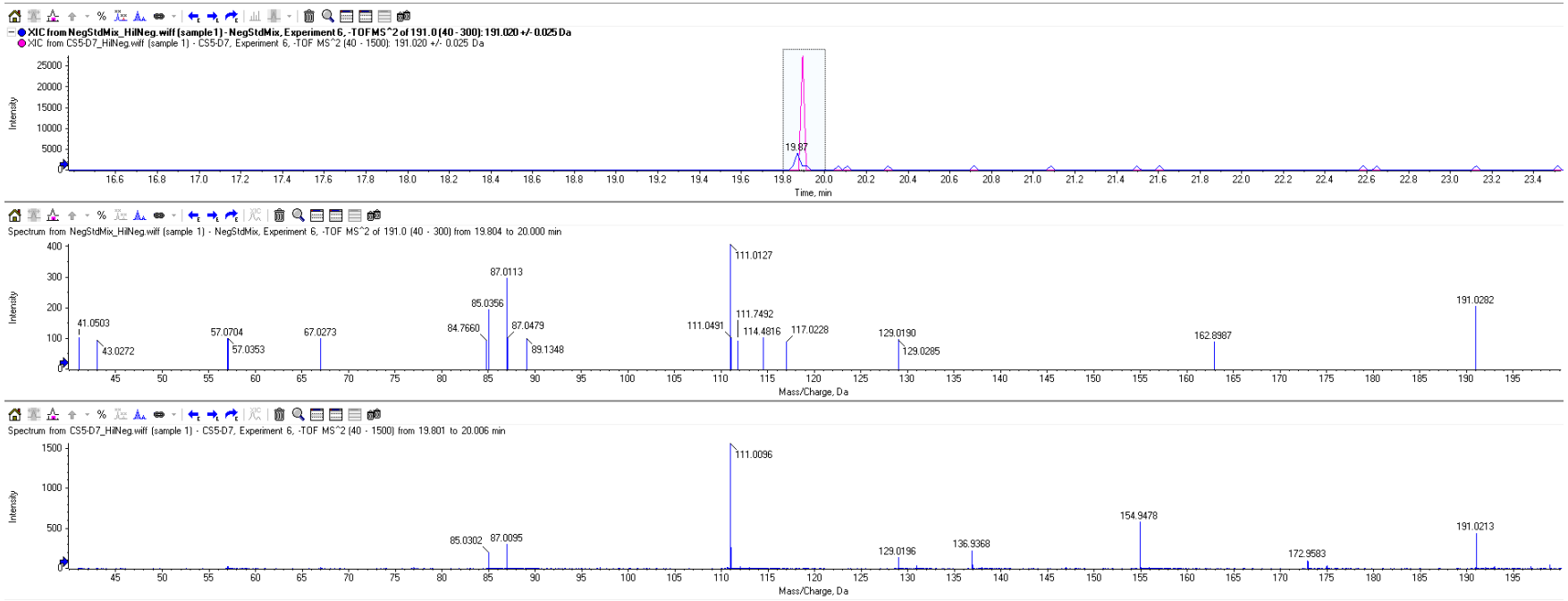

Figure S7. Example chromatogram from untargeted LC-MS analysis. The top panel is the XIC (extracted ion chromatogram) showing the retention time for citrate when run in the negative ionization mode using the HILIC column. The next panels are the MS/MS spectra from the selected XIC window for a mix of standards including citrate (center panel) and a sample (bottom panel).

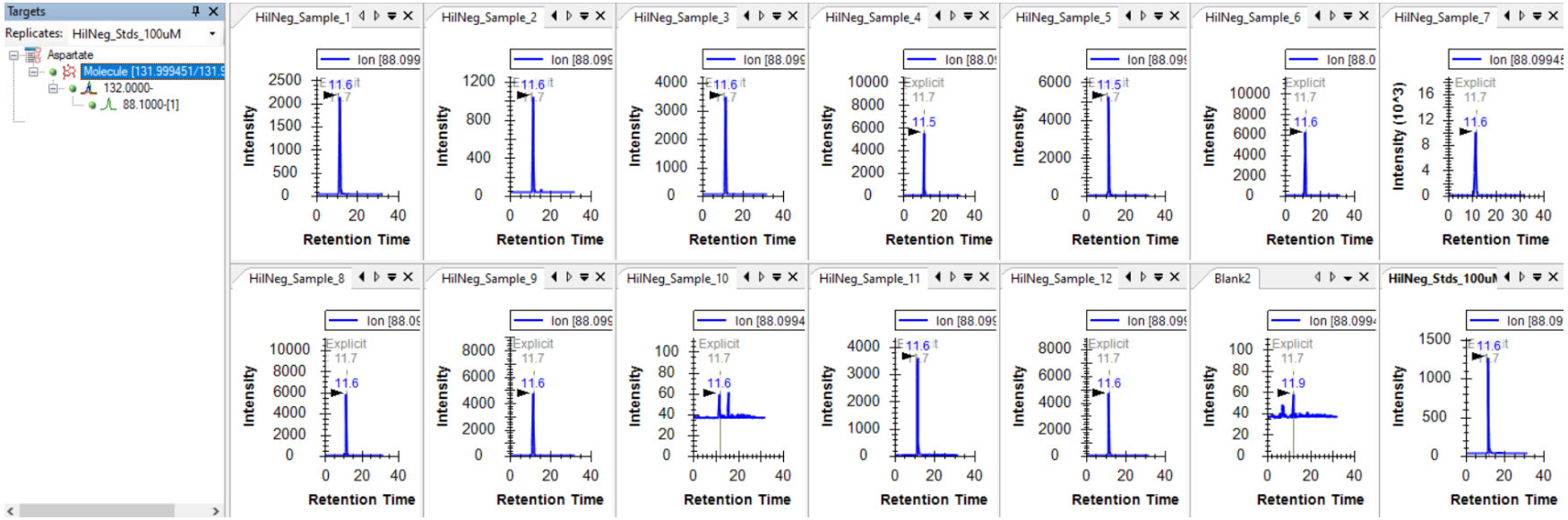

Figure S8. Example chromatograms from targeted LC-MS analysis. Varying intensities can be seen for aspartate in supernatant samples. The last two panels show a very low intensity in a blank sample and a higher intensity for a chemical standard.

Chapter 3. ^{13}C Metabolic Flux Analysis to Understand the Impact of Citrate Addition on Productivity of CHO Cells

3.1 Abstract

Addition of TCA cycle metabolites such as citrate to CHO cell cultures has been shown to improve volumetric titer and specific productivity (qP) of monoclonal antibodies. To gain insight into the mechanism of this productivity improvement, we used stable isotope labeling of citric acid-$^{13}C_6$ in ambr250 bioreactors for multiple industrial CHO clones. We analyzed cell pellets and supernatants from mid-exponential and early-stationary timepoints using LC-MS for key TCA cycle intermediates and other select metabolites connected to citrate metabolism. We used mass isotopomer distributions (MIDs) derived from this analysis along with amino acid exchange data to estimate intracellular fluxes using ^{13}C-metabolic flux analysis (MFA) and found several fluxes that significantly correlated with either qP or clonal response in glycolysis, mitochondrial exchange, and amino acid metabolism pathways.

3.2 Introduction

In the previous chapter, we discovered that the addition of sodium citrate solution as a bolus to cell culture could lead to a dose-dependent increase in qP for multiple CHO cell lines expressing two different molecules, mAb A or mAb B. To better understand the mechanism of qP increase, we decided to follow the fate of the added citrate by repeating the experiment but with ^{13}C stable isotope labeling in the high-dose conditions. One hypothesis for how the citrate could be improving qP is that it is acting as a direct substrate into the TCA cycle, preventing a bottleneck and enhancing oxidative TCA flux (Zhang et al., 2020). The increased ATP could reduce the amount of glutamine and glutamate metabolism towards α-ketoglutarate by inhibiting glutamate dehydrogenase, thereby also reducing production of ammonium, a toxic byproduct (Gilbert et al., 2013). If citrate directly enters the TCA cycle, pyruvate oxidation to acetyl-CoA and eventually citrate may be reduced, and the pyruvate would be driven more towards a glycolytic flux resulting in lactate production (Figure 1). Accumulation of lactate may have negative impacts on cell growth, although our cell lines have historically been robust to lactate accumulation below 6-8 g/L. We explored this hypothesis by measuring the MIDs of several metabolites involved in the TCA cycle, as well as of palmitic acid which could potentially also accumulate labeled carbons from citrate via acetyl-CoA.

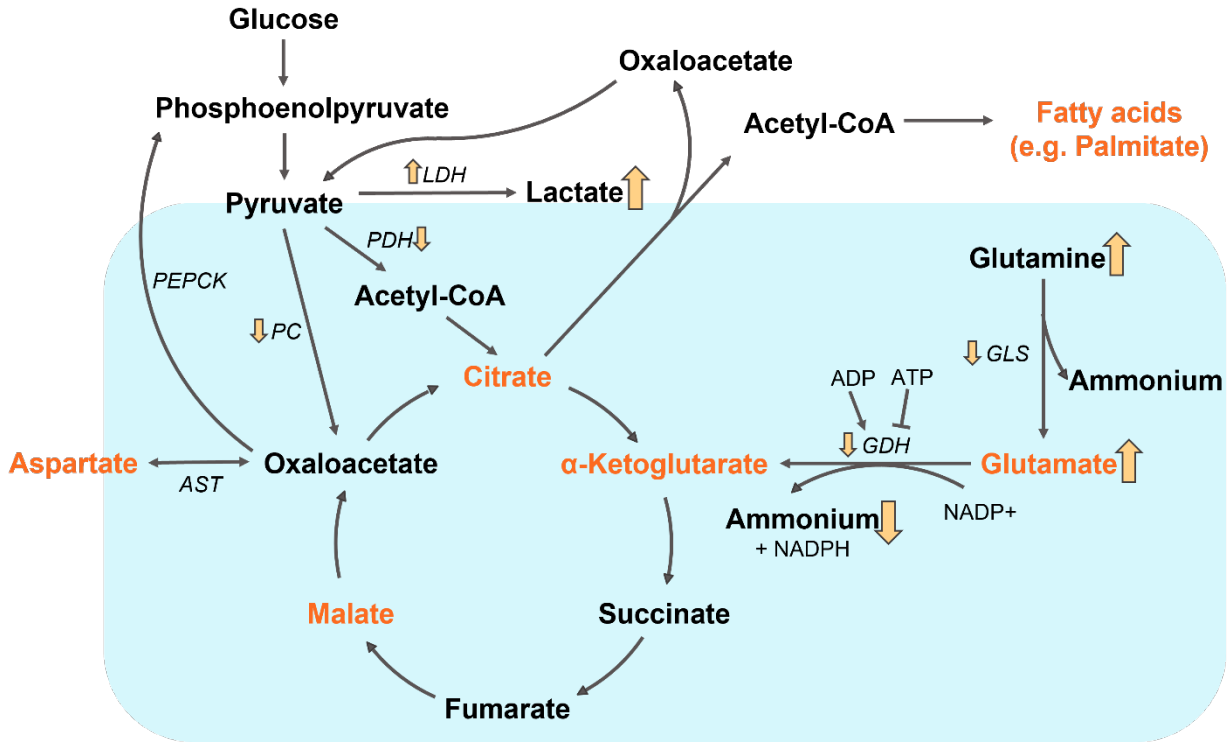

Figure 1. A simplified view of main pathways connected to citrate metabolism. Large yellow arrows indicate trends previously observed upon citrate addition: increased accumulation of glutamate, glutamine, and lactate and decreased accumulation of ammonium. Small yellow arrows indicate hypothetical flux changes that could explain those metabolite trends. Metabolites in orange were targeted for LC-MS analysis to investigate this hypothesis. (LDH: lactate dehydrogenase, PDH: pyruvate dehydrogenase, PC: pyruvate carboxylase, PEPCK: phosphoenolpyruvate carboxykinase, AST: aspartate transaminase, GDH: glutamate dehydrogenase, GLS: glutaminase)

3.3 Materials and Methods

3.3.1 Cell Culture Experiment

Cell lines A-1, A-2, A-3, B-1, B-2, and B-3 from Chapter 2 were used in this study. 14-day fed-batch experiments were carried out in an ambr250 as in described section 2.5.2, with sodium citrate

bolus additions on day 3 as described in 2.5.7. The 3mM sodium citrate bolus was unlabeled due to material constraints. The 6mM sodium citrate bolus included 20% fully labeled citric acid-$^{13}C_6$ (Sigma-Aldrich), neutralized with sodium hydroxide, and 80% unlabeled sodium citrate. Pellets containing 1×10^6 cells were washed with PBS and snap frozen in liquid nitrogen on days 4 and 7. The supernatants from these timepoints were also frozen. Amino acid quantitation was performed on the supernatant samples using the REBEL Cell Culture Media Analyzer (908 Devices, Boston, MA, USA). Cell growth and productivity characteristics were calculated as previously described in section 2.5.5.

3.3.2 LC-MS Experiment

Supernatant samples were diluted 1:10 for LC-MS analysis. Cell pellets were extracted by first resuspending and vortexing in a methanol/water mixture (91:9 v/v). Samples were subjected to three freeze-thaw cycles in liquid nitrogen, then centrifuged at 15,000 ×g for 5 minutes at 4°C. The supernatant was dried in a SpeedVac concentrator using no heat and stored at -20°C prior to reconstitution in 100uL methanol/water mixture (1:1 v/v). Analysis was performed on a quadrupole time-of flight (TOF) mass spectrometer (TripleTOF 5600+, AB Sciex, Framingham, MA, USA) with a HILIC column (Phenomenex Luna NH2, Torrance, CA, USA) as described in section 2.5.3. The gradient and settings used were identical to the ones used in the QQQ targeted experiment in section 2.6. Each sample was run multiple times in negative mode, each time with a TOF scan and multiple product ion scans for targeted masses.

3.3.3 Mass Isotopomer Distribution (MID) Calculations

Peaks from product ion scans were identified based on precursor-product transitions and the retention times of pure unlabeled chemical standards for all metabolites and quantified in Skyline 21.2.0.425 (Pino et al., 2020). Retention times and transitions used to identify the metabolites and

their isotopologues can be found in supplementary information (Table S1). MS/MS spectra were used to verify metabolite identities. Measurements from blank samples were used to remove background in M+2 and higher forms. A metabolite's MID was calculated by normalizing the area-under-the curve (AUC) of each isotopologue to the sum of the peak areas for all isotopologues of the metabolite.

3.3.4 Metabolic Flux Analysis

Fluxes for amino acids, ammonia, glucose, and lactate were calculated from day 4 to day 7 with a simple regression on concentrations from each day and converted to millimoles per gram of dry cell weight per hour (mmol/gDW/hr). Lacking experimental cell weight measurements, we assumed a literature value of 300 pg as the dry weight of a cell (Chen et al., 2019). Asparagine and cysteine concentrations were not used due to insufficient data from the REBEL. These fluxes were used along with the MIDs for glutamate, malate, and citrate for elementary metabolite unit (EMU)-based flux optimization of a 66-reaction network (Supplementary Information Table S2) as described previously (Si et al., 2009). Twenty iterations were performed for each day/clone pair and averaged. These averaged flux estimates were then correlated with qP as well as each clone's response to citrate addition, and significant correlations ($p<0.05$) were examined (Supplementary Information Table S3). The response to citrate addition was calculated as such for each clone:

$$\Delta qP_{citrate} = \frac{qP\ with\ 6\ mM\ citrate - qP\ with\ 0\ mM\ citrate}{qP\ with\ 0\ mM\ citrate}.$$

3.4 Results

3.4.1 Dose-dependent qP and titer improvement observed

In this labeling experiment, results were similar to those observed in the previous experiment without labeling (Figure 5 of section 2.3.3), with a qP and titer increase seen in the majority of

clones upon citrate addition (Figure 2). Unfortunately, the 6mM condition in clone A-3 was lost by day 7 to bacterial contamination, so this clone was removed from the flux analysis. As seen previously, clone B-2 saw the most benefit from the citrate addition while clone A-1 showed a negative impact on specific and volumetric productivity.

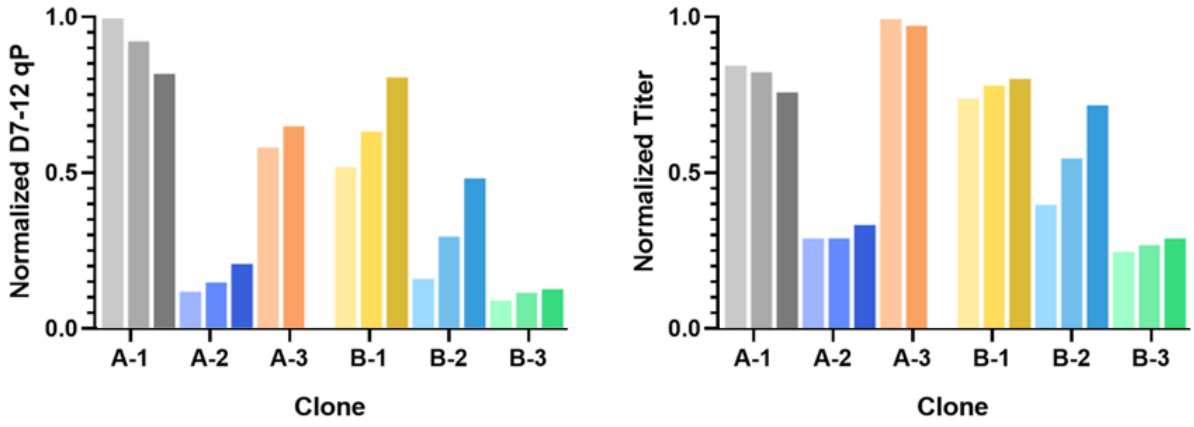

Figure 2. Specific productivity (qP) and volumetric productivity (final titer) of six industrial CHO clones, normalized to the maximum qP or titer among all conditions. For each clone, bars from left to right represent addition of 0mM, 3mM, or 6mM citrate on day 3. Addition of citrate to the cultures at 3mM or 6mM impacts both qP and titer in a dose-dependent manner, with most clones responding positively and one clone (A-1) responding negatively.

Viable cell density trends were similar as well, with some clones showing a negative impact from citrate and others showing minimal impact (Figure 3). In a departure from the previous experiment, for clone B-1, the increase in qP was enough to overcome detrimental effects on growth, resulting in slightly higher final titer.

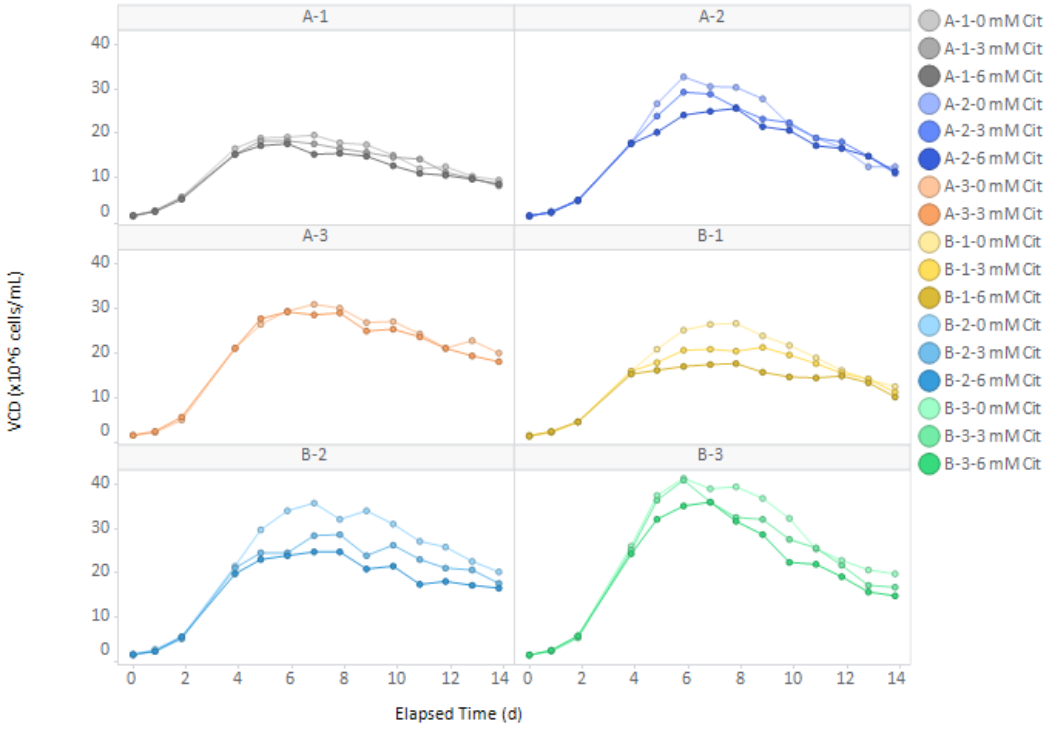

Figure 3. Viable cell densities across the 14-day fed-batch production culture. Addition of citrate impacts some clones minimally, while other clones show a negative impact on growth resulting in a lower peak VCD. (Legend applies to all graphs in this section.)

For some of the clones, the lower peak VCD with increasing citrate amounts correlated with improved longevity (Figure 4).

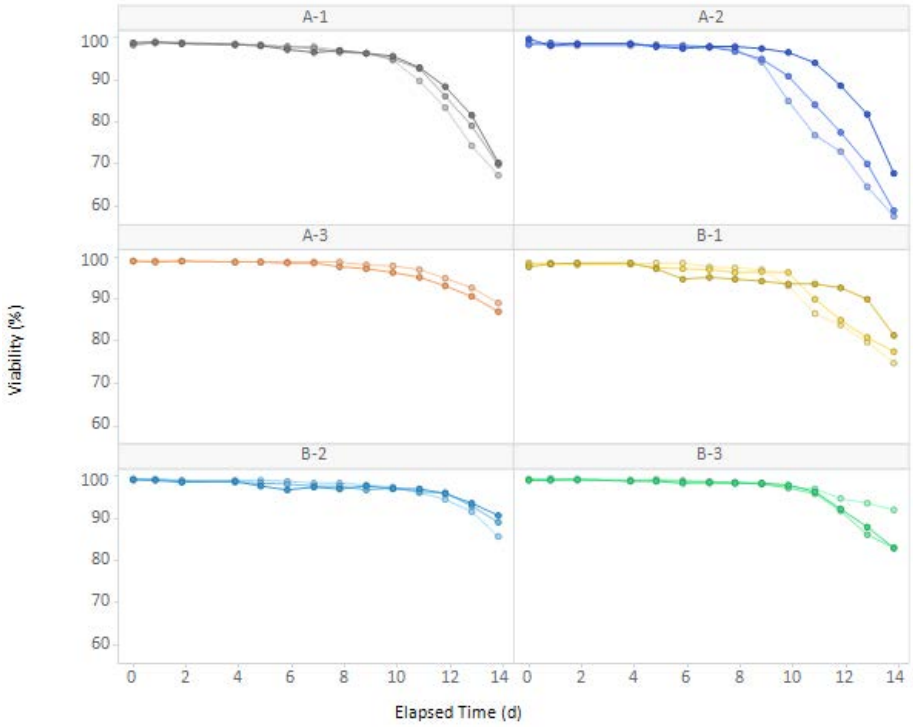

Figure 4. Viabilities across the 14-day fed batch production culture. Higher viability towards the end of the culture was observed in most clones upon citrate addition. Clones A-2 and B-1, which had lower peak VCDs with citrate, especially showed improved longevity in a dose-dependent manner.

As observed in the previous experiment, citrate addition also generally led to increased lactate, glutamate, and glutamine accumulation and decreased ammonium buildup, although the degree of change varies by clone, and again clone A-1 showed little impact (Figures 5-8).

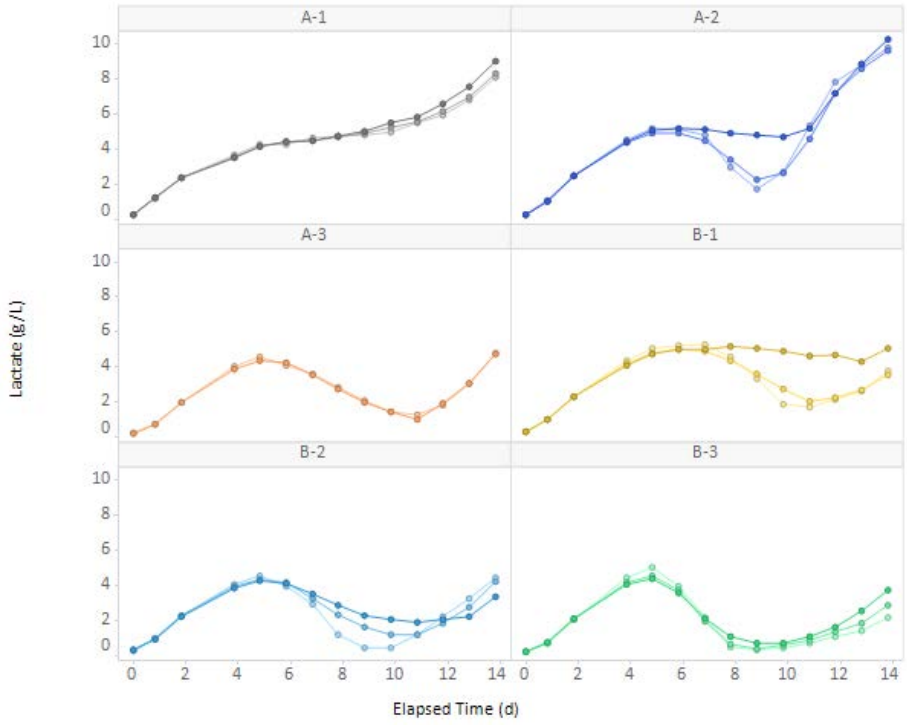

Figure 5. Lactate concentrations in supernatant.

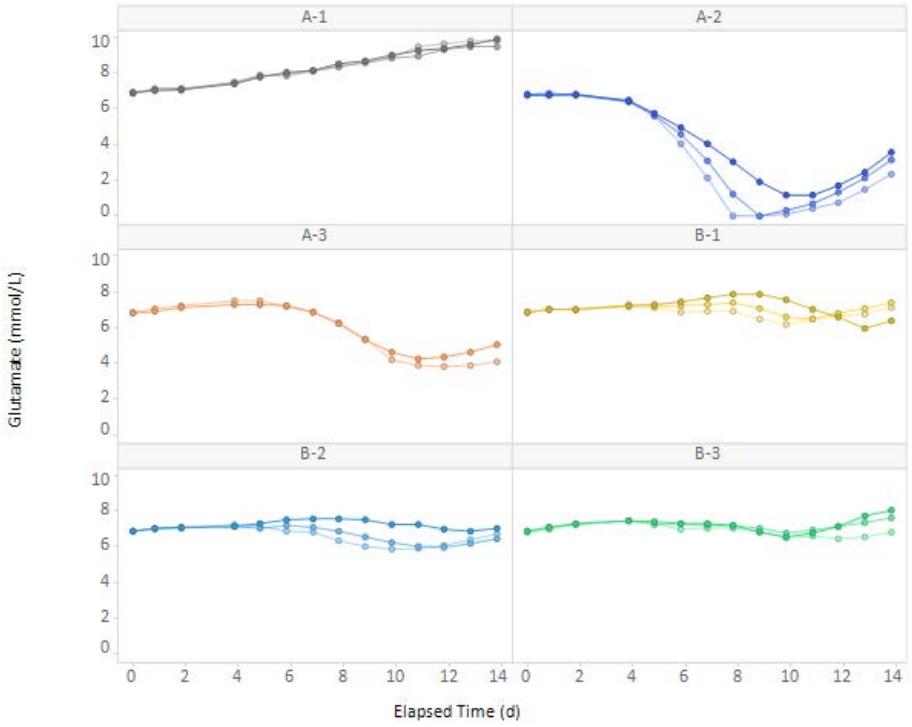

Figure 6. Glutamate concentrations in supernatant.

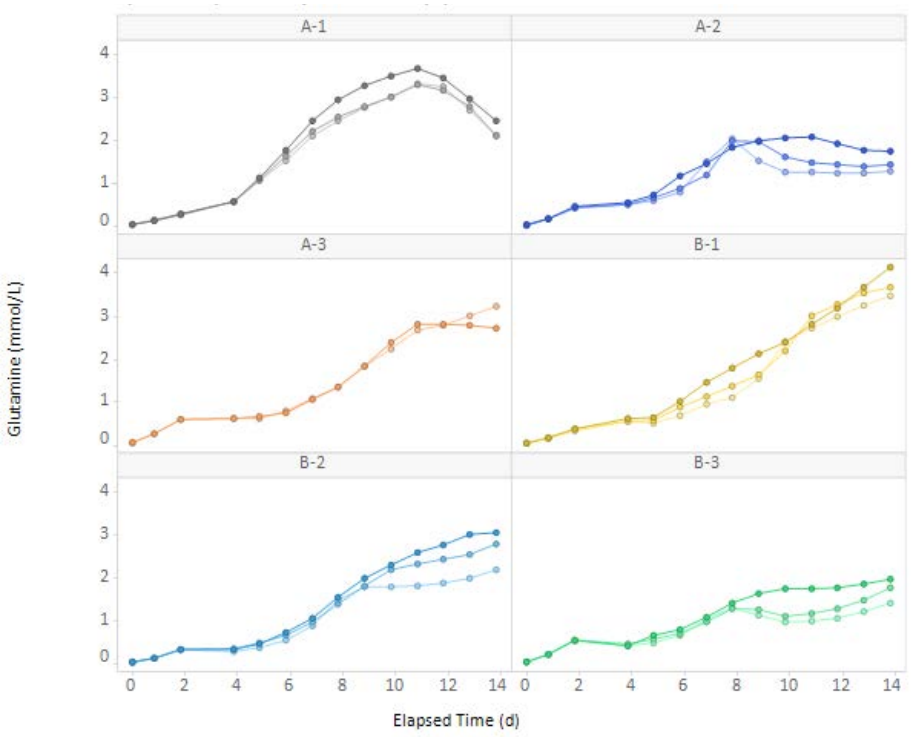

Figure 7. Glutamine concentrations in supernatant.

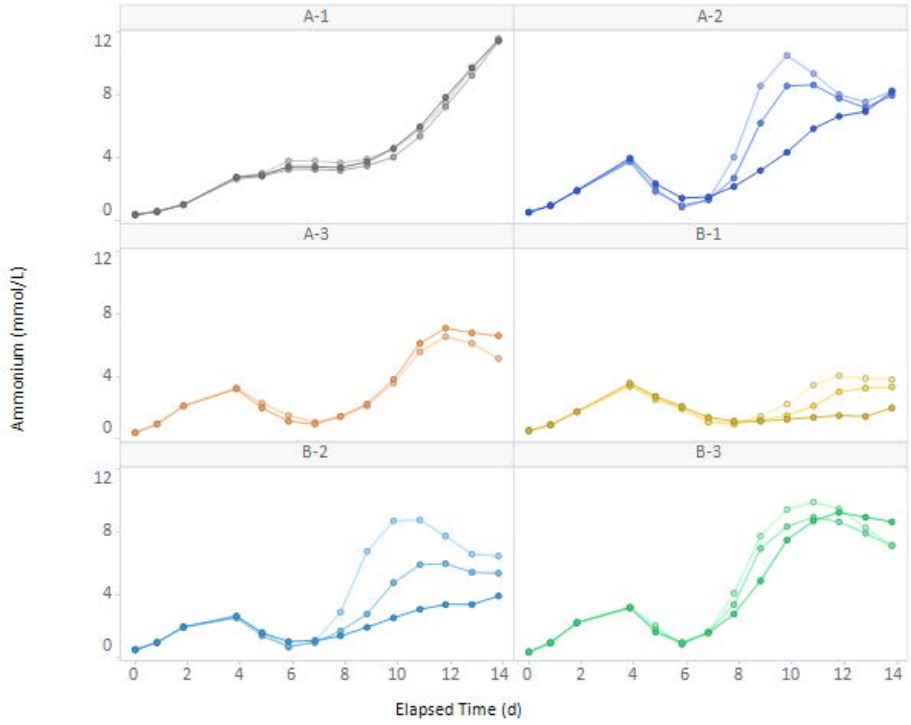

Figure 8. Ammonium concentrations in supernatant.

Cell diameters, which often correlate with titer, increased over time as expected (Figure 9). For some clones, citrate addition also increased cell size.

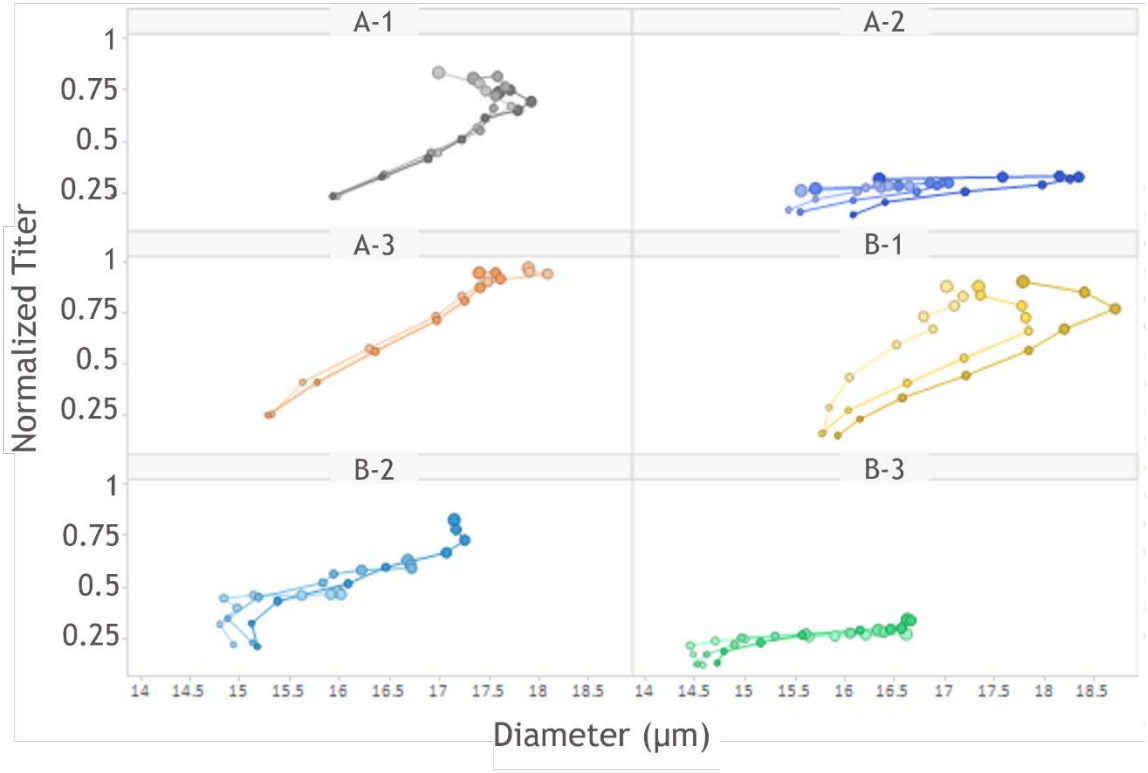

Figure 9. Cell diameters and titers (normalized to the maximum titer) over the 14-day production culture. Marker size indicates day, with the smallest markers for day 6 and the largest for day 14. Cultures with 6mM citrate had increased cell diameters for some clones, such as A-2 and B-1.

3.4.2 Citrate was not completely consumed by cells

Supernatants from day 7 were analyzed using LC-MS to confirm labeling in the 6mM citrate bioreactors. As expected, M+6 labeling was observed in these conditions (Figure 10).

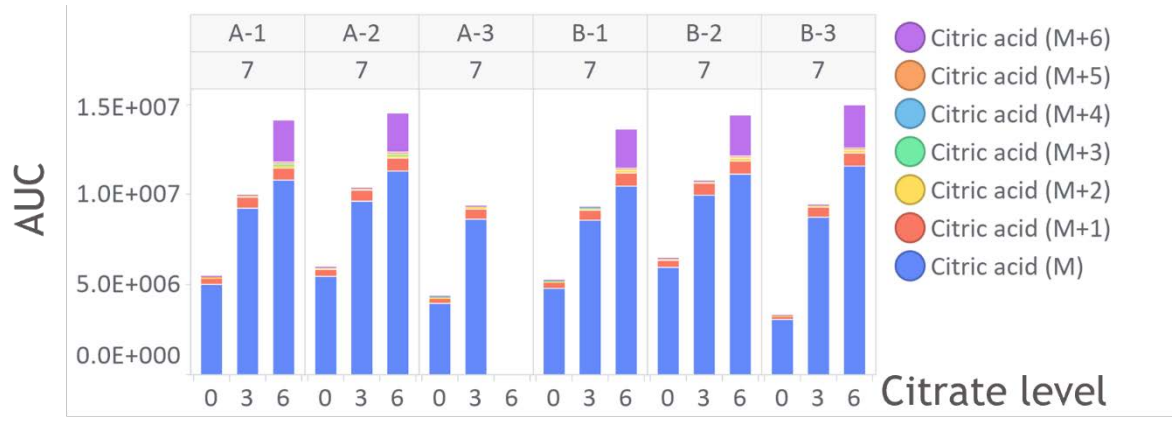

Figure 10. Peak areas for all isotopologues of citric acid in the supernatant. Areas under the curve (AUC) were integrated for peaks chosen based on retention time, precursor-product transitions, and MS/MS spectra. M+6 peaks were present in the labeled 6mM conditions as expected.

None of the other metabolites in the supernatant were labeled, suggesting that the citrate was not metabolized within cells into other products that were then secreted. Cell pellet samples from days 4 and 7 for each clone were analyzed using LC-MS to examine intracellular metabolism. Out of these intracellular metabolites, citrate showed the most incorporation of the label while the other metabolites each had a very small amount of labeling. While the total amount of intracellular citrate was higher in the supplemented cultures as expected, the proportion of intracellular citrate that was labeled was much lower than that of the extracellular citrate, indicating that not all added citrate was taken up by the cells. Isotopologue AUCs for citrate, glutamate, malate, and aspartate can be found in Supplementary Information Figures S1-S4.

3.4.3 Flux estimation shows correlations with qP and citrate response

The MIDs of glutamate, malate, and citrate in the 6mM citrate conditions were calculated by normalizing the total AUCs for all isotopomers to 100% and used in EMU-based flux estimation.

Exchange fluxes for glucose, lactate, ammonium, and all amino acids except for asparagine and cysteine were calculated between days 4 and 7 and used for flux estimation for both timepoints. Because these initial input fluxes were the same, estimated fluxes were similar, differing slightly because of changed MIDs. Day 7 estimated fluxes are shown in Figure 11.

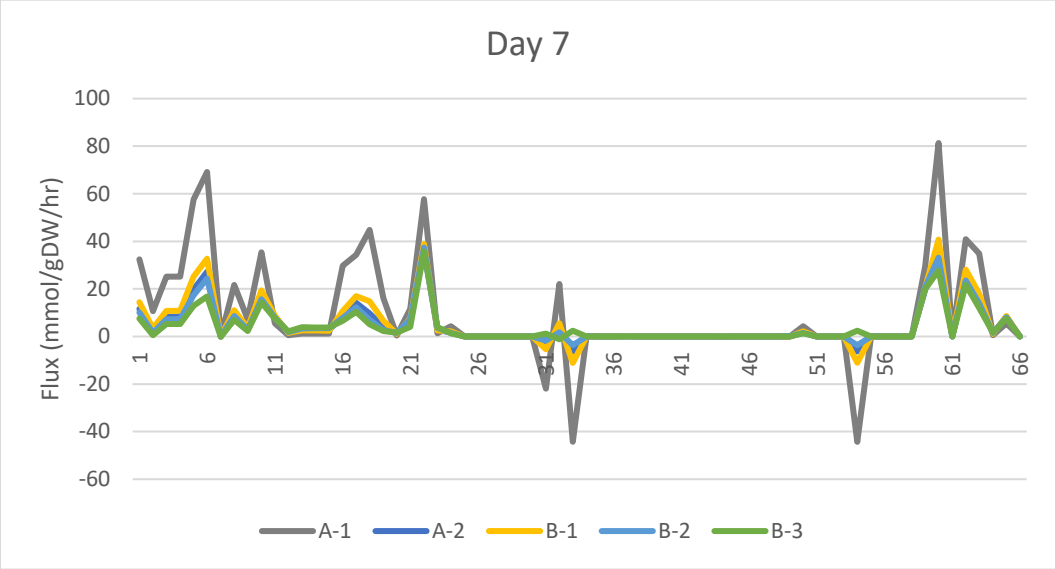

Figure 11. Day 7 reaction fluxes averaged from 20 iterations of EMU-based flux estimation for each clone. Reaction numbers across the x-axis correspond to those in SI Table 2.

The average estimated fluxes for each clone at each timepoint were used in correlation analyses against the qP for each clone and against the qP response to citrate addition.

All estimated fluxes and correlation coefficients can be found in Supplementary Information Tables S2 and S3. There were no significant correlations between estimated day 4 fluxes and qP. For estimated day 7 fluxes, 3 reactions were significantly positively correlated with qP: the production of lactate from pyruvate via lactate dehydrogenase, the production of alanine from pyruvate via alanine dehydrogenase, and serine uptake by cells (Figure 12). When looking at the

response to citrate addition, the day 4 flux through the malate-α-ketoglutarate transporter was positively correlated. Day 7 fluxes for metabolism of phenylalanine, tyrosine, isoleucine, and leucine were also significantly correlated to $\Delta qP_{citrate}$, with all positive correlations except for leucine catabolism.

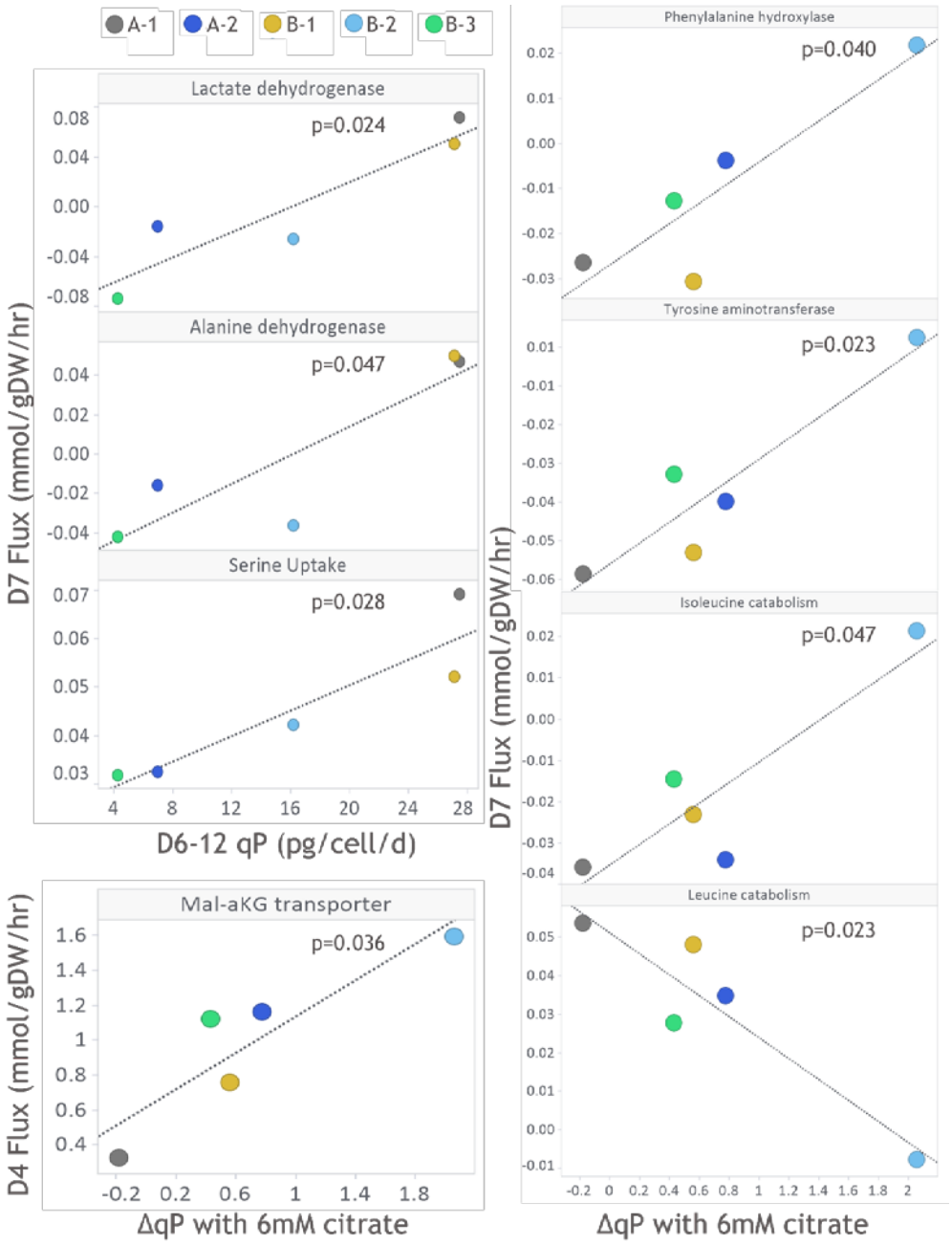

Figure 12. Estimated fluxes that were significantly correlated with qP or $\Delta qP_{citrate}$.

3.5 Discussion

Overall, results from adding citrate to fed-batch production cell cultures of CHO clones showed reproducible trends in qP/titer improvement as well as the previously observed decrease in ammonium production and increases in glutamine, glutamate, and lactate accumulation. However, the mechanism of qP increase (Figure 1) may not necessarily be due to direct incorporation of citrate as a substrate for the TCA cycle as initially hypothesized. The abundance of labeled citrate remaining in the media four days after feeding is high compared to the lower amount of labeled intracellular citrate, and minimal incorporation into other measured intracellular and extracellular metabolites was detected. Taken together, these measurements suggest that much of the citrate remained in the medium and did not become metabolized in the TCA cycle.

Upon correlation analysis between estimated fluxes from ^{13}C-MFA and qP from 6mM citrate conditions, we found that increased conversion of pyruvate to lactate and alanine was positively correlated with higher qP (Figure 13). We did not estimate intracellular fluxes in the 0 mM control conditions for comparison, but this result is in line with the overall increased extracellular lactate seen in the citrate-supplemented cultures (Figure 5). However, it seems to be contrary to many publications suggesting a negative association between lactate production and titer as well as industry-wide efforts to promote a lactate consumption phenotype (Le et al., 2012; Pereira et al., 2018; Templeton et al., 2013; Templeton, Smith, et al., 2017; Xu et al., 2016; Zhang et al., 2020). It is possible that although lactate is known to be a toxic metabolite in terms of cell growth, our cell lines are less sensitive to lactate buildup below an inhibitory threshold and more sensitive to accumulation of ammonium. There may potentially be a clone-specific range of lactate concentrations that can slightly dampen growth but lead to more energy being directed towards producing antibody. Indeed, the 6 mM conditions with the highest qP (clones A-1 and B-1) had

lower peak VCDs than the others yet relatively high titers. Alanine has also been shown to have a negative effect on cell growth as it can inhibit pyruvate kinase and the TCA cycle (Xing et al., 2011). Its presence signals that TCA cycle intermediates are abundant, so this correlation with qP may simply reflect adequate TCA cycle flux for high productivity (Reinhart et al., 2019). Indeed, in our previous untargeted metabolomics experiment investigating pathway correlations with qP, the two pathways identified through Metaboanalyst to be both significantly enriched and impacted were the TCA cycle and alanine, aspartate, and glutamate metabolism, again reflecting the strong influence of these reactions on qP (Yao et al., 2021).

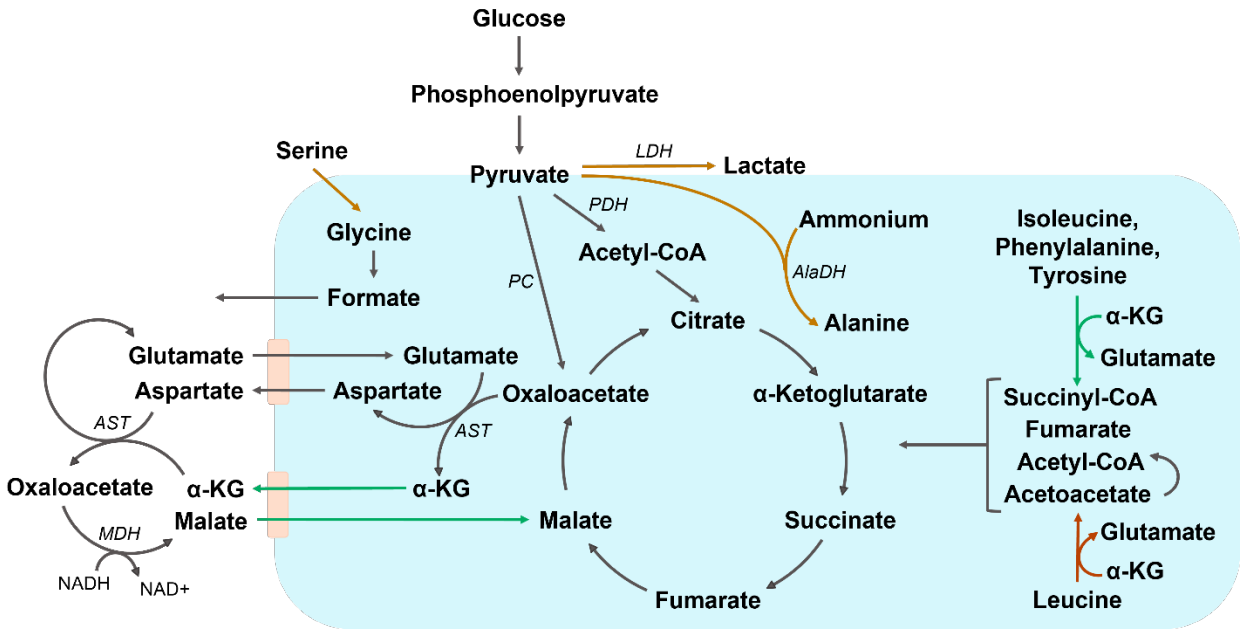

Figure 13. Intracellular pathways associated with qP and citrate response. Estimated fluxes in brown were positively correlated with qP. Fluxes in green were positively correlated with clonal response to citrate, or $\Delta qP_{citrate,}$ while the flux in red had a negative correlation with $\Delta qP_{citrate}$. (MDH: malate dehydrogenase)

Another flux that was positively correlated with qP was serine consumption. Serine uptake can lead to production of glycine, formate, or pyruvate (Carinhas et al., 2013; Coulet et al., 2022).

Based on simulated fluxes (Table S2), it is more likely that the increased consumption led to glycine and formate production rather than that of pyruvate. Formate has been identified as a putative growth inhibitor and reducing the levels of its precursors serine and glycine was suggested as a way to control formate to a minimum (Mulukutla et al., 2017). Possibly similar to lactate and alanine production, a small flux increase in this growth-inhibitory reaction may be beneficial enough to qP that overall titer is enhanced.

When examining estimated fluxes associated with $\Delta qP_{citrate}$, we found five significant correlations. Increased flux through the exchange reaction of α-ketoglutarate (α-KG) and malate was correlated with a positive response to citrate addition: clone B-2, which saw the highest increase in qP, had high flux while clone A-1, which had a negative response, had the lowest flux. This reaction is part of the malate-aspartate shuttle, which requires concerted action by two transporters in the mitochondrial membrane: the α-KG-malate transporter and the aspartate-glutamate transporter (Borst, 2020). Working together, these two carriers transfer cytosolic NADH into the mitochondria for ATP production via oxidative metabolism (Lasorsa et al., 2003). As can be seen in Figure 15, malate dehydrogenase (MDH) is closely connected with the activity of this shuttle. An enzymatic bottleneck at MDH along with excess aspartate in media can result in malate efflux, resulting in secretion of a molecule which should be moving through the TCA cycle. Metabolic engineering to overexpress MDH in CHO cells can remove this bottleneck and result in increased intracellular ATP and NADH (Chong et al., 2010). Extracellular aspartate concentration was previously found to be positively associated with qP (Yao et al., 2021). If cells can support higher flux through MDH and the malate-aspartate shuttle while aspartate is readily available, as seen in cultures that saw increased qP after citrate supplementation, then potentially this flux increase can drive higher antibody productivity by fueling ATP production.

In addition to the malate-aspartate shuttle, malate participates in the citrate-malate shuttle, which transports acetyl-CoA into the mitochondria for fatty acid synthesis (Matuszczyk et al., 2015). Flux through this reaction (Table S2 reaction 63) was higher for the clone that did not show higher qP with citrate addition compared to other clones, so potentially this clone processed the signal from excess citrate differently than the others and caused less malate to be available for the malate-aspartate shuttle.

The other four significantly correlated reactions were involved in catabolism of two aromatic amino acids (phenylalanine and tyrosine), and two branched-chain amino acids (isoleucine and leucine). Interestingly, correlations were positive with degradation of phenylalanine, tyrosine, and isoleucine but negative with degradation of leucine, the only one of the four that is only ketogenic, not both glucogenic and ketogenic. Phenylalanine hydroxylase converts phenylalanine to tyrosine, which is transaminated with α-KG to form glutamate and 4-hydroxy-phenylpyruvate. 4-hydroxy-phenylpyruvate is then further degraded through a series of steps to form acetoacetate and fumarate (Matthews, 2007). Fumarate can directly enter the TCA cycle, while acetoacetate can also enter the TCA cycle after degradation by 3-oxoacid-CoA transferase and acetoacetyl-CoA thiolase into acetyl-CoA (Williamson, 1998). As for isoleucine and leucine, these branched-chain amino acids (BCAAs) are first transaminated with α-KG by branched-chain aminotransferase (BCAT). Isoleucine is then further converted into 2-methylbutyryl-CoA, then to acetyl-CoA and succinyl-CoA to enter the TCA cycle. Leucine is similarly catabolized to isovaleryl-CoA, then acetyl-CoA and acetoacetate. Because the three glucogenic amino acids were positively correlated with $\Delta qP_{citrate}$ while the ketogenic amino acid was negatively correlated, it is possible that increased flux in this case is feeding into the TCA cycle, indirectly impacted by citrate but still driving ATP production to support greater product biosynthesis.

BCAA catabolism has previously been observed to be higher in perfusion processes compared to fed-batch (Templeton, Xu, et al., 2017). Lower BCAA degradation rates have also been associated with high-producing phenotypes, although this association was based on titer and strong growth, not specific productivity (Popp et al., 2016). Intermediates in each of these pathways have been identified to be growth inhibitors, and enzymes in both pathways have been genetically targeted to curtail their production resulting in improved growth (Mulukutla et al., 2019). In a follow-up to that work, short-chain fatty acid (SCFA) byproducts of BCAA catabolism were found to enhance qP in CHO cells by inhibiting histone deacetylases (Harrington et al., 2021). This mechanism could be an alternative explanation for our observations. Furthermore, citrate can dampen the activity of the TCA cycle by inhibiting PDH and succinate dehydrogenase (Iacobazzi & Infantino, 2014). Thus, we may be seeing the accumulation of citrate signaling cells to favor anabolism (fatty acid synthesis) including these qP-promoting SCFAs over catabolism (TCA cycle) (Frezza, 2017). RNA-seq or proteomics analysis to investigate enzyme activity around pyruvate, citrate, acetyl-CoA, and these SCFAs is warranted to explore this possibility.

Some further work can be done to improve the calculation of MIDs and exchange fluxes used to estimate intracellular fluxes for the clones on days 4 and 7. For the MID calculations, corrections for natural isotope abundance could improve accuracy. Ideally, pure chemical standards would be analyzed using these same LC-MS methods in product ion mode to generate isotope distributions that could be used for correction (Midani et al., 2017). Known natural abundance values could also be used, although in this experiment, due to the low uptake and metabolism of the labeled citrate, the impact on overall analysis may be minimal. The exchange fluxes were calculated by obtaining metabolite concentrations supernatant samples from these two timepoints and performing a regression between them, accounting for viable cell densities and feeds. If sample analysis

capability is not a constraint, future work could consider flux changes over time to provide greater accuracy by calculating a separate set of fluxes for each timepoint, for example one set from days 3 to 5 and another set from days 6 to 8. However, in this work, due to sample availability, only one set of fluxes was obtained for each clone. Also, input fluxes could be further improved by incorporating cell dry weights, either by using an approximation such as 0.25*cell volume based on cell diameters, or by empirical measurements (Niklas et al., 2011). Nevertheless, the MIDs and fluxes used in this work helped us gain interesting insights into productivity differences among clones.

We found that rather than increasing qP by directly entering the TCA cycle as a substrate, citrate addition led to increased glucogenic fluxes from isoleucine, phenylalanine, and tyrosine, decreased ketogenic flux from leucine, and increased flux through the α-KG-malate transporter for clones that responded positively. Further elucidation of these pathways and citrate's role as a regulatory molecule could provide engineering targets for additional cell line improvements.

3.6 Acknowledgements

I would like to thank Karin Yanagi for her help with processing mass spectrometry data in Skyline.

References

Borst, P. (2020). The malate–aspartate shuttle (Borst cycle): How it started and developed into a major metabolic pathway. *IUBMB Life, 72*(11), 2241-2259. doi:https://doi.org/10.1002/iub.2367

Carinhas, N., Duarte, T. M., Barreiro, L. C., Carrondo, M. J. T., Alves, P. M., & Teixeira, A. P. (2013). Metabolic signatures of GS-CHO cell clones associated with butyrate treatment and culture phase transition. *Biotechnology and Bioengineering, 110*(12), 3244-3257. doi:doi:10.1002/bit.24983

Chen, Y., McConnell, B., Dhara, G., Naik, H. M., Li, C.-T., Antoniewicz, M., & Betenbaugh, M. (2019). An unconventional uptake rate objective function approach enhances applicability of genome-scale models for mammalian cells. *npj Systems Biology and Applications, 5*. doi:10.1038/s41540-019-0103-6

Chong, W., Reddy, S., Yusufi, F., Lee, D.-Y., Wong, N., Heng, C.-K., . . . Ho, Y. (2010). Metabolomics-driven approach for the improvement of Chinese hamster ovary cell growth: Overexpression of malate dehydrogenase II. *Journal of Biotechnology, 147*, 116-121. doi:10.1016/j.jbiotec.2010.03.018

Coulet, M., Kepp, O., Kroemer, G., & Basmaciogullari, S. (2022). Metabolic Profiling of CHO Cells during the Production of Biotherapeutics. *Cells, 11*(12). doi:10.3390/cells11121929

Frezza, C. (2017). Mitochondrial metabolites: undercover signalling molecules. *Interface Focus, 7*(2), 20160100. doi:doi:10.1098/rsfs.2016.0100

Gilbert, A., McElearney, K., Kshirsagar, R., Sinacore, M. S., & Ryll, T. (2013). Investigation of metabolic variability observed in extended fed batch cell culture. *Biotechnol Prog, 29*(6), 1519-1527. doi:10.1002/btpr.1787

Harrington, C., Jacobs, M., Bethune, Q., Kalomeris, T., Hiller, G. W., & Mulukutla, B. C. (2021). Production of butyrate and branched-chain amino acid catabolic byproducts by CHO cells in fed-batch culture enhances their specific productivity. *Biotechnol Bioeng, 118*(12), 4786-4799. doi:10.1002/bit.27942

Iacobazzi, V., & Infantino, V. (2014). Citrate--new functions for an old metabolite. *Biol Chem, 395*(4), 387-399. doi:10.1515/hsz-2013-0271

Lasorsa, F. M., Pinton, P., Palmieri, L., Fiermonte, G., Rizzuto, R., & Palmieri, F. (2003). Recombinant Expression of the Ca2+-sensitive Aspartate/Glutamate Carrier Increases Mitochondrial ATP Production in Agonist-stimulated Chinese Hamster Ovary Cells*. *Journal of Biological Chemistry, 278*(40), 38686-38692. doi:https://doi.org/10.1074/jbc.M304988200

Le, H., Kabbur, S., Pollastrini, L., Sun, Z., Mills, K., Johnson, K., . . . Hu, W. S. (2012). Multivariate analysis of cell culture bioprocess data--lactate consumption as process indicator. *J Biotechnol, 162*(2-3), 210-223. doi:10.1016/j.jbiotec.2012.08.021

Matthews, D. E. (2007). An Overview of Phenylalanine and Tyrosine Kinetics in Humans. *The Journal of Nutrition, 137*(6), 1549S-1555S. doi:10.1093/jn/137.6.1549S

Matuszczyk, J.-C., Teleki, A., Pfizenmaier, J., & Takors, R. (2015). Compartment-specific metabolomics for CHO reveals that ATP pools in mitochondria are much lower than in cytosol. *Biotechnol J, 10*(10), 1639-1650. doi:https://doi.org/10.1002/biot.201500060

Midani, F. S., Wynn, M. L., & Schnell, S. (2017). The importance of accurately correcting for the natural abundance of stable isotopes. *Anal Biochem, 520*, 27-43. doi:10.1016/j.ab.2016.12.011

Mulukutla, B. C., Kale, J., Kalomeris, T., Jacobs, M., & Hiller, G. W. (2017). Identification and control of novel growth inhibitors in fed-batch cultures of Chinese hamster ovary cells. *Biotechnol Bioeng, 114*(8), 1779-1790. doi:10.1002/bit.26313

Mulukutla, B. C., Mitchell, J., Geoffroy, P., Harrington, C., Krishnan, M., Kalomeris, T., . . . Hiller, G. W. (2019). Metabolic engineering of Chinese hamster ovary cells towards reduced biosynthesis and accumulation of novel growth inhibitors in fed-batch cultures. *Metabolic Engineering, 54*, 54-68. doi:https://doi.org/10.1016/j.ymben.2019.03.001

Niklas, J., Schräder, E., Sandig, V., Noll, T., & Heinzle, E. (2011). Quantitative characterization of metabolism and metabolic shifts during growth of the new human cell line AGE1.HN using time resolved metabolic flux analysis. *Bioprocess Biosyst Eng, 34*(5), 533-545. doi:10.1007/s00449-010-0502-y

Pereira, S., Kildegaard, H. F., & Andersen, M. R. (2018). Impact of CHO Metabolism on Cell Growth and Protein Production: An Overview of Toxic and Inhibiting Metabolites and Nutrients. *Biotechnol J, 13*(3), e1700499. doi:10.1002/biot.201700499

Pino, L. K., Searle, B. C., Bollinger, J. G., Nunn, B., MacLean, B., & MacCoss, M. J. (2020). The Skyline ecosystem: Informatics for quantitative mass spectrometry proteomics. *Mass Spectrom Rev, 39*(3), 229-244. doi:10.1002/mas.21540

Popp, O., Müller, D., Didzus, K., Paul, W., Lipsmeier, F., Kirchner, F., . . . Beaucamp, N. (2016). A hybrid approach identifies metabolic signatures of high-producers for chinese hamster ovary clone selection and process optimization. *Biotechnol Bioeng, 113*(9), 2005-2019. doi:10.1002/bit.25958

Reinhart, D., Damjanovic, L., Kaisermayer, C., Sommeregger, W., Gili, A., Gasselhuber, B., . . . Kunert, R. (2019). Bioprocessing of Recombinant CHO-K1, CHO-DG44, and CHO-S:

CHO Expression Hosts Favor Either mAb Production or Biomass Synthesis. *Biotechnol J, 14*(3), 1700686. doi:https://doi.org/10.1002/biot.201700686

Si, Y., Shi, H., & Lee, K. (2009). Impact of perturbed pyruvate metabolism on adipocyte triglyceride accumulation. *Metab Eng, 11*(6), 382-390. doi:10.1016/j.ymben.2009.08.001

Templeton, N., Dean, J., Reddy, P., & Young, J. D. (2013). Peak antibody production is associated with increased oxidative metabolism in an industrially relevant fed-batch CHO cell culture. *Biotechnol Bioeng, 110*(7), 2013-2024. doi:10.1002/bit.24858

Templeton, N., Smith, K. D., McAtee-Pereira, A. G., Dorai, H., Betenbaugh, M. J., Lang, S. E., & Young, J. D. (2017). Application of (13)C flux analysis to identify high-productivity CHO metabolic phenotypes. *Metab Eng, 43*(Pt B), 218-225. doi:10.1016/j.ymben.2017.01.008

Templeton, N., Xu, S., Roush, D. J., & Chen, H. (2017). (13)C metabolic flux analysis identifies limitations to increasing specific productivity in fed-batch and perfusion. *Metab Eng, 44*, 126-133. doi:10.1016/j.ymben.2017.09.010

Williamson, D. H. (1998). KETOSIS*. In B. Caballero (Ed.), *Encyclopedia of Human Nutrition (Second Edition)* (pp. 91-98). Oxford: Elsevier.

Xing, Z., Kenty, B., Koyrakh, I., Borys, M., Pan, S.-H., & Li, Z. J. (2011). Optimizing amino acid composition of CHO cell culture media for a fusion protein production. *Process Biochemistry, 46*(7), 1423-1429. doi:https://doi.org/10.1016/j.procbio.2011.03.014

Xu, S., Hoshan, L., & Chen, H. (2016). Improving lactate metabolism in an intensified CHO culture process: productivity and product quality considerations. *Bioprocess and Biosystems Engineering, 39*(11), 1689-1702. doi:10.1007/s00449-016-1644-3

Yao, G., Aron, K., Borys, M., Li, Z., Pendse, G., & Lee, K. (2021). A Metabolomics Approach to Increasing Chinese Hamster Ovary (CHO) Cell Productivity. *Metabolites, 11*(12), 823. Retrieved from https://www.mdpi.com/2218-1989/11/12/823

Zhang, X., Jiang, R., Lin, H., & Xu, S. (2020). Feeding tricarboxylic acid cycle intermediates improves lactate consumption and antibody production in Chinese hamster ovary cell cultures. *Biotechnol Prog, n/a*(n/a), e2975. doi:10.1002/btpr.2975

3.7 Supplementary Information

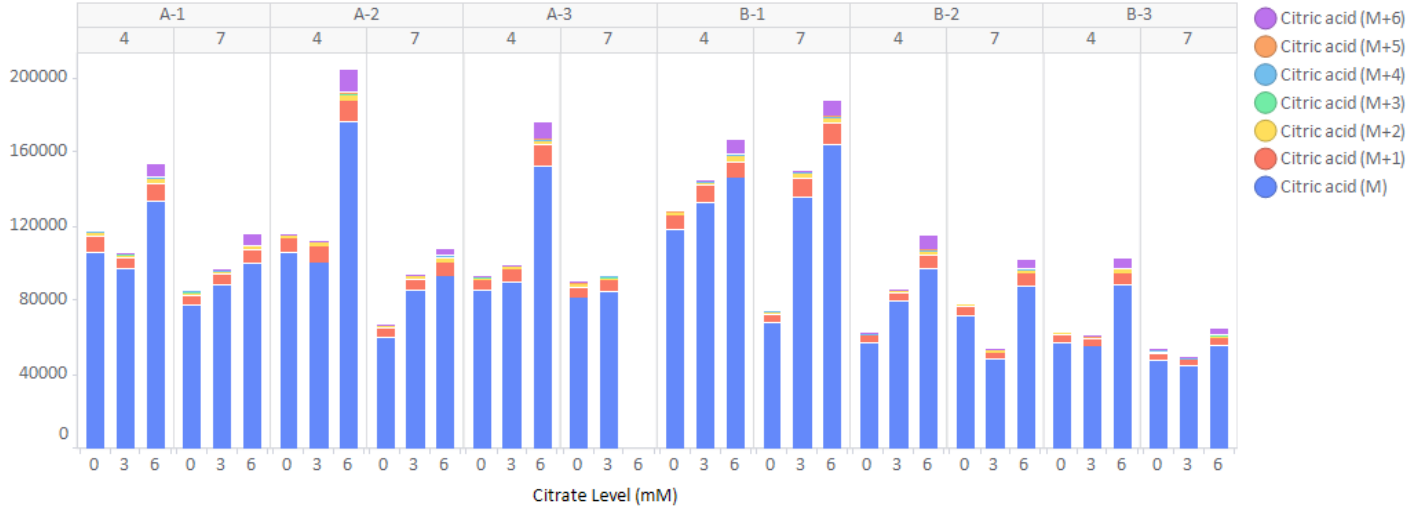

Figure S1. Citric acid isotopologue AUCs from cell pellet samples on days 4 and 7.

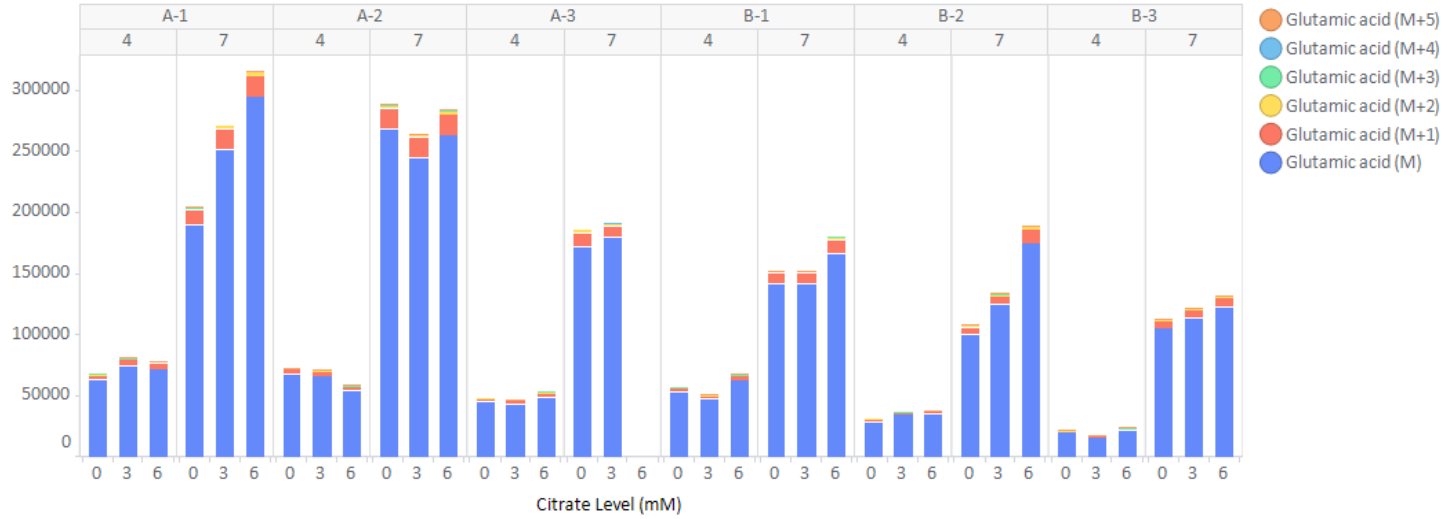

Figure S2. Glutamic acid isotopologue AUCs from cell pellet samples on days 4 and 7.

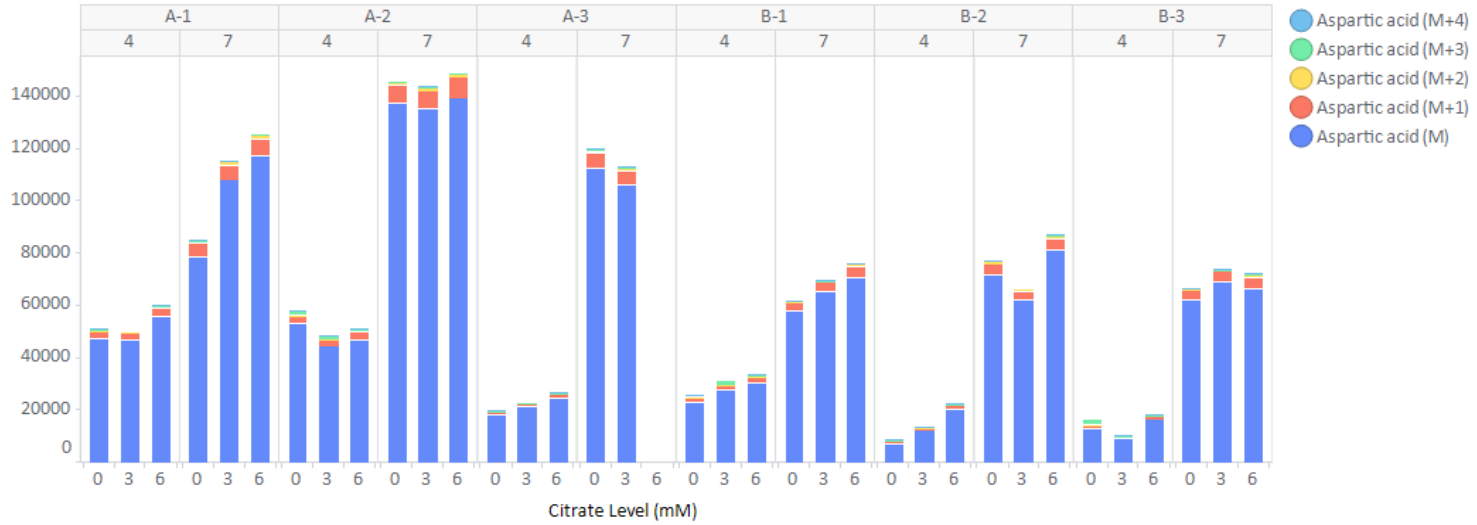

Figure S3. Aspartic acid isotopologue AUCs from cell pellet samples on days 4 and 7.

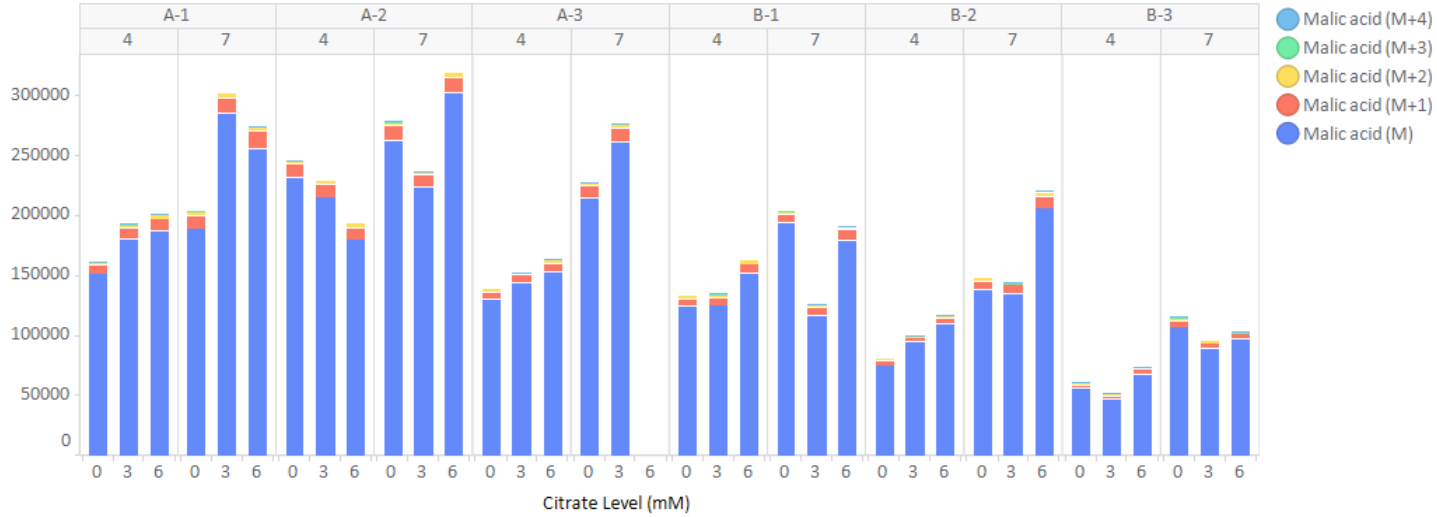

Figure S4. Malic acid isotopologue AUCs from cell pellet samples on days 4 and 7.

Table S1. Retention times and precursor-product transitions used for peak selection. Although peaks were integrated for each of these transitions, they were not all ultimately used in the final analysis because some metabolite isotopologues had overlapping mz at the same retention time so could not be distinguished from each other.

Molecule	Retention Time (min)	Precursor Adduct	Precursor Mz	Fragment Ion	Product Adduct	Product Mz
Citric acid	20.4	[M-H]	191.020	M	[M-H]	111.009
		[M-1C+1C'-H]	192.023	M	[M-H]	111.009
		[M-1C+1C'-H]	192.023	M+1	[M-1C+1C'-H]	112.012
		[M-2C+2C'-H]	193.026	M	[M-H]	111.009
		[M-2C+2C'-H]	193.026	M+1	[M-1C+1C'-H]	112.012
		[M-2C+2C'-H]	193.026	M+2	[M-2C+2C'-H]	113.015
		[M-3C+3C'-H]	194.030	M	[M-H]	111.009
		[M-3C+3C'-H]	194.030	M+1	[M-1C+1C'-H]	112.012
		[M-3C+3C'-H]	194.030	M+2	[M-2C+2C'-H]	113.015
		[M-3C+3C'-H]	194.030	M+3	[M-3C+3C'-H]	114.019
		[M-4C+4C'-H]	195.033	M	[M-H]	111.009
		[M-4C+4C'-H]	195.033	M+1	[M-1C+1C'-H]	112.012
		[M-4C+4C'-H]	195.033	M+2	[M-2C+2C'-H]	113.015
		[M-4C+4C'-H]	195.033	M+3	[M-3C+3C'-H]	114.019
		[M-4C+4C'-H]	195.033	M+4	[M-4C+4C'-H]	115.022
		[M-5C+5C'-H]	196.037	M	[M-H]	111.009
		[M-5C+5C'-H]	196.037	M+1	[M-1C+1C'-H]	112.012
		[M-5C+5C'-H]	196.037	M+2	[M-2C+2C'-H]	113.015
		[M-5C+5C'-H]	196.037	M+3	[M-3C+3C'-H]	114.019
		[M-5C+5C'-H]	196.037	M+4	[M-4C+4C'-H]	115.022
		[M-5C+5C'-H]	196.037	M+5	[M-5C+5C'-H]	116.026
		[M-6C+6C'-H]	197.040	M	[M-H]	111.009
		[M-6C+6C'-H]	197.040	M+1	[M-1C+1C'-H]	112.012
		[M-6C+6C'-H]	197.040	M+2	[M-2C+2C'-H]	113.015
		[M-6C+6C'-H]	197.040	M+3	[M-3C+3C'-H]	114.019
		[M-6C+6C'-H]	197.040	M+4	[M-4C+4C'-H]	115.022
		[M-6C+6C'-H]	197.040	M+5	[M-5C+5C'-H]	116.026
Fumaric acid	19.2	[M-H]	115.004	M	[M-H]	71.014
		[M-1C+1C'-H]	116.007	M	[M-H]	71.014
		[M-1C+1C'-H]	116.007	M+1	[M-1C+1C'-H]	72.017
		[M-2C+2C'-H]	117.010	M	[M-H]	71.014
		[M-2C+2C'-H]	117.010	M+1	[M-1C+1C'-H]	72.017
		[M-2C+2C'-H]	117.010	M+2	[M-2C+2C'-H]	73.021
		[M-3C+3C'-H]	118.014	M	[M-H]	71.014
		[M-3C+3C'-H]	118.014	M+1	[M-1C+1C'-H]	72.017

		[M-3C+3C'-H]	118.014	M+2	[M-2C+2C'-H]	73.021
		[M-3C+3C'-H]	118.014	M+3	[M-3C+3C'-H]	74.024
		[M-4C+4C'-H]	119.017	M	[M-H]	71.014
		[M-4C+4C'-H]	119.017	M+1	[M-1C+1C'-H]	72.017
		[M-4C+4C'-H]	119.017	M+2	[M-2C+2C'-H]	73.021
		[M-4C+4C'-H]	119.017	M+3	[M-3C+3C'-H]	74.024
Glutamic acid	15.3	[M-H]	146.046	M	[M-H]	102.056
		[M-1C+1C'-H]	147.049	M	[M-H]	102.056
		[M-1C+1C'-H]	147.049	M+1	[M-1C+1C'-H]	103.059
		[M-2C+2C'-H]	148.053	M	[M-H]	102.056
		[M-2C+2C'-H]	148.053	M+1	[M-1C+1C'-H]	103.059
		[M-2C+2C'-H]	148.053	M+2	[M-2C+2C'-H]	104.063
		[M-3C+3C'-H]	149.056	M	[M-H]	102.056
		[M-3C+3C'-H]	149.056	M+1	[M-1C+1C'-H]	103.059
		[M-3C+3C'-H]	149.056	M+2	[M-2C+2C'-H]	104.063
		[M-3C+3C'-H]	149.056	M+3	[M-3C+3C'-H]	105.066
		[M-4C+4C'-H]	150.059	M	[M-H]	102.056
		[M-4C+4C'-H]	150.059	M+1	[M-1C+1C'-H]	103.059
		[M-4C+4C'-H]	150.059	M+2	[M-2C+2C'-H]	104.063
		[M-4C+4C'-H]	150.059	M+3	[M-3C+3C'-H]	105.066
		[M-4C+4C'-H]	150.059	M+4	[M-4C+4C'-H]	106.069
		[M-5C+5C'-H]	151.063	M	[M-H]	102.056
		[M-5C+5C'-H]	151.063	M+1	[M-1C+1C'-H]	103.059
		[M-5C+5C'-H]	151.063	M+2	[M-2C+2C'-H]	104.063
		[M-5C+5C'-H]	151.063	M+3	[M-3C+3C'-H]	105.066
		[M-5C+5C'-H]	151.063	M+4	[M-4C+4C'-H]	106.069
		[M-5C+5C'-H]	151.063	M+5	[M-5C+5C'-H]	107.073
Malic acid	19.2	[M-H]	133.014	M	[M-H]	115.004
		[M-1C+1C'-H]	134.018	M	[M-H]	115.004
		[M-1C+1C'-H]	134.018	M+1	[M-1C+1C'-H]	116.007
		[M-2C+2C'-H]	135.021	M	[M-H]	115.004
		[M-2C+2C'-H]	135.021	M+1	[M-1C+1C'-H]	116.007
		[M-2C+2C'-H]	135.021	M+2	[M-2C+2C'-H]	117.010
		[M-3C+3C'-H]	136.024	M	[M-H]	115.004
		[M-3C+3C'-H]	136.024	M+1	[M-1C+1C'-H]	116.007
		[M-3C+3C'-H]	136.024	M+2	[M-2C+2C'-H]	117.010
		[M-3C+3C'-H]	136.024	M+3	[M-3C+3C'-H]	118.014
		[M-4C+4C'-H]	137.028	M	[M-H]	115.004
		[M-4C+4C'-H]	137.028	M+1	[M-1C+1C'-H]	116.007
		[M-4C+4C'-H]	137.028	M+2	[M-2C+2C'-H]	117.010
		[M-4C+4C'-H]	137.028	M+3	[M-3C+3C'-H]	118.014

		[M-4C+4C'-H]	137.028	M+4	[M-4C+4C'-H]	119.017
Aspartic Acid	15.3	[M-H]	132.030	M	[M-H]	88.040
		[M-1C+1C'-H]	133.034	M	[M-H]	88.040
		[M-1C+1C'-H]	133.034	M+1	[M-1C+1C'-H]	89.044
		[M-2C+2C'-H]	134.037	M	[M-H]	88.040
		[M-2C+2C'-H]	134.037	M+1	[M-1C+1C'-H]	89.044
		[M-2C+2C'-H]	134.037	M+2	[M-2C+2C'-H]	90.047
		[M-3C+3C'-H]	135.040	M	[M-H]	88.040
		[M-3C+3C'-H]	135.040	M+1	[M-1C+1C'-H]	89.044
		[M-3C+3C'-H]	135.040	M+2	[M-2C+2C'-H]	90.047
		[M-3C+3C'-H]	135.040	M+3	[M-3C+3C'-H]	91.050
		[M-4C+4C'-H]	136.044	M	[M-H]	88.040
		[M-4C+4C'-H]	136.044	M+1	[M-1C+1C'-H]	89.044
		[M-4C+4C'-H]	136.044	M+2	[M-2C+2C'-H]	90.047
		[M-4C+4C'-H]	136.044	M+3	[M-3C+3C'-H]	91.050
Succinic acid	19.2	[M-H]	117.019	M	[M-H]	73.030
		[M-1C+1C'-H]	118.023	M	[M-H]	73.030
		[M-1C+1C'-H]	118.023	M+1	[M-1C+1C'-H]	74.033
		[M-2C+2C'-H]	119.026	M	[M-H]	73.030
		[M-2C+2C'-H]	119.026	M+1	[M-1C+1C'-H]	74.033
		[M-2C+2C'-H]	119.026	M+2	[M-2C+2C'-H]	75.036
		[M-3C+3C'-H]	120.029	M	[M-H]	73.030
		[M-3C+3C'-H]	120.029	M+1	[M-1C+1C'-H]	74.033
		[M-3C+3C'-H]	120.029	M+2	[M-2C+2C'-H]	75.036
		[M-3C+3C'-H]	120.029	M+3	[M-3C+3C'-H]	76.040
		[M-4C+4C'-H]	121.033	M	[M-H]	73.030
		[M-4C+4C'-H]	121.033	M+1	[M-1C+1C'-H]	74.033
		[M-4C+4C'-H]	121.033	M+2	[M-2C+2C'-H]	75.036
		[M-4C+4C'-H]	121.033	M+3	[M-3C+3C'-H]	76.040
a-Ketoglutaric acid	19.2	[M-H]	145.014	M	[M-H]	101.024
		[M-1C+1C'-H]	146.018	M	[M-H]	101.024
		[M-1C+1C'-H]	146.018	M+1	[M-1C+1C'-H]	102.028
		[M-2C+2C'-H]	147.021	M	[M-H]	101.024
		[M-2C+2C'-H]	147.021	M+1	[M-1C+1C'-H]	102.028
		[M-2C+2C'-H]	147.021	M+2	[M-2C+2C'-H]	103.031
		[M-3C+3C'-H]	148.024	M	[M-H]	101.024
		[M-3C+3C'-H]	148.024	M+1	[M-1C+1C'-H]	102.028
		[M-3C+3C'-H]	148.024	M+2	[M-2C+2C'-H]	103.031
		[M-3C+3C'-H]	148.024	M+3	[M-3C+3C'-H]	104.034
		[M-4C+4C'-H]	149.028	M	[M-H]	101.024
		[M-4C+4C'-H]	149.028	M+1	[M-1C+1C'-H]	102.028

		[M-4C+4C'-H]	149.028	M+2	[M-2C+2C'-H]	103.031
		[M-4C+4C'-H]	149.028	M+3	[M-3C+3C'-H]	104.034
		[M-4C+4C'-H]	149.028	M+4	[M-4C+4C'-H]	105.038
		[M-5C+5C'-H]	150.031	M	[M-H]	101.024
		[M-5C+5C'-H]	150.031	M+1	[M-1C+1C'-H]	102.028
		[M-5C+5C'-H]	150.031	M+2	[M-2C+2C'-H]	103.031
		[M-5C+5C'-H]	150.031	M+3	[M-3C+3C'-H]	104.034
		[M-5C+5C'-H]	150.031	M+4	[M-4C+4C'-H]	105.038
Palmitic acid	8.4	[M-H]	255.233	M	[M-H]	237.222
		[M-1C+1C'-H]	256.236	M	[M-H]	237.222
		[M-1C+1C'-H]	256.236	M+1	[M-1C+1C'-H]	238.226
		[M-2C+2C'-H]	257.240	M	[M-H]	237.222
		[M-2C+2C'-H]	257.240	M+1	[M-1C+1C'-H]	238.226
		[M-2C+2C'-H]	257.240	M+2	[M-2C+2C'-H]	239.229
		[M-3C+3C'-H]	258.243	M	[M-H]	237.222
		[M-3C+3C'-H]	258.243	M+1	[M-1C+1C'-H]	238.226
		[M-3C+3C'-H]	258.243	M+2	[M-2C+2C'-H]	239.229
		[M-3C+3C'-H]	258.243	M+3	[M-3C+3C'-H]	240.232
		[M-4C+4C'-H]	259.246	M	[M-H]	237.222
		[M-4C+4C'-H]	259.246	M+1	[M-1C+1C'-H]	238.226
		[M-4C+4C'-H]	259.246	M+2	[M-2C+2C'-H]	239.229
		[M-4C+4C'-H]	259.246	M+3	[M-3C+3C'-H]	240.232
		[M-4C+4C'-H]	259.246	M+4	[M-4C+4C'-H]	241.236
		[M-5C+5C'-H]	260.250	M	[M-H]	237.222
		[M-5C+5C'-H]	260.250	M+1	[M-1C+1C'-H]	238.226
		[M-5C+5C'-H]	260.250	M+2	[M-2C+2C'-H]	239.229
		[M-5C+5C'-H]	260.250	M+3	[M-3C+3C'-H]	240.232
		[M-5C+5C'-H]	260.250	M+4	[M-4C+4C'-H]	241.236
		[M-5C+5C'-H]	260.250	M+5	[M-5C+5C'-H]	242.239
		[M-6C+6C'-H]	261.253	M	[M-H]	237.222
		[M-6C+6C'-H]	261.253	M+1	[M-1C+1C'-H]	238.226
		[M-6C+6C'-H]	261.253	M+2	[M-2C+2C'-H]	239.229
		[M-6C+6C'-H]	261.253	M+3	[M-3C+3C'-H]	240.232
		[M-6C+6C'-H]	261.253	M+4	[M-4C+4C'-H]	241.236
		[M-6C+6C'-H]	261.253	M+5	[M-5C+5C'-H]	242.239
		[M-6C+6C'-H]	261.253	M+6	[M-6C+6C'-H]	243.243
		[M-7C+7C'-H]	262.256	M	[M-H]	237.222
		[M-7C+7C'-H]	262.256	M+1	[M-1C+1C'-H]	238.226
		[M-7C+7C'-H]	262.256	M+2	[M-2C+2C'-H]	239.229
		[M-7C+7C'-H]	262.256	M+3	[M-3C+3C'-H]	240.232
		[M-7C+7C'-H]	262.256	M+4	[M-4C+4C'-H]	241.236

		[M-7C+7C'-H]	262.256	M+5	[M-5C+5C'-H]	242.239
		[M-7C+7C'-H]	262.256	M+6	[M-6C+6C'-H]	243.243
		[M-7C+7C'-H]	262.256	M+7	[M-7C+7C'-H]	244.246
		[M-8C+8C'-H]	263.260	M	[M-H]	237.222
		[M-8C+8C'-H]	263.260	M+1	[M-1C+1C'-H]	238.226
		[M-8C+8C'-H]	263.260	M+2	[M-2C+2C'-H]	239.229
		[M-8C+8C'-H]	263.260	M+3	[M-3C+3C'-H]	240.232
		[M-8C+8C'-H]	263.260	M+4	[M-4C+4C'-H]	241.236
		[M-8C+8C'-H]	263.260	M+5	[M-5C+5C'-H]	242.239
		[M-8C+8C'-H]	263.260	M+6	[M-6C+6C'-H]	243.243
		[M-8C+8C'-H]	263.260	M+7	[M-7C+7C'-H]	244.246
		[M-8C+8C'-H]	263.260	M+8	[M-8C+8C'-H]	245.249
		[M-9C+9C'-H]	264.263	M	[M-H]	237.222
		[M-9C+9C'-H]	264.263	M+1	[M-1C+1C'-H]	238.226
		[M-9C+9C'-H]	264.263	M+2	[M-2C+2C'-H]	239.229
		[M-9C+9C'-H]	264.263	M+3	[M-3C+3C'-H]	240.232
		[M-9C+9C'-H]	264.263	M+4	[M-4C+4C'-H]	241.236
		[M-9C+9C'-H]	264.263	M+5	[M-5C+5C'-H]	242.239
		[M-9C+9C'-H]	264.263	M+6	[M-6C+6C'-H]	243.243
		[M-9C+9C'-H]	264.263	M+7	[M-7C+7C'-H]	244.246
		[M-9C+9C'-H]	264.263	M+8	[M-8C+8C'-H]	245.249
		[M-9C+9C'-H]	264.263	M+9	[M-9C+9C'-H]	246.253
		[M-10C+10C'-H]	265.267	M	[M-H]	237.222
		[M-10C+10C'-H]	265.267	M+1	[M-1C+1C'-H]	238.226
		[M-10C+10C'-H]	265.267	M+10	[M-10C+10C'-H]	247.256
		[M-10C+10C'-H]	265.267	M+2	[M-2C+2C'-H]	239.229
		[M-10C+10C'-H]	265.267	M+3	[M-3C+3C'-H]	240.232
		[M-10C+10C'-H]	265.267	M+4	[M-4C+4C'-H]	241.236
		[M-10C+10C'-H]	265.267	M+5	[M-5C+5C'-H]	242.239
		[M-10C+10C'-H]	265.267	M+6	[M-6C+6C'-H]	243.243
		[M-10C+10C'-H]	265.267	M+7	[M-7C+7C'-H]	244.246
		[M-10C+10C'-H]	265.267	M+8	[M-8C+8C'-H]	245.249
		[M-10C+10C'-H]	265.267	M+9	[M-9C+9C'-H]	246.253
		[M-11C+11C'-H]	266.270	M	[M-H]	237.222
		[M-11C+11C'-H]	266.270	M+1	[M-1C+1C'-H]	238.226
		[M-11C+11C'-H]	266.270	M+10	[M-10C+10C'-H]	247.256
		[M-11C+11C'-H]	266.270	M+11	[M-11C+11C'-H]	248.259
		[M-11C+11C'-H]	266.270	M+2	[M-2C+2C'-H]	239.229
		[M-11C+11C'-H]	266.270	M+3	[M-3C+3C'-H]	240.232
		[M-11C+11C'-H]	266.270	M+4	[M-4C+4C'-H]	241.236
		[M-11C+11C'-H]	266.270	M+5	[M-5C+5C'-H]	242.239

		[M-11C+11C'-H]	266.270	M+6	[M-6C+6C'-H]	243.243
		[M-11C+11C'-H]	266.270	M+7	[M-7C+7C'-H]	244.246
		[M-11C+11C'-H]	266.270	M+8	[M-8C+8C'-H]	245.249
		[M-11C+11C'-H]	266.270	M+9	[M-9C+9C'-H]	246.253
		[M-12C+12C'-H]	267.273	M	[M-H]	237.222
		[M-12C+12C'-H]	267.273	M+1	[M-1C+1C'-H]	238.226
		[M-12C+12C'-H]	267.273	M+10	[M-10C+10C'-H]	247.256
		[M-12C+12C'-H]	267.273	M+11	[M-11C+11C'-H]	248.259
		[M-12C+12C'-H]	267.273	M+12	[M-12C+12C'-H]	249.263
		[M-12C+12C'-H]	267.273	M+2	[M-2C+2C'-H]	239.229
		[M-12C+12C'-H]	267.273	M+3	[M-3C+3C'-H]	240.232
		[M-12C+12C'-H]	267.273	M+4	[M-4C+4C'-H]	241.236
		[M-12C+12C'-H]	267.273	M+5	[M-5C+5C'-H]	242.239
		[M-12C+12C'-H]	267.273	M+6	[M-6C+6C'-H]	243.243
		[M-12C+12C'-H]	267.273	M+7	[M-7C+7C'-H]	244.246
		[M-12C+12C'-H]	267.273	M+8	[M-8C+8C'-H]	245.249
		[M-12C+12C'-H]	267.273	M+9	[M-9C+9C'-H]	246.253
		[M-13C+13C'-H]	268.277	M	[M-H]	237.222
		[M-13C+13C'-H]	268.277	M+1	[M-1C+1C'-H]	238.226
		[M-13C+13C'-H]	268.277	M+10	[M-10C+10C'-H]	247.256
		[M-13C+13C'-H]	268.277	M+11	[M-11C+11C'-H]	248.259
		[M-13C+13C'-H]	268.277	M+12	[M-12C+12C'-H]	249.263
		[M-13C+13C'-H]	268.277	M+13	[M-13C+13C'-H]	250.266
		[M-13C+13C'-H]	268.277	M+2	[M-2C+2C'-H]	239.229
		[M-13C+13C'-H]	268.277	M+3	[M-3C+3C'-H]	240.232
		[M-13C+13C'-H]	268.277	M+4	[M-4C+4C'-H]	241.236
		[M-13C+13C'-H]	268.277	M+5	[M-5C+5C'-H]	242.239
		[M-13C+13C'-H]	268.277	M+6	[M-6C+6C'-H]	243.243
		[M-13C+13C'-H]	268.277	M+7	[M-7C+7C'-H]	244.246
		[M-13C+13C'-H]	268.277	M+8	[M-8C+8C'-H]	245.249
		[M-13C+13C'-H]	268.277	M+9	[M-9C+9C'-H]	246.253
		[M-14C+14C'-H]	269.280	M	[M-H]	237.222
		[M-14C+14C'-H]	269.280	M+1	[M-1C+1C'-H]	238.226
		[M-14C+14C'-H]	269.280	M+10	[M-10C+10C'-H]	247.256
		[M-14C+14C'-H]	269.280	M+11	[M-11C+11C'-H]	248.259
		[M-14C+14C'-H]	269.280	M+12	[M-12C+12C'-H]	249.263
		[M-14C+14C'-H]	269.280	M+13	[M-13C+13C'-H]	250.266
		[M-14C+14C'-H]	269.280	M+14	[M-14C+14C'-H]	251.269
		[M-14C+14C'-H]	269.280	M+2	[M-2C+2C'-H]	239.229
		[M-14C+14C'-H]	269.280	M+3	[M-3C+3C'-H]	240.232
		[M-14C+14C'-H]	269.280	M+4	[M-4C+4C'-H]	241.236

		[M-14C+14C'-H]	269.280	M+5	[M-5C+5C'-H]	242.239
		[M-14C+14C'-H]	269.280	M+6	[M-6C+6C'-H]	243.243
		[M-14C+14C'-H]	269.280	M+7	[M-7C+7C'-H]	244.246
		[M-14C+14C'-H]	269.280	M+8	[M-8C+8C'-H]	245.249
		[M-14C+14C'-H]	269.280	M+9	[M-9C+9C'-H]	246.253
		[M-15C+15C'-H]	270.283	M	[M-H]	237.222
		[M-15C+15C'-H]	270.283	M+1	[M-1C+1C'-H]	238.226
		[M-15C+15C'-H]	270.283	M+10	[M-10C+10C'-H]	247.256
		[M-15C+15C'-H]	270.283	M+11	[M-11C+11C'-H]	248.259
		[M-15C+15C'-H]	270.283	M+12	[M-12C+12C'-H]	249.263
		[M-15C+15C'-H]	270.283	M+13	[M-13C+13C'-H]	250.266
		[M-15C+15C'-H]	270.283	M+14	[M-14C+14C'-H]	251.269
		[M-15C+15C'-H]	270.283	M+15	[M-15C+15C'-H]	252.273
		[M-15C+15C'-H]	270.283	M+2	[M-2C+2C'-H]	239.229
		[M-15C+15C'-H]	270.283	M+3	[M-3C+3C'-H]	240.232
		[M-15C+15C'-H]	270.283	M+4	[M-4C+4C'-H]	241.236
		[M-15C+15C'-H]	270.283	M+5	[M-5C+5C'-H]	242.239
		[M-15C+15C'-H]	270.283	M+6	[M-6C+6C'-H]	243.243
		[M-15C+15C'-H]	270.283	M+7	[M-7C+7C'-H]	244.246
		[M-15C+15C'-H]	270.283	M+8	[M-8C+8C'-H]	245.249
		[M-15C+15C'-H]	270.283	M+9	[M-9C+9C'-H]	246.253
		[M-16C+16C'-H]	271.287	M	[M-H]	237.222
		[M-16C+16C'-H]	271.287	M+1	[M-1C+1C'-H]	238.226
		[M-16C+16C'-H]	271.287	M+10	[M-10C+10C'-H]	247.256
		[M-16C+16C'-H]	271.287	M+11	[M-11C+11C'-H]	248.259
		[M-16C+16C'-H]	271.287	M+12	[M-12C+12C'-H]	249.263
		[M-16C+16C'-H]	271.287	M+13	[M-13C+13C'-H]	250.266
		[M-16C+16C'-H]	271.287	M+14	[M-14C+14C'-H]	251.269
		[M-16C+16C'-H]	271.287	M+15	[M-15C+15C'-H]	252.273
		[M-16C+16C'-H]	271.287	M+16	[M-16C+16C'-H]	253.276
		[M-16C+16C'-H]	271.287	M+2	[M-2C+2C'-H]	239.229
		[M-16C+16C'-H]	271.287	M+3	[M-3C+3C'-H]	240.232
		[M-16C+16C'-H]	271.287	M+4	[M-4C+4C'-H]	241.236
		[M-16C+16C'-H]	271.287	M+5	[M-5C+5C'-H]	242.239
		[M-16C+16C'-H]	271.287	M+6	[M-6C+6C'-H]	243.243
		[M-16C+16C'-H]	271.287	M+7	[M-7C+7C'-H]	244.246
		[M-16C+16C'-H]	271.287	M+8	[M-8C+8C'-H]	245.249
		[M-16C+16C'-H]	271.287	M+9	[M-9C+9C'-H]	246.253

Table S2. Reactions and estimated fluxes. Average of 20 iterations of flux estimation based on MIDs of glutamate, citrate, and malate and 20 highlighted exchange fluxes. Bolded metabolites are extracellular.

			Day 4					Day 7				
	Pathway	**Reaction**	**A-1**	**A-2**	**B-1**	**B-2**	**B-3**	**A-1**	**A-2**	**B-1**	**B-2**	**B-3**
1	Glycolysis	**Glucose** + ATP = Glucose 6-P + ADP	3.24E+01	1.15E+01	1.44E+01	1.01E+01	7.62E+00	3.24E+01	1.15E+01	1.44E+01	1.01E+01	7.61E+00
2	Glycolysis	Glucose 6-P = Fructose 6-P	1.22E+01	2.19E+00	2.82E+00	1.28E+00	4.55E-01	1.07E+01	1.72E+00	3.41E+00	1.48E+00	5.42E-01
3	Glycolysis	Fructose 6-P + ATP = Glyceraldehyde 3-P + Glycerone-P + ADP	2.56E+01	8.40E+00	1.06E+01	7.15E+00	5.23E+00	2.52E+01	8.25E+00	1.07E+01	7.22E+00	5.25E+00
4	Glycolysis	Glycerone-P = Glyceraldehyde 3-P	2.56E+01	8.40E+00	1.06E+01	7.15E+00	5.23E+00	2.52E+01	8.25E+00	1.07E+01	7.22E+00	5.25E+00
5	Glycolysis	Glyceraldehyde 3-P + NAD+ + ADP + Pi = P-Enolpyruvate + ATP + H2O	5.80E+01	1.99E+01	2.50E+01	1.72E+01	1.28E+01	5.75E+01	1.98E+01	2.51E+01	1.73E+01	1.29E+01
6	Glycolysis	P-Enolpyruvate + ADP + H+ = Pyruvate + ATP	6.85E+01	2.70E+01	3.31E+01	2.37E+01	1.70E+01	6.91E+01	2.72E+01	3.26E+01	2.44E+01	1.69E+01
7	Glycolysis	Pyruvate + NADH + H+ = **Lactate** + NAD+	7.63E-02	1.70E-02	1.39E-02	-1.95E-02	-6.95E-02	7.19E-02	-1.57E-02	5.09E-02	-2.57E-02	-7.35E-02
8	Pentose phosphate pathway	Glucose 6-P + 2 NADP+ + H2O = Ribulose 5-P + CO2 + 2 NADPH + 2 H+	2.02E+01	9.31E+00	1.16E+01	8.80E+00	7.16E+00	2.17E+01	9.80E+00	1.10E+01	8.61E+00	7.06E+00
9	Pentose phosphate pathway	3 Ribulose 5-P = 2 Fructose 6-P + Glyceraldehyde 3-P	6.74E+00	3.10E+00	3.87E+00	2.93E+00	2.39E+00	7.23E+00	3.27E+00	3.66E+00	2.87E+00	2.35E+00
10	TCA cycle (mitochondria)	***Pyruvate*** + ***Oxaloacetate*** + NAD+ + H2O = ***Citrate*** + CO2 + NADH + H+	3.39E+01	1.60E+01	1.89E+01	1.60E+01	1.41E+01	3.54E+01	1.67E+01	1.94E+01	1.57E+01	1.42E+01
11	TCA cycle (mitochondria)	***Pyruvate*** + HCO3- + ATP = ***Oxaloacetate*** + ADP + Pi	4.25E+00	7.58E+00	8.24E+00	8.83E+00	7.79E+00	5.57E+00	8.21E+00	8.74E+00	7.92E+00	7.60E+00
12	TCA cycle (mitochondria)	***Citrate*** + NAD+ = ***2-Oxoglutarate*** + CO2 + NADH + H+	3.50E-01	1.16E+00	1.13E+00	1.41E+00	2.50E+00	5.59E-01	1.41E+00	1.46E+00	1.84E+00	2.19E+00
13	TCA cycle (mitochondria)	***2-Oxoglutarate*** + NAD+ + CoA = ***Succinyl-CoA*** + CO2 + NADH	6.77E-01	2.32E+00	1.89E+00	3.01E+00	3.62E+00	1.16E+00	2.69E+00	2.55E+00	3.37E+00	3.85E+00
14	TCA cycle (mitochondria)	***Succinyl-CoA*** + FAD + Pi + ADP = ***Fumarate*** + FADH2 + ATP + CoA	6.22E-01	2.40E+00	1.81E+00	3.04E+00	3.66E+00	1.21E+00	2.67E+00	2.50E+00	3.51E+00	3.82E+00
15	TCA cycle (mitochondria)	***Fumarate*** + H2O = ***Malate***	5.28E-01	2.33E+00	1.72E+00	3.01E+00	3.64E+00	1.16E+00	2.64E+00	2.46E+00	3.52E+00	3.80E+00
16	TCA cycle (mitochondria)	***Malate*** + NAD+ = ***Oxaloacetate*** + NADH + H+	2.96E+01	8.41E+00	1.06E+01	7.15E+00	6.26E+00	2.98E+01	8.47E+00	1.07E+01	7.77E+00	6.62E+00
17	TCA cycle	Citrate + CoA + ATP = Acetyl-CoA + Oxaloacetate + ADP + Pi	3.33E+01	1.38E+01	1.71E+01	1.31E+01	1.03E+01	3.44E+01	1.41E+01	1.69E+01	1.23E+01	1.04E+01
18	TCA cycle	Oxaloacetate + NADH + H+ = Malate + NAD+	4.68E+01	1.04E+01	1.49E+01	7.85E+00	5.19E+00	4.48E+01	9.70E+00	1.48E+01	7.01E+00	5.16E+00
19	TCA cycle	Malate + NADP+ = Pyruvate + CO2 + NADPH	1.77E+01	4.37E+00	6.03E+00	3.70E+00	2.57E+00	1.62E+01	3.87E+00	6.62E+00	2.76E+00	2.33E+00
20	TCA cycle	Citrate + NADP+ = 2-Oxoglutarate + CO2 + NADPH + H+	1.94E-01	1.05E+00	6.15E-01	1.51E+00	1.24E+00	4.23E-01	1.16E+00	1.03E+00	1.55E+00	1.66E+00

21	TCA cycle	Oxaloacetate + ATP = P-Enolpyruvate + CO2 + ADP	1.05E+01	7.06E+00	8.16E+00	6.44E+00	4.14E+00	1.16E+01	7.47E+00	7.54E+00	7.09E+00	4.03E+00
22	Oxidative phosphorylation	NADH + 0.5 O2 + 3 ADP + 3 Pi + 4 H+ = NAD+ + 3 ATP + 4 H2O	5.17E+01	3.39E+01	3.66E+01	3.59E+01	3.55E+01	5.78E+01	3.62E+01	3.88E+01	3.74E+01	3.58E+01
23	Oxidative phosphorylation	FADH2 + 0.5 O2 + 2 ADP + 2 Pi + 3 H+ = FAD + 2 ATP + 3 H2O	6.95E-01	2.49E+00	1.86E+00	3.10E+00	3.72E+00	1.30E+00	2.70E+00	2.56E+00	3.61E+00	3.86E+00
24	Palmitate biosynthesis	8 Acetyl-CoA + 14 NADPH + 7 ATP + 7 HCO3- + 14 H+ = Palmitate + 14 NADP+ + 8 CoA + 7 ADP + 7 Pi + 7 CO2 + 6 H2O	4.17E+00	1.72E+00	2.14E+00	1.63E+00	1.29E+00	4.30E+00	1.76E+00	2.11E+00	1.54E+00	1.30E+00
25	Tripalmitoylglycerol biosynthesis	Glycerone-P + 3 Palmitate + NADH + 3 ATP + H2O + H+ = Tripalmitoylglycerol + NAD+ + Pi + 3 AMP + 3 PPi	9.61E-07	1.75E-07	2.43E-07	5.79E-07	-2.33E-09	1.72E-06	1.29E-06	7.83E-07	1.24E-06	-8.18E-07
26	Tripalmitoylglycerol biosynthesis	Tripalmitoylglycerol + 3 H2O = **Glycerol** + 3 Palmitate	4.31E-07	-1.05E-07	-2.43E-07	3.68E-07	-1.19E-09	3.06E-07	3.05E-07	-4.70E-07	-1.24E-06	9.21E-07
27	Metabolism of ketone bodies	2 ***Acetyl-CoA*** = ***Acetoacetate*** + 2 CoA	8.11E-07	-1.14E-07	1.71E-08	5.18E-08	8.19E-09	-6.21E-06	1.81E-06	2.53E-06	-6.19E-09	-1.05E-07
28	Metabolism of ketone bodies	***Acetoacetyl-CoA*** = ***Acetoacetate*** + CoA	3.27E-06	8.64E-08	8.54E-09	4.30E-08	2.48E-09	4.50E-07	-2.27E-06	6.47E-07	2.18E-08	1.76E-07
29	Metabolism of ketone bodies	***Acetoacetate*** + NADH = **3-Hydroxybutyrate**	3.57E-06	2.30E-07	-8.06E-09	-1.29E-07	-3.73E-09	3.55E-06	-6.07E-07	-4.23E-06	2.30E-08	4.46E-07
30	Amino acid metabolism	Pyruvate + NH4+ + NADPH = Alanine	2.63E-02	1.11E-02	2.07E-02	2.67E-02	1.27E-03	4.74E-02	-1.54E-02	5.00E-02	-3.59E-02	-4.18E-02
31	Amino acid metabolism	Aspartate + NH4+ = **Asparagine**	-2.39E+01	-3.68E+00	-5.92E+00	-1.17E+00	1.05E+00	-2.19E+01	-3.01E+00	-5.42E+00	-1.76E+00	1.24E+00
32	Amino acid metabolism	Aspartate = Oxaloacetate + NH4+ + NADH	2.40E+01	3.71E+00	5.98E+00	1.22E+00	-9.87E-01	2.20E+01	3.06E+00	5.47E+00	1.81E+00	-1.18E+00
33	Amino acid metabolism	Cysteine = Pyruvate + NH4+ + NADH	-4.81E+01	-7.63E+00	-1.20E+01	-2.54E+00	2.22E+00	-4.43E+01	-6.29E+00	-1.11E+01	-3.65E+00	2.41E+00
34	Amino acid metabolism	Glutamate = 2-Oxoglutarate + NH4+ + NADH	1.33E-01	1.15E-01	1.44E-01	8.87E-02	-1.21E-01	1.75E-01	1.16E-01	6.03E-02	-1.93E-02	3.91E-03
35	Amino acid metabolism	**Glutamine** = Glutamate + NH4+ + ATP	-1.60E-02	-1.29E-02	-1.87E-02	2.69E-02	9.01E-02	-4.66E-02	-1.01E-02	9.55E-03	-5.13E-03	4.30E-02
36	Amino acid metabolism	Serine + THF = Glycine	8.50E-03	2.92E-02	5.78E-02	3.30E-02	1.41E-02	5.05E-02	1.26E-03	2.64E-02	-5.33E-03	-1.86E-03
37	Amino acid metabolism	**Histidine** + THF = Glutamate + NH4+	8.60E-02	1.06E-01	8.99E-02	1.19E-01	3.38E-02	9.56E-02	1.08E-01	1.66E-01	-7.60E-03	3.98E-02
38	Amino acid metabolism	**Isoleucine** + 2 CoA = ***Succinyl-CoA*** + ***Acetyl-CoA*** + NH4+ + FADH2 + 2 NADH	-7.22E-02	-5.54E-02	-5.47E-02	-1.11E-02	-8.35E-03	-3.58E-02	-3.40E-02	-2.30E-02	2.14E-02	-1.44E-02
39	Amino acid metabolism	**Leucine** + CoA + CO2 + ATP = ***Acetoacetate*** + ***Acetyl-CoA*** + NH4+ + FADH2 + 2 NADH	9.31E-02	6.50E-02	9.33E-02	3.10E-02	1.79E-02	5.36E-02	3.48E-02	4.81E-02	-7.59E-03	2.78E-02
40	Amino acid metabolism	**Lysine** = 2-Oxoadipate + 2 NH4+ + 3 NADH	-1.55E-02	1.29E-02	5.11E-03	9.75E-03	-7.69E-03	2.19E-02	-3.02E-02	1.74E-02	-4.59E-02	-3.33E-02
41	Amino acid metabolism	2-Oxoadipate + CoA = ***Acetoacetyl-CoA*** + 2 CO2 + FADH2 + 2 NADH	2.98E-06	2.78E-06	9.57E-06	7.64E-07	2.48E-09	-7.19E-07	8.18E-06	1.55E-05	1.69E-05	-1.04E-05
42	Amino acid metabolism	**Methionine** + Serine + ATP + CoA + THF = ***Succinyl-CoA*** + Cysteine + NH4+ + NADH	-3.65E-02	4.67E-02	-3.46E-02	6.29E-03	3.13E-03	1.48E-02	-4.42E-03	-5.04E-02	3.24E-02	-3.40E-02
43	Amino acid metabolism	**Phenylalanine** + O2 + NADH = Tyrosine	-4.21E-02	-3.42E-02	-5.24E-02	-1.92E-02	-1.14E-02	-2.65E-02	-3.81E-03	-3.06E-02	2.19E-02	-1.27E-02
44	Amino acid metabolism	Glutamate + ATP + 2 NADPH = **Proline**	-1.38E-03	-4.99E-02	-6.20E-02	-2.87E-02	4.07E-02	-6.83E-02	-3.36E-02	-4.12E-03	1.32E-02	-6.90E-03

45	Amino acid metabolism	Serine = Pyruvate + NH4+	1.04E-01	-8.32E-02	3.76E-03	-2.22E-02	-3.13E-03	4.08E-03	3.58E-02	7.62E-02	1.52E-02	6.77E-02
46	Amino acid metabolism	**Threonine** + CoA = Glycine + ***Acetyl-CoA*** + NADH	-2.09E-02	-9.58E-03	-3.86E-02	-1.99E-02	-9.50E-03	-1.78E-02	-7.14E-04	-2.50E-02	-1.38E-02	-1.34E-02
47	Amino acid metabolism	**Tryptophan** + 3 O2 + NADPH = 2-Oxoadipate + Alanine + CO2 + NH4+	1.55E-02	-1.29E-02	-5.11E-03	-9.75E-03	7.69E-03	-2.19E-02	3.02E-02	-1.74E-02	4.59E-02	3.33E-02
48	Amino acid metabolism	Tyrosine + 2 O2 = ***Acetoacetate*** + ***Fumarate*** + CO2 + NH4+ + NADH	-9.31E-02	-6.50E-02	-9.33E-02	-3.10E-02	-1.79E-02	-5.36E-02	-3.48E-02	-4.81E-02	7.60E-03	-2.78E-02
49	Amino acid metabolism	**Valine** + CoA = ***Succinyl-CoA*** + CO2 + 4 NADH + FADH2 + NH4+	5.29E-02	8.62E-02	5.93E-03	3.74E-02	4.82E-02	7.43E-02	2.46E-02	2.62E-02	8.52E-02	2.04E-02
50	Plasma exchange	Palmitate = **Palmitate**	4.17E+00	1.72E+00	2.14E+00	1.63E+00	1.29E+00	4.30E+00	1.76E+00	2.11E+00	1.54E+00	1.30E+00
51	Plasma exchange	***Acetoacetate*** = **Acetoacetate**	3.24E-06	2.38E-07	-7.93E-09	4.13E-07	-2.95E-09	3.75E-06	-7.97E-07	-5.18E-06	2.17E-08	4.61E-07
52	Plasma exchange	Alanine = **Alanine**	4.18E-02	-1.85E-03	1.56E-02	1.70E-02	8.96E-03	2.55E-02	1.48E-02	3.27E-02	1.00E-02	-8.56E-03
53	Plasma exchange	**Aspartate** = Aspartate	7.39E-02	3.39E-02	6.62E-02	5.31E-02	6.29E-02	8.69E-02	5.10E-02	4.36E-02	5.44E-02	5.87E-02
54	Plasma exchange	**Cysteine** = Cysteine	-4.81E+01	-7.68E+00	-1.20E+01	-2.54E+00	2.22E+00	-4.43E+01	-6.28E+00	-1.11E+01	-3.68E+00	2.45E+00
55	Plasma exchange	**Glutamate =** Glutamate	2.97E-02	-5.38E-02	-2.64E-02	-3.17E-02	-2.36E-02	-3.50E-02	-3.56E-02	-1.00E-01	-3.57E-03	2.42E-04
56	Plasma exchange	Glycine = **Glycine**	-1.24E-02	1.96E-02	1.92E-02	1.31E-02	4.57E-03	3.27E-02	5.45E-04	1.39E-03	-1.92E-02	-1.52E-02
57	Plasma exchange	**Serine** = Serine	7.62E-02	-7.38E-03	2.70E-02	1.72E-02	1.41E-02	6.94E-02	3.26E-02	5.23E-02	4.22E-02	3.18E-02
58	Plasma exchange	**Tyrosine** = Tyrosine	-5.10E-02	-3.08E-02	-4.09E-02	-1.18E-02	-6.46E-03	-2.71E-02	-3.09E-02	-1.74E-02	-1.42E-02	-1.51E-02
59	Plasma exchange	**O2 =** O2	2.60E+01	1.80E+01	1.90E+01	1.94E+01	1.96E+01	2.93E+01	1.95E+01	2.05E+01	2.07E+01	1.99E+01
60	Plasma exchange	CO2 = **CO2**	7.92E+01	3.36E+01	3.99E+01	3.20E+01	2.75E+01	8.13E+01	3.48E+01	4.08E+01	3.31E+01	2.77E+01
61	Plasma exchange	NH4+ = **NH4+**	1.28E-02	-1.01E-02	2.93E-02	2.56E-02	3.64E-02	2.89E-02	2.34E-02	-1.50E-02	4.14E-02	3.17E-02
62	Mitochondrial exchange	Pyruvate = ***Pyruvate***	3.81E+01	2.36E+01	2.71E+01	2.48E+01	2.18E+01	4.09E+01	2.49E+01	2.81E+01	2.36E+01	2.18E+01
63	Mitochondrial exchange	***Citrate*** + Malate = Citrate + ***Malate***	3.35E+01	1.48E+01	1.77E+01	1.46E+01	1.16E+01	3.48E+01	1.53E+01	1.79E+01	1.38E+01	1.20E+01
64	Mitochondrial exchange	2-Oxoglutarate + ***Malate*** = ***2-Oxoglutarate*** + Malate	3.27E-01	1.16E+00	7.60E-01	1.60E+00	1.12E+00	5.98E-01	1.28E+00	1.09E+00	1.53E+00	1.66E+00
65	Mitochondrial exchange	***Malate*** + Pi = Malate + ***Pi***	4.10E+00	7.59E+00	8.06E+00	8.83E+00	7.81E+00	5.57E+00	8.16E+00	8.64E+00	8.06E+00	7.54E+00
66	Tripalmitoylglycerol accumulation	Tripalmitoylglycerol = **Tripalmitoylglycerol**	5.79E-07	-9.93E-08	-2.39E-07	-1.29E-07	-1.14E-09	2.59E-07	3.06E-07	-4.97E-07	-1.24E-06	9.24E-07

Table S3. Correlation coefficients and p-values for correlations between estimated fluxes and qP or $\Delta qP_{citrate}$. Cells with a significant p-value of <0.05 are highlighted.

			Correlation w/ qP						Correlation w/ CIT response					
			D4			D7			D4			D7		
	Pathway	Reaction	CC	t	p-value	CC	t	p-value	CC	t	p-value	CC	t	p-value
1	Glycolysis	**Glucose** + ATP = Glucose 6-P + ADP	0.718	1.787	0.172	0.717	1.782	0.173	-0.618	1.363	0.266	-0.618	1.361	0.267
2	Glycolysis	Glucose 6-P = Fructose 6-P	0.667	1.549	0.219	0.736	1.882	0.156	-0.628	1.396	0.257	-0.620	1.370	0.264
3	Glycolysis	Fructose 6-P + ATP = Glyceraldehyde 3-P + Glycerone-P + ADP	0.708	1.739	0.180	0.720	1.799	0.170	-0.621	1.371	0.264	-0.618	1.363	0.266
4	Glycolysis	Glycerone-P = Glyceraldehyde 3-P	0.708	1.739	0.180	0.720	1.799	0.170	-0.621	1.371	0.264	-0.618	1.363	0.266
5	Glycolysis	Glyceraldehyde 3-P + NAD+ + ADP + Pi = P-Enolpyruvate + ATP + H2O	0.714	1.765	0.176	0.719	1.789	0.171	-0.619	1.367	0.265	-0.618	1.362	0.267
6	Glycolysis	P-Enolpyruvate + ADP + H+ = Pyruvate + ATP	0.736	1.882	0.156	0.730	1.847	0.162	-0.603	1.310	0.281	-0.590	1.265	0.295
7	Glycolysis	Pyruvate + NADH + H+ = **Lactate** + NAD+	0.722	1.806	0.169	0.925	4.212	0.024	-0.431	0.828	0.468	-0.445	0.860	0.453
8	Pentose phosphate pathway	Glucose 6-P + 2 NADP+ + H2O = Ribulose 5-P + CO2 + 2 NADPH + 2 H+	0.762	2.039	0.134	0.703	1.711	0.186	-0.607	1.323	0.278	-0.615	1.351	0.269
9	Pentose phosphate pathway	3 Ribulose 5-P = 2 Fructose 6-P + Glyceraldehyde 3-P	0.762	2.039	0.134	0.703	1.711	0.186	-0.607	1.323	0.278	-0.615	1.351	0.269
10	TCA cycle (mitochondria)	***Pyruvate*** + ***Oxaloacetate*** + NAD+ + H2O = ***Citrate*** + CO2 + NADH + H+	0.718	1.784	0.172	0.707	1.731	0.182	-0.608	1.326	0.277	-0.633	1.416	0.252
11	TCA cycle (mitochondria)	***Pyruvate*** + HCO3- + ATP = ***Oxaloacetate*** + ADP + Pi	-0.418	0.798	0.483	-0.305	0.554	0.618	0.765	2.060	0.132	0.527	1.075	0.361
12	TCA cycle (mitochondria)	***Citrate*** + NAD+ = ***2-Oxoglutarate*** + CO2 + NADH + H+	-0.758	2.011	0.138	-0.692	1.660	0.196	0.266	0.477	0.666	0.552	1.147	0.335
13	TCA cycle (mitochondria)	***2-Oxoglutarate*** + NAD+ + CoA = ***Succinyl-CoA*** + CO2 + NADH	-0.791	2.241	0.111	-0.734	1.873	0.158	0.566	1.188	0.320	0.588	1.259	0.297
14	TCA cycle (mitochondria)	***Succinyl-CoA*** + FAD + Pi + ADP = ***Fumarate*** + FADH2 + ATP + CoA	-0.814	2.426	0.094	-0.723	1.813	0.167	0.569	1.197	0.317	0.634	1.419	0.251
15	TCA cycle (mitochondria)	***Fumarate*** + H2O = ***Malate***	-0.815	2.435	0.093	-0.721	1.800	0.170	0.569	1.198	0.317	0.644	1.459	0.241
16	TCA cycle (mitochondria)	***Malate*** + NAD+ = ***Oxaloacetate*** + NADH + H+	0.671	1.567	0.215	0.669	1.559	0.217	-0.644	1.457	0.241	-0.631	1.409	0.254
17	TCA cycle	Citrate + CoA + ATP = Acetyl-CoA + Oxaloacetate + ADP + Pi	0.738	1.894	0.155	0.713	1.759	0.177	-0.605	1.315	0.280	-0.634	1.419	0.251
18	TCA cycle	Oxaloacetate + NADH + H+ = Malate + NAD+	0.695	1.675	0.193	0.702	1.705	0.187	-0.637	1.430	0.248	-0.650	1.482	0.235
19	TCA cycle	Malate + NADP+ = Pyruvate + CO2 + NADPH	0.696	1.681	0.191	0.739	1.898	0.154	-0.626	1.391	0.259	-0.670	1.562	0.216

20	TCA cycle	Citrate + NADP+ = 2-Oxoglutarate + CO2 + NADPH + H+	-0.729	1.844	0.162	-0.738	1.896	0.154	0.817	2.453	0.091	0.657	1.510	0.228
21	TCA cycle	Oxaloacetate + ATP = P-Enolpyruvate + CO2 + ADP	0.842	2.707	0.073	0.755	1.993	0.140	-0.423	0.809	0.478	-0.363	0.674	0.548
22	Oxidative phosphorylation	NADH + 0.5 O2 + 3 ADP + 3 Pi + 4 H+ = NAD+ + 3 ATP + 4 H2O	0.650	1.480	0.236	0.667	1.552	0.218	-0.598	1.292	0.287	-0.597	1.290	0.287
23	Oxidative phosphorylation	FADH2 + 0.5 O2 + 2 ADP + 2 Pi + 3 H+ = FAD + 2 ATP + 3 H2O	-0.823	2.507	0.087	-0.710	1.746	0.179	0.567	1.194	0.318	0.649	1.478	0.236
24	Palmitate biosynthesis	8 Acetyl-CoA + 14 NADPH + 7 ATP + 7 HCO3- + 14 H+ = Palmitate + 14 NADP+ + 8 CoA + 7 ADP + 7 Pi + 7 CO2 + 6 H2O	0.738	1.894	0.155	0.713	1.759	0.177	-0.605	1.315	0.280	-0.634	1.419	0.251
25	Tripalmitoylglycerol biosynthesis	Glycerone-P + 3 Palmitate + NADH + 3 ATP + H2O + H+ = Tripalmitoylglycerol + NAD+ + Pi + 3 AMP + 3 PPi	0.692	1.660	0.196	0.580	1.235	0.305	-0.108	0.188	0.863	0.079	0.138	0.899
26	Tripalmitoylglycerol biosynthesis	Tripalmitoylglycerol + 3 H2O = **Glycerol** + 3 Palmitate	0.240	0.427	0.698	-0.425	0.813	0.476	0.137	0.239	0.826	-0.767	2.073	0.130
27	Metabolism of ketone bodies	2 ***Acetyl-CoA*** = ***Acetoacetate*** + 2 CoA	0.625	1.387	0.260	-0.383	0.718	0.525	-0.554	1.153	0.332	0.470	0.922	0.424
28	Metabolism of ketone bodies	***Acetoacetyl-CoA*** = ***Acetoacetate*** + CoA	0.563	1.179	0.323	0.605	1.314	0.280	-0.612	1.339	0.273	-0.166	0.291	0.790
29	Metabolism of ketone bodies	***Acetoacetate*** + NADH = **3-Hydroxybutyrate**	0.539	1.108	0.349	-0.047	0.081	0.940	-0.649	1.479	0.236	-0.290	0.524	0.636
30	Amino acid metabolism	Pyruvate + NH4+ + NADPH = Alanine	0.817	2.450	0.092	0.883	3.257	0.047	0.229	0.407	0.712	-0.592	1.273	0.293
31	Amino acid metabolism	Aspartate + NH4+ = **Asparagine**	-0.706	1.726	0.183	-0.723	1.812	0.168	0.631	1.409	0.254	0.599	1.294	0.286
32	Amino acid metabolism	Aspartate = Oxaloacetate + NH4+ + NADH	0.706	1.728	0.183	0.722	1.809	0.168	-0.631	1.410	0.253	-0.599	1.295	0.286
33	Amino acid metabolism	Cysteine = Pyruvate + NH4+ + NADH	-0.707	1.732	0.182	-0.723	1.814	0.167	0.628	1.396	0.257	0.599	1.296	0.286
34	Amino acid metabolism	Glutamate = 2-Oxoglutarate + NH4+ + NADH	0.708	1.737	0.181	0.418	0.796	0.484	0.039	0.067	0.950	-0.725	1.825	0.166
35	Amino acid metabolism	**Glutamine** = Glutamate + NH4+ + ATP	-0.670	1.563	0.216	-0.594	1.279	0.291	0.169	0.297	0.786	0.193	0.341	0.756
36	Amino acid metabolism	Serine + THF = Glycine	0.310	0.565	0.611	0.823	2.506	0.087	0.372	0.694	0.538	-0.723	1.814	0.167
37	Amino acid metabolism	**Histidine** + THF = Glutamate + NH4+	0.343	0.632	0.572	0.462	0.903	0.433	0.554	1.154	0.332	-0.601	1.303	0.284
38	Amino acid metabolism	**Isoleucine** + 2 CoA = ***Succinyl-CoA*** + ***Acetyl-CoA*** + NH4+ + FADH2 + 2 NADH	-0.605	1.315	0.280	-0.148	0.259	0.812	0.631	1.408	0.254	0.883	3.252	0.047
39	Amino acid metabolism	**Leucine** + CoA + CO2 + ATP = ***Acetoacetate*** + ***Acetyl-CoA*** + NH4+ + FADH2 + 2 NADH	0.788	2.216	0.113	0.423	0.810	0.477	-0.535	1.096	0.353	-0.928	4.323	0.023
40	Amino acid metabolism	**Lysine** = 2-Oxoadipate + 2 NH4+ + 3 NADH	-0.280	0.505	0.648	0.826	2.542	0.084	0.732	1.858	0.160	-0.729	1.845	0.162
41	Amino acid metabolism	2-Oxoadipate + CoA = ***Acetoacetyl-CoA*** + 2 CO2 + FADH2 + 2 NADH	0.664	1.537	0.222	0.407	0.772	0.496	-0.254	0.456	0.680	0.635	1.425	0.249
42	Amino acid metabolism	**Methionine** + Serine + ATP + CoA + THF = ***Succinyl-CoA*** + Cysteine + NH4+ + NADH	-0.839	2.674	0.075	0.049	0.084	0.938	0.429	0.823	0.471	0.428	0.821	0.472
43	Amino acid metabolism	**Phenylalanine** + O2 + NADH = Tyrosine	-0.775	2.124	0.124	-0.477	0.941	0.416	0.425	0.813	0.476	0.896	3.495	0.040

44	Amino acid metabolism	Glutamate + ATP + 2 NADPH = **Proline**	-0.389	0.732	0.517	-0.290	0.526	0.635	-0.303	0.551	0.620	0.772	2.105	0.126
45	Amino acid metabolism	Serine = Pyruvate + NH4+	0.686	1.635	0.201	-0.219	0.388	0.724	-0.573	1.212	0.312	-0.142	0.249	0.820
46	Amino acid metabolism	**Threonine** + CoA = Glycine + ***Acetyl-CoA*** + NADH	-0.840	2.686	0.075	-0.762	2.041	0.134	0.037	0.064	0.953	0.207	0.366	0.739
47	Amino acid metabolism	**Tryptophan** + 3 O2 + NADPH = 2-Oxoadipate + Alanine + CO2 + NH4+	0.280	0.505	0.648	-0.826	2.540	0.085	-0.732	1.859	0.160	0.729	1.847	0.162
48	Amino acid metabolism	Tyrosine + 2 O2 = ***Acetoacetate*** + ***Fumarate*** + CO2 + NH4+ + NADH	-0.788	2.216	0.113	-0.423	0.810	0.477	0.535	1.097	0.353	0.928	4.323	0.023
49	Amino acid metabolism	**Valine** + CoA = ***Succinyl-CoA*** + CO2 + 4 NADH + FADH2 + NH4+	-0.601	1.303	0.283	0.449	0.870	0.448	-0.103	0.179	0.870	0.356	0.661	0.556
50	Plasma exchange	Palmitate = **Palmitate**	0.738	1.894	0.154	0.713	1.759	0.177	-0.605	1.315	0.280	-0.634	1.418	0.251
51	Plasma exchange	***Acetoacetate*** = **Acetoacetate**	0.554	1.153	0.332	-0.086	0.150	0.890	-0.521	1.059	0.368	-0.255	0.456	0.679
52	Plasma exchange	Alanine = **Alanine**	0.765	2.054	0.132	0.863	2.960	0.060	-0.393	0.741	0.512	-0.233	0.415	0.706
53	Plasma exchange	**Aspartate** = Aspartate	0.647	1.468	0.238	0.310	0.565	0.612	-0.491	0.975	0.401	-0.535	1.096	0.353
54	Plasma exchange	**Cysteine** = Cysteine	-0.706	1.728	0.182	-0.723	1.812	0.168	0.628	1.396	0.257	0.598	1.292	0.287
55	Plasma exchange	**Glutamate =** Glutamate	0.631	1.409	0.254	-0.643	1.453	0.242	-0.593	1.276	0.292	0.317	0.579	0.603
56	Plasma exchange	Glycine = **Glycine**	-0.301	0.547	0.623	0.630	1.405	0.255	0.571	1.205	0.314	-0.756	1.998	0.140
57	Plasma exchange	**Serine** = Serine	0.760	2.028	0.136	0.918	4.006	0.028	-0.543	1.121	0.344	-0.460	0.896	0.436
58	Plasma exchange	**Tyrosine** = Tyrosine	-0.768	2.075	0.130	-0.024	0.041	0.970	0.610	1.335	0.274	0.471	0.925	0.423
59	Plasma exchange	**O2 =** O2	0.575	1.218	0.310	0.639	1.438	0.246	-0.575	1.217	0.311	-0.562	1.176	0.324
60	Plasma exchange	CO2 = **CO2**	0.706	1.728	0.182	0.706	1.728	0.182	-0.619	1.364	0.266	-0.609	1.331	0.275
61	Plasma exchange	NH4+ = **NH4+**	0.130	0.227	0.835	-0.480	0.947	0.413	0.102	0.177	0.871	0.319	0.583	0.601
62	Mitochondrial exchange	Pyruvate = ***Pyruvate***	0.782	2.170	0.118	0.750	1.965	0.144	-0.548	1.135	0.339	-0.631	1.410	0.253
63	Mitochondrial exchange	***Citrate*** + Malate = Citrate + ***Malate***	0.733	1.866	0.159	0.709	1.741	0.180	-0.587	1.257	0.298	-0.630	1.407	0.254
64	Mitochondrial exchange	2-Oxoglutarate + ***Malate*** = ***2-Oxoglutarate*** + Malate	-0.634	1.420	0.251	-0.786	2.201	0.115	0.903	3.633	0.036	0.632	1.412	0.253
65	Mitochondrial exchange	***Malate*** + Pi = Malate + ***Pi***	-0.457	0.891	0.439	-0.307	0.558	0.615	0.772	2.107	0.126	0.591	1.269	0.294
66	Tripalmitoylglycerol accumulation	Tripalmitoylglycerol = **Tripalmitoylglycerol**	0.343	0.633	0.572	-0.448	0.869	0.449	-0.623	1.379	0.262	-0.751	1.969	0.144

Chapter 4. Improvement of Genome Scale CHO Models Using Secondary Parameters in Objective Functions

4.1 Abstract

In this work, we tested several strategies to improve the accuracy of growth rate predictions from a genome-scale metabolic model for CHO cells. The original model used was the consensus model iCHO1766 using the COBRA toolbox for objective function optimization (Hefzi et al., 2016). Tested strategies include model reduction, implementing a two-step optimization including different objective functions, eliminating select constraints, and modifying antibody production parameters. While some of these strategies led to slight improvement in predictions, the improvements were inconsistent among cell lines.

4.2 Introduction

After the *Cricetulus griseus* genome became publicly available in 2011, researchers have been able to develop genome scale metabolic models used for understanding CHO phenotypes (Xu et al., 2011). The main component of a metabolic model is a stoichiometric matrix (known as the S matrix) of reactions in a cell and the metabolites that are consumed or produced in those reactions. The CHO consensus genome scale model reconciled from multiple independent research groups was published in 2016 with 1766 genes, encompassing over 6000 reactions and 4000 metabolites (Hefzi et al., 2016). Under a pseudo steady-state assumption, flux balance analysis (FBA) is applied using the GIMME algorithm (Gene Inactivity Moderated by Metabolism and Expression) and measured values as lower- and upper-bound constraints for certain fluxes to calculate the optimal set of metabolic fluxes for an assumed cellular objective (Becker & Palsson, 2008). In this case, the open-source COBRA (COnstraint-Based Reconstruction and Analysis, v3.0) toolbox in MATLAB (v2019b, Mathworks, Natick, MA) was used for the objective function optimization (Heirendt et al., 2019) The consensus model includes a biomass reaction that accounts for RNA, DNA, proteins, amino acids, fatty acids, ATP costs, etc. and uses it as the default objective function. Hefzi et al. modified the global CHO reconstruction to represent 3 protein-producing cell lines (CHO-K1, CHO-S, and CHO-DG44) more accurately and demonstrated growth rate predictions for multiple datasets.

For this work, we wanted to modify the CHO-K1 cell line model further to better represent BMSCHO1 cells, which are generated from a double GS knockout by random integration of a plasmid that contains the GS gene along with the gene for the protein of interest. We gathered data from six BMSCHO1 clones and attempted to implement several strategies towards this aim. First, we wanted to reduce to the model to simplify and speed up further work. Next, we wanted

to incorporate some known information about protein production in our cell lines. Finally, we tried a two-step objective function optimization. A case study for multi-objective optimization has previously been performed by Villaverde et al. on a large-scale CHO metabolic model using biomass, antibody composition, and other experimental data available in the literature (Nolan & Lee, 2010; Villaverde et al., 2016). They obtained a Pareto front that described the tradeoff between two conflicting objectives: maximize productivity while minimizing enzymatic modifications. We expected to also see tradeoffs within the cell based on this and other previous work on multi-objective optimizations.

4.3 Materials and Methods

4.3.1 CHO cell data

The data for this work come from the control conditions of the 6 different clones in the citrate addback experiment described in section 3.3.1. Daily culture maintenance activities are described in section 2.5.2, including the cell counts used for determining integral VCD. Instead of using the REBEL for amino acid analysis on select days, a high-throughput HPLC analysis was performed with supernatants taken each day from day 0 through day 14. This measurement was also performed on the feed media for use in calculating metabolite fluxes.

4.3.2 Flux Balance Analysis

Fluxes for all amino acids, glucose, lactate, and ammonia were calculated for each condition. For simpler calculation, concentration time course data from the fed-batch production culture were transformed into batch culture. Transformation of glucose concentration data provides an illustrative example. Glucose was consumed by cells at variable rates throughout the process but generally more quickly than other nutrients. Once the measured value dropped below the action

limit, we supplemented more glucose. This led to a glucose profile that fluctuated over the course of the fed-batch culture due to intermittent feeds. We summed up the total amount of glucose fed over the course of the culture and added it to the measured glucose concentration on day 0. By adding all the glucose at the beginning instead of on a daily basis, we transformed the glucose profile so that the glucose concentration consistently decreased, allowing for easier calculation of glucose consumption rates over multiple days. This transformation was applied to all measured metabolites. Linear regressions were then performed on the metabolite data normalized to daily integral VCD, to obtain the exchange fluxes. These exchange fluxes were inputted as the lower-bound and upper-bound constraints in the model using the changeRxnBounds function in the COBRA toolbox. FBA was then performed using the optimizeCbModel function, also from the COBRA toolbox (see script in the Supplementary Information). For initial optimizations, biomass production was used as the objective function.

4.3.3 Model Reduction

Following a published extraction process for the human genome, we applied a model reduction strategy based on metabolic data and an input of core reactions (Quek & Turner, 2019) We adapted pseudocode and a spreadsheet template from the supplementary data, and we modified MATLAB scripts provided by Quek and Turner to execute the model reduction. Briefly, exchange reactions were restricted to force uptake of substrates not in the cell culture media to be zero, while cofactor-producing reactions were also restricted to a few conventional reactions. A check was performed to make sure the model was still feasible, then mixed-integer linear programming was used to minimize reactions not in the core set.

4.3.4 Modifying antibody production parameters

The amino acid composition for the IgG formation reactions in the original iCHO1766 model differs from that of the IgGs produced by the BMSCHO1 cells in this study. We updated the S matrix of the model to reflect the correct number of each of the amino acids. Another parameter to note was the flux input for the IgG reaction, which was initially set to 0 for growth phase simulations. However, a small amount of antibody is being made during this time, so we calculated IgG fluxes in the same manner as we calculated all other input fluxes. We added these updated fluxes to the lower- and upper-bound constraints.

4.3.5 Two-Step Objective Function Optimization

We tested bilevel objective function optimization following previous work by Schinn et al. which had shown improvement in predictions (Schinn et al., 2021). Based on their results, we tried adding a layer to the default objective function to maximize biomass formation: minimization of either cytosolic NADPH regeneration or mitochondrial NADH regeneration, as these both were shown to have positive effects on accuracy. Essentially this involved implementing an additional objective function before optimizing the fluxes for biomass production. For each of these tested functions, a dummy metabolite was created and added to the model to minimize related reactions. For example, all reactions including mitochondrial NADH regeneration were annotated to receive this penalty by being added to the dummy "NADH regeneration metabolite." Minimizing a new reaction that keeps track of the dummy metabolite was used as the first objective function in FBA. The solution for the new objective function in this optimization was then used as the lower bound for the dummy metabolite in a new optimization maximizing biomass.

4.4 Results

Although we were able to reduce iCHO1766 significantly, the resulting networks were too small, i.e., too many reactions were removed, and we were unable to obtain a satisfactory reduced model that included all the reactions we designated as core reactions. One possible explanation is that the sets of essential reactions and constraints between the example model, Recon 2, and our CHO cell model were too different. We proceeded to test alternative strategies for modifying the genome-scale model without reducing it.

Our initial simulated growth rates, without making any adjustments to the published model, were not on the same order of magnitude as experimental results. We hypothesized that one or more measured fluxes were inaccurately determined and artificially limited the growth rates that could be achieved. After excluding some measured metabolic flux data, we were able to achieve higher growth rates in the range of the experimental results. Removing different inputs led to different simulated growth rates, as can be seen in Figures 1-3, which represent the optimized maximum biomass with different sets of constraints (see constraint sets in Table S1). As we were interested in eventually evaluating the model's capability for predicting protein production as well as cell growth, we decided to focus on timeframes that were likely to include some amount of antibody production: days 1-6 and days 3-6. We still wanted to observe results in the earliest timeframe, days 1-3, but little protein is thought to be produced during this time while the cells were in an exponential growth phase. Thus, in the rest of the work, the constraint set 1 was used, since it is more closely aligned with the experimental data in Figure 2.

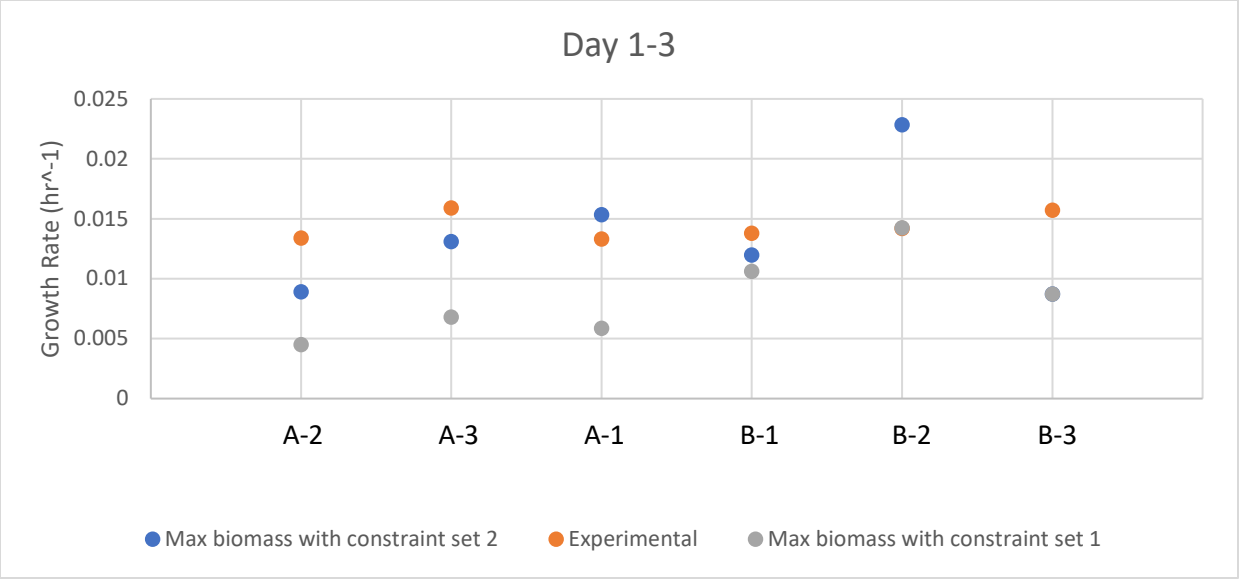

Figure 1: Results of model optimization with two different sets of constraints on fluxes calculated from days 1-3.

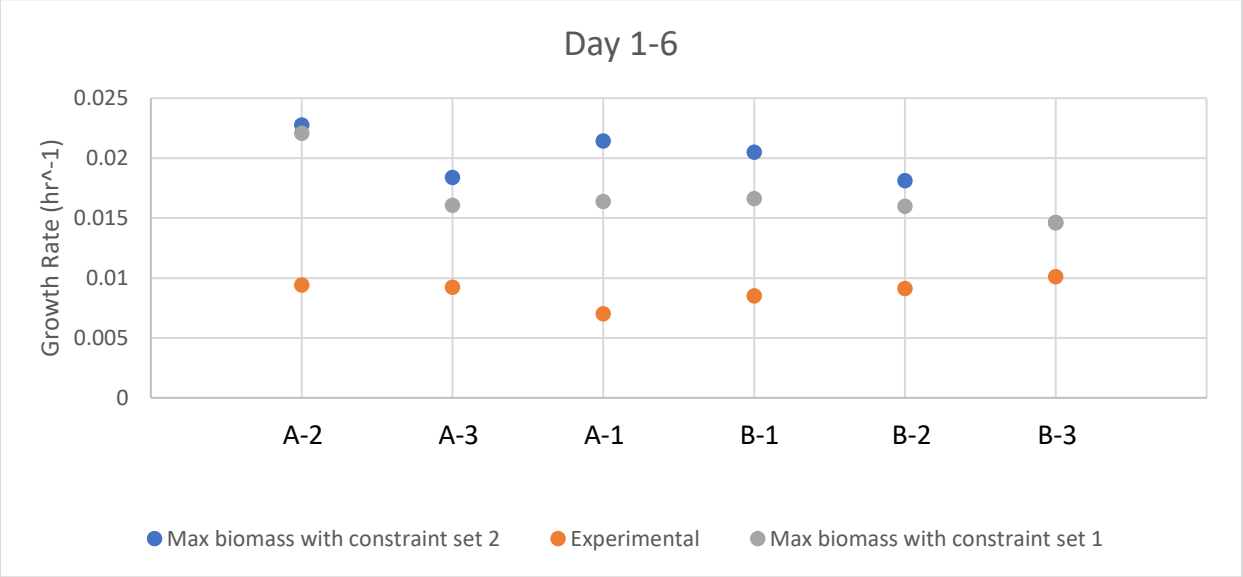

Figure 2: Results of model optimization with two different sets of constraints on fluxes calculated from days 1-6.

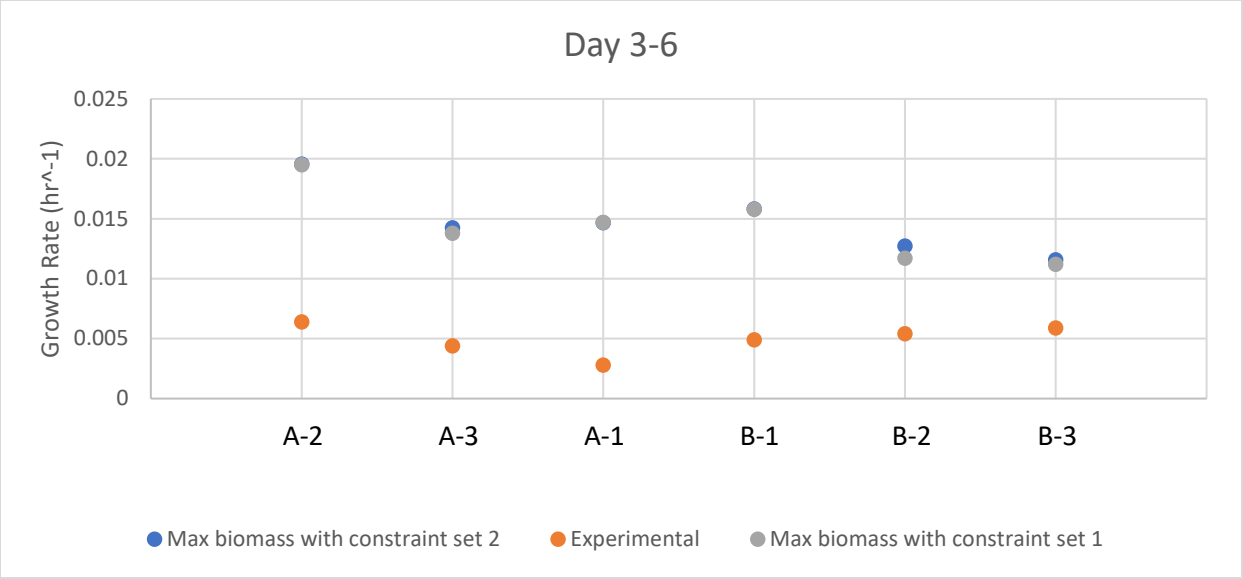

Figure 3: Results of model optimization with two different sets of constraints on fluxes calculated from days 3-6.

Updating the IgG composition and flux impacted the predicted growth rate but the change was inconsistent for the two tested timespans. For days 1-6 (Figure 4), the predicted growth rate increased for half of the clones, resulting in a greater difference between predicted and experimental rates. For the other three clones, there was only a very minimal decrease in simulated growth rate. For days 3-6 (Figure 5), the improvement was slightly greater and more consistent. Because the protein production is occurring to a larger extent during this time compared to days 1-3, it is not surprising that we see more improvement for days 3-6. We also added a 10% tolerance to the input IgG fluxes to account for measurement error, but this had a minimal impact on simulated growth rates. Overall, estimated fluxes were still at least double the experimental fluxes for most cases, suggesting that additional constraints need to be considered.

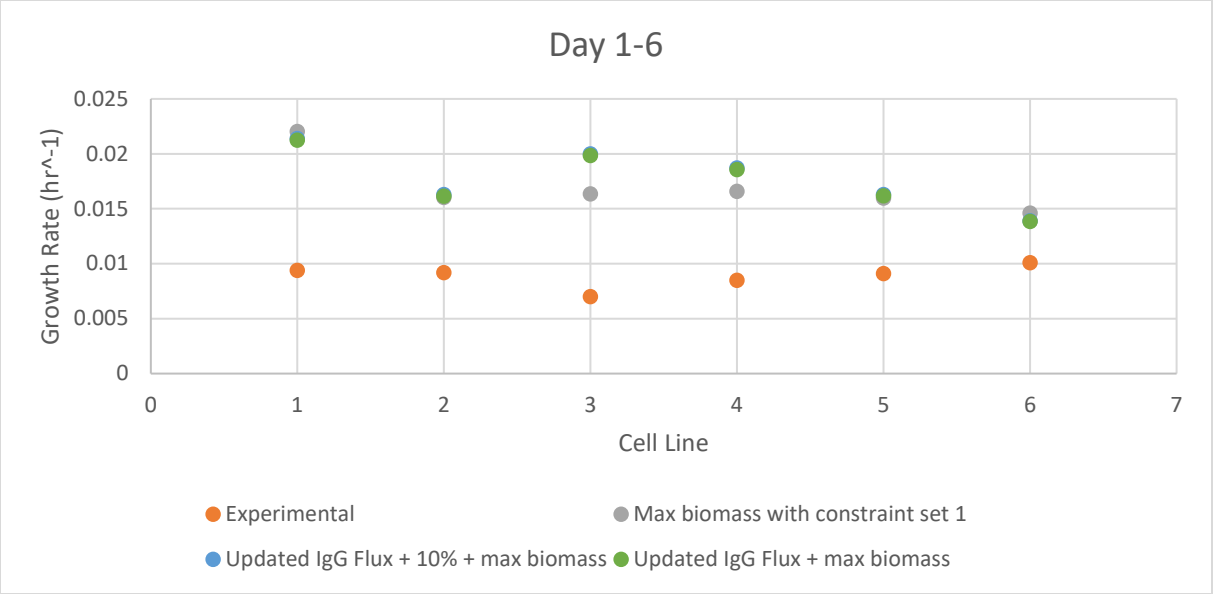

Figure 4: Results of model optimization with updated IgG flux and updated IgG flux with a 10% tolerance from days 1-6. For this timespan, adding the 10% tolerance did not impact the simulated growth rate at all.

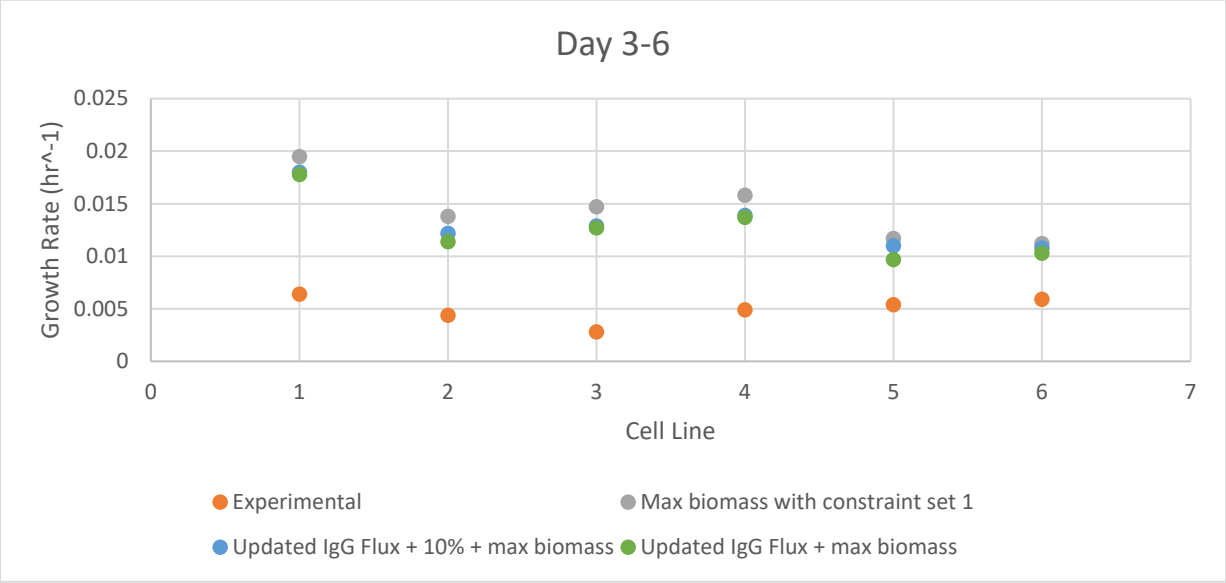

Figure 5: Results of model optimization with updated IgG flux and updated IgG flux with a 10% tolerance from days 3-6.

In the two-step objective function testing, we saw that the bilevel objective function results in growth rates much closer to the experimental values as can be seen in Figures 6 and 7, with minimizing mitochondrial NADH regeneration as the additional objective layer. Minimizing cytosolic NADPH regeneration similarly led to improved results. As expected, the added constraints limited the amount of flux in the biomass reaction. However, though growth rates were reduced, the trend among clones was not always consistent with experimental data. For example, experimental data shows that clone A-1 has the slowest growth rate during these timeframes, but the bilevel optimization estimates the second fastest growth rate for A-1 among the six clones. Nevertheless, the bilevel optimization strategy was still the most successful in quantitatively improving estimated growth rate calculations.

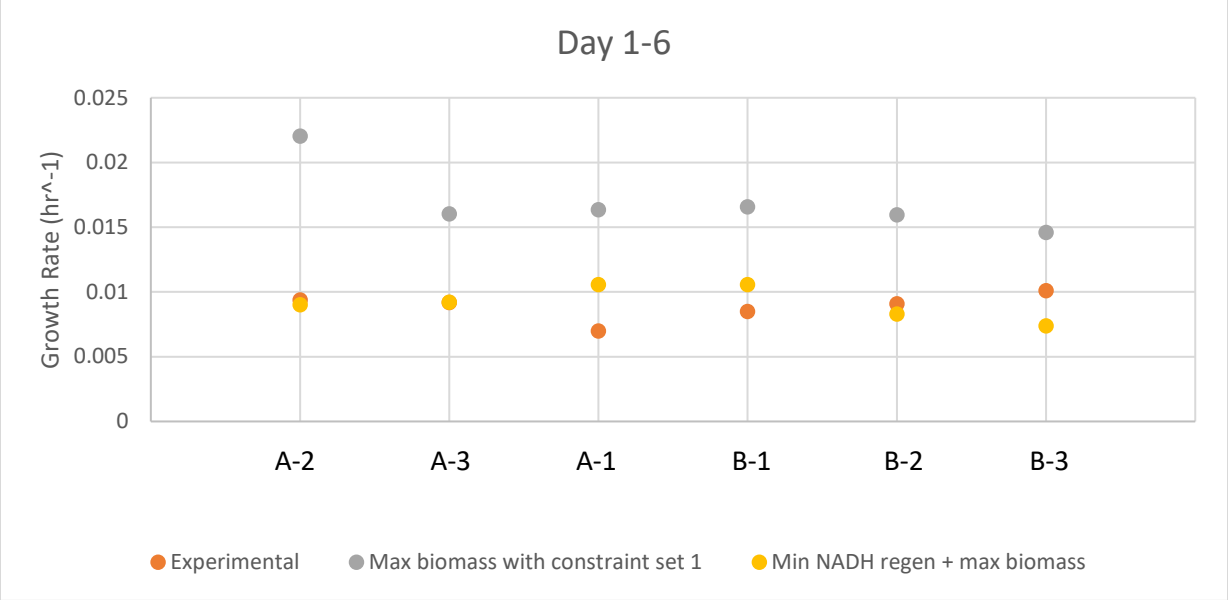

Figure 6: Results of model optimization with minimization of mitochondrial NADH regeneration as the additional objective function from days 1-6.

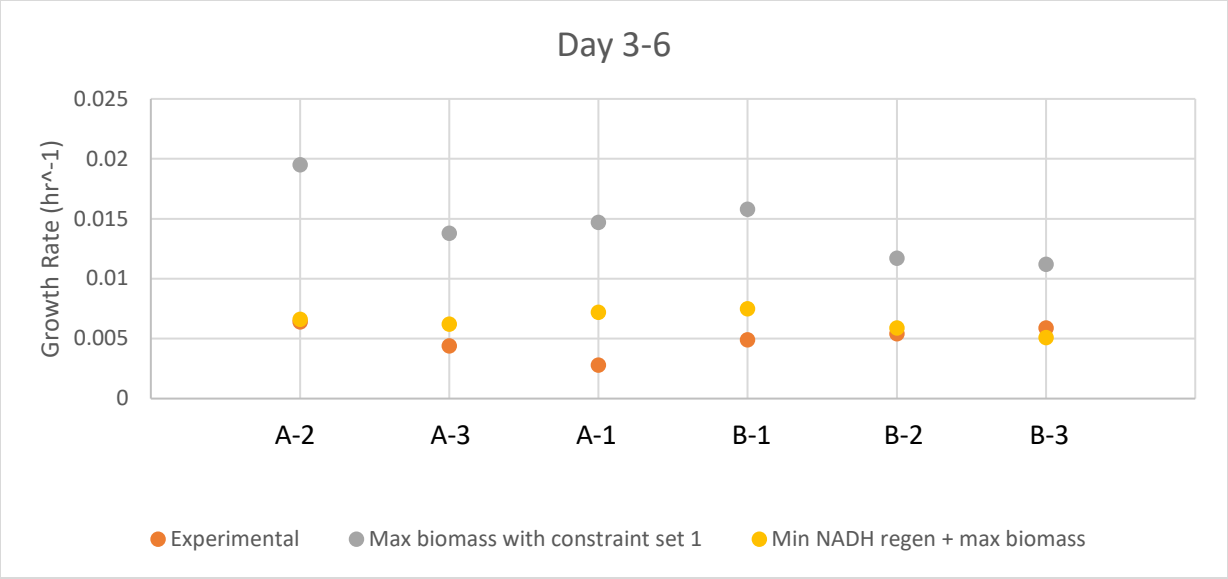

Figure 7: Results of model optimization with minimization of mitochondrial NADH regeneration as the additional objective function from days 3-6.

4.5 Conclusion

After testing several strategies for improving cell growth prediction for our specific cell lines, we found that the most effective strategy was implementing a two-step optimization, where the first step solves an optimization problem to generate additional constraints for the second optimization step. We tried two "penalties" suggested by Schinn et al.; others may be more consistent or more accurate. Although our predictions were quantitatively closer to experimental results compared to the conventional FBA solutions, growth rates between cell lines did not trend correctly. The difficulty in modifying the genome-scale model to better fit BMSCHO1 cells may reflect the rigidity of the underlying consensus model. However, we only had a limited dataset from which we could determine exchange fluxes as model inputs. An annotated genome for BMSCHO1could be useful in more specifically curating the reactions in the model and further improving predictions.

4.6 Acknowledgements

I would like to thank two impressive undergraduate students from our lab, Jenner Tresan for his initial work in calculating fluxes from raw data and modifying the existing model to better fit our data and Sophie Girard for implementing these strategies and generating these results figures. I am so grateful to both for their major contributions. I would also like to acknowledge the work of Ayushi Patel and Zhuangrong Huang in developing the final template for regression-based flux calculations.

References

Becker, S. A., & Palsson, B. O. (2008). Context-specific metabolic networks are consistent with experiments. *PLoS Comput Biol, 4*(5), e1000082. doi:10.1371/journal.pcbi.1000082

Hefzi, H., Ang, K. S., Hanscho, M., Bordbar, A., Ruckerbauer, D., Lakshmanan, M., . . . Lewis, N. E. (2016). A Consensus Genome-scale Reconstruction of Chinese Hamster Ovary Cell Metabolism. *Cell Systems, 3*(5), 434-443.e438. doi:https://doi.org/10.1016/j.cels.2016.10.020

Heirendt, L., Arreckx, S., Pfau, T., Mendoza, S. N., Richelle, A., Heinken, A., . . . Fleming, R. M. T. (2019). Creation and analysis of biochemical constraint-based models using the COBRA Toolbox v.3.0. *Nature Protocols, 14*(3), 639-702. doi:10.1038/s41596-018-0098-2

Nolan, R., & Lee, K. (2010). Dynamic model of CHO cell metabolism. *Metabolic Engineering, 13*, 108-124. doi:10.1016/j.ymben.2010.09.003

Quek, L.-E., & Turner, N. (2019). Using the Human Genome-Scale Metabolic Model Recon 2 for Steady-State Flux Analysis of Cancer Cell Metabolism. In M. Haznadar (Ed.), *Cancer Metabolism: Methods and Protocols* (pp. 479-489). New York, NY: Springer New York.

Schinn, S. M., Morrison, C., Wei, W., Zhang, L., & Lewis, N. E. (2021). Systematic evaluation of parameters for genome-scale metabolic models of cultured mammalian cells. *Metab Eng, 66*, 21-30. doi:10.1016/j.ymben.2021.03.013

Villaverde, A. F., Bongard, S., Mauch, K., Balsa-Canto, E., & Banga, J. R. (2016). Metabolic engineering with multi-objective optimization of kinetic models. *Journal of Biotechnology, 222*, 1-8. doi:https://doi.org/10.1016/j.jbiotec.2016.01.005

Xu, X., Nagarajan, H., Lewis, N. E., Pan, S., Cai, Z., Liu, X., . . . Wang, J. (2011). The genomic sequence of the Chinese hamster ovary (CHO)-K1 cell line. *Nature Biotechnology, 29*(8), 735-741. doi:10.1038/nbt.1932

4.7 Supplementary Information

Matlab script for Flux Balance Analysis

```
m =6;
sol = [0,0,0,0,0,0];
changeCobraSolver('gurobi');
fileName = 'iCHOv1_final.mat';
%load model
if ~exist('modelCHO','var')
    modelCHO = readCbModel(fileName);
end

%load constraint data
[constraints,names] = xlsread('constraintsNewZero.xlsx','3-6');
names = names(2:end,1);
exp = names(1,2:end);
gr = constraints(end,:);
%iterate through different experiments
for v =1:6
    model1 = modelCHO;

    %constraint names
    names = string(names);
    %constraint lower bounds
    boundsX = constraints(:,v);
    %boundsX = table2array(boundsX);

    %do not want every single constraint in excel table
    %Predicted 2
    %want = [3:6, 9, 11:14, 17,18,20,22,23,25,26, 28,30:33,38:41]';
    %Predicted 1
    %want = [3, 4, 6, 11, 12, 13, 14, 16, 17, 18, 19, 20,22, 23, 25, 26, 28,
30, 31, 32, 33, 38, 39, 40, 41]';
    %Predicted 3
    want = [3:6, 9,11:14, 16, 17, 19,20,22,25,26,28,30:33,38:41];
    n = length(want);

        %initialize
    s = zeros(n,m);
        %create array of selectred constraints
    for k = 1:n
        t = want(k);
        s(k,:) = boundsX(t,:);
    end
    c = names(want);

        %iterate through constraints to set lower bounds
    for i = 1:n
        model1 = changeRxnBounds(model1,c(i),s(i),'l');
    end

        %model1 = changeRxnBounds(model1,c2,5*s2,'b');
```

```
        %iterate through constraints to set upper bounds
    for j = 1:n-4
        model1 = changeRxnBounds(model1,c(j),s(j),'u');
    end

        %add in tolerances for Igg 10%
    tol = 0;
    model1 = changeRxnBounds(model1,names(1),boundsX(1)*(1-tol),'l');
    model1 = changeRxnBounds(model1,names(1),boundsX(1)*(1+tol),'u');
        %find growth rate for each expermient
    %obj_func = 'igg_formation';
    %model1 = changeObjective(model1,  obj_func);
    FBAsolution = optimizeCbModel(model1,'max');
    % try other Igg models
    sol(v) = FBAsolution.f;

end
sol = sol'
```

Table S1. Constraint Sets For Simulating Growth Rates

Constraint Set 1	Constraint Set 2
DM_igg[g]	DM_igg[g]
EX_ala_L_e_	EX_ala_L_e_
EX_arg_L_e_	EX_arg_L_e_
EX_asp_L_e_	EX_asn_L_e_
EX_cys_L_e_	EX_asp_L_e_
EX_glc_e_	EX_cys_L_e_
EX_gln_L_e_	EX_glc_e_
EX_glu_L_e_	EX_gln_L_e_
EX_gly_e_	EX_glu_L_e_
EX_his_L_e_	EX_gly_e_
EX_ile_L_e_	EX_ile_L_e_
EX_lac_L_e_	EX_lys_L_e_
EX_leu_L_e_	EX_nh4_e_
EX_lys_L_e_	EX_o2_e_
EX_met_L_e_	EX_phe_L_e_
EX_nh4_e_	EX_pro_L_e_
EX_o2_e_	EX_ser_L_e_
EX_phe_L_e_	EX_thr_L_e_
EX_pro_L_e_	EX_trp_L_e_
EX_ser_L_e_	EX_tyr_L_e_
EX_thr_L_e_	EX_val_L_e_
EX_trp_L_e_	SK_Asn_X_Ser/Thr[r]
EX_tyr_L_e_	SK_Tyr_ggn[c]
EX_val_L_e_	SK_Ser/Thr[g]
SK_Asn_X_Ser/Thr[r]	SK_pre_prot[r]
SK_Tyr_ggn[c]	
SK_Ser/Thr[g]	
SK_pre_prot[r]	

Chapter 5. Conclusions & Future Directions

In Chapter 2, we aimed to better understand specific productivity in CHO cells starting with an untargeted metabolomics approach on a library of industrial clones. Using this approach, we were able to identify several pathways associated with productivity and select metabolites of interest from these pathways to investigate further in hopes of finding rational interventions that can enhance qP during commercial process development. Some metabolites that positively correlated with qP, like citrate, directly improved both qP and titer in multiple cell lines when supplemented to the cell culture. A simple screening study with only four metabolites at three concentrations was performed to find this additive, but potentially others could be found by experimenting more with timing and amount. Others, like aspartic acid and cysteine, were found to be potential early indicators of high-qP cell lines and could be useful in clone selection. Intracellular mechanisms behind how the extracellular concentrations of these amino acids correlate to qP are not well understood. ^{13}C tracer experiments could reveal more about these associations. For example, according to our experimental fluxes, aspartate is consumed by cells, at least between days 4-7. Feeding labeled aspartate and targeting metabolites involved in aspartate catabolism pathways (purine biosynthesis, urea cycle, and the malate-aspartate shuttle) followed by flux analysis comparing high- and low-qP clones could provide more clues about the relationship between aspartate and qP.

This ^{13}C-MFA strategy was used for exploring how citrate addition improved qP in Chapter 3, and we were able to estimate fluxes and pinpoint more pathways related to qP and clonal qP response to citrate addition. These pathways included catabolism of aromatic and branched-chain amino acids (BCAAs), glycolysis, and mitochondrial exchange. Unfortunately, the proportion of labeled citrate combined with the amount of citrate consumed was too low to see significant labeling of

other metabolites and trace the fate of citrate in the cells as originally intended. Other labeling strategies have been used for CHO cells such as parallel labeling of glucose and glutamine, which has been shown to be effective for providing insights into CHO cell metabolism (Ahn & Antoniewicz, 2013). However, because we do not feed our GS knockout cells glutamine, it may be necessary to find an alternative feed source to label, e.g., glutamate. Compartment-specific analysis of isotopic label distribution by separating cytosolic components from mitochondrial compartments may be another more sophisticated, though laborious, option that can provide greater detail (Matuszczyk et al., 2015) Especially because we observed that some intercompartmental fluxes may be key factors in qP or response to qP, such as malate-aspartate transport, α-KG-glutamate transport, and the citrate-malate shuttle, clarifying these subcellular fluxes along with the resulting cofactor balances could be essential in narrowing down engineering targets (Junghans et al., 2019; Wijaya et al., 2021). Furthermore, the LC-MS methods used could be refined to resolve metabolites based on retention times as well as product ion spectra. We observed similar retention times for some pairs of metabolites that had overlapping m/z for their isotopologues such as pyruvate and lactate, or succinate and fumarate.

To augment LC-MS data, some orthogonal methods could be used. For example, we examined glycolytic versus mitochondrial ATP generation using the Seahorse XFe96 Analyzer (Agilent, Santa Clara, CA, USA) and saw preliminary results suggesting that increased ATP in citrate-supplemented cultures was largely due to increased glycolytic ATP production rather than mitochondrial ATP production. However, due to poor replicate consistency, this experiment would need to be repeated to provide a more definitive evidence of increased ATP production from glycolysis. Another option is to acquire genomic data that may reveal differences between clones. Because our clones are generated through random integration, the insertion sites are unknown. We

are planning to target our plasmids using Cas9 and sequence outwards to discover the insertion sites and what genes, if any, are disrupted. If a pattern emerges between these disrupted genes and clonal productivity, this knowledge could be used in choosing hotspots while developing new host cell lines. Epigenetic data that can be acquired during sequencing may also be useful, especially in light of the potential role of BCAA catabolism byproducts as histone deacetylase (HDAC) inhibitors (Harrington et al., 2021).

We explored a consensus genome-scale metabolic model for CHO cells in Chapter 4. Strategies such as correcting amino acid composition in the antibody production reactions did not lead to significant improvement towards matching the experimental data we had generated. One strategy that did lead to improvement in estimating the growth rate was implementation of a bilevel optimization scheme for FBA, which added a constraint reflecting cellular limitations to growth. Different cellular objectives could be tested as the additional constraint. Furthermore, there are several updated versions of the genome-scale model that may be examined; for example, some curation has been done to better represent industrial cell lines or the model has been enhanced with more reactions in the secretory pathway. Also, one limitation of this work was that data for each clone was from a single reactor due to experimental restrictions. Multiple replicates from different reactor runs would help ensure that the input (exchange flux) data more accurately capture experimental variability.

Finally, the approaches described in this thesis were used to explore CHO cell productivity, while product quality was considered out of scope. However, the metabolomics approach of this thesis study could also be helpful in investigating metabolites and pathways related to glycosylation and other quality attributes.

References

Ahn, W. S., & Antoniewicz, M. R. (2013). Parallel labeling experiments with [1,2-13C]glucose and [U-13C]glutamine provide new insights into CHO cell metabolism. *Metabolic Engineering, 15*, 34-47. doi:https://doi.org/10.1016/j.ymben.2012.10.001

Harrington, C., Jacobs, M., Bethune, Q., Kalomeris, T., Hiller, G. W., & Mulukutla, B. C. (2021). Production of butyrate and branched-chain amino acid catabolic byproducts by CHO cells in fed-batch culture enhances their specific productivity. *Biotechnol Bioeng, 118*(12), 4786-4799. doi:10.1002/bit.27942

Junghans, L., Teleki, A., Wijaya, A. W., Becker, M., Schweikert, M., & Takors, R. (2019). From nutritional wealth to autophagy: In vivo metabolic dynamics in the cytosol, mitochondrion and shuttles of IgG producing CHO cells. *Metabolic Engineering, 54*, 145-159. doi:https://doi.org/10.1016/j.ymben.2019.02.005

Matuszczyk, J.-C., Teleki, A., Pfizenmaier, J., & Takors, R. (2015). Compartment-specific metabolomics for CHO reveals that ATP pools in mitochondria are much lower than in cytosol. *Biotechnol J, 10*(10), 1639-1650. doi:https://doi.org/10.1002/biot.201500060

Wijaya, A. W., Ulmer, A., Hundsdorfer, L., Verhagen, N., Teleki, A., & Takors, R. (2021). Compartment-specific metabolome labeling enables the identification of subcellular fluxes that may serve as promising metabolic engineering targets in CHO cells. *Bioprocess and Biosystems Engineering, 44*(12), 2567-2578. doi:10.1007/s00449-021-02628-1